UNIVERSITÀ DEGLI STUDI DI TRIESTE

UNIVERSITÀ DEGLI STUDI DI TRIESTE

XXXV CICLO DEL DOTTORATO DI RICERCA IN

BIOMEDICINA MOLECOLARE

miR-30d suppresses innate immune signalling in BC cells by attenuating the cGAS/STING/IFN-I pathway

Settore scientifico-disciplinare: BIO/11

DOTTORANDO / A
Federica Di Camillo

COORDINATORE
Prof. Germana Meroni

SUPERVISORE DI TESI
Prof. Giannino Del Sal

ANNO ACCADEMICO 2021/2022

To my parents,
Dino and Luciana,
for their constant support

Index

Abstract

Tumors are complex ecosystems composed by heterogeneous populations of cancer cells embedded in a dynamic tumor microenvironment (TME). Communication of cancer cells with the TME displays both local and systemic tumor-promoting effects, including angiogenesis, ECM remodeling, and modulation of immune/inflammatory cells, to support tumor growth and progression, and escape from immune surveillance. Understanding immune evasion mechanisms that generate non-immunogenic "cold" tumors represents a key issue for improving the efficacy of anticancer immune therapies. Accumulating evidence has established that oncogenic drivers, such as mutant p53 and HIF1α, contribute to tumor progression and immune evasion by attenuating the cGAS/STING/IFN-I pathway in cancer cells. This cascade involves cGAS-dependent sensing of cell-intrinsic DNA damage with consequent induction of STING ER-Golgi trafficking, activation of the transcription factor IRF3 and expression of downstream type-I interferons (IFN) response target genes, thus engaging anti-tumor immune surveillance. Recently, our research group highlighted an oncogenic axis affecting tumor-stroma crosstalk. We discovered that miR-30d, a secreted onco-miRNA cooperatively induced by HIF1α and mutp53 oncoproteins, regulates targets involved in the secretory pathway, causing structural alterations of ER and Golgi compartments. This promotes the release of a pro-malignant secretome, which alters the TME and fosters tumor growth and metastatic colonization.

Transcriptomic analysis in metastatic breast cancer (BC) cells upon downregulation of miR-30d highlighted a putative inhibitory effect of miR-30d on the categories of "cellular response to DNA damage", "type-I interferon production" and "antiviral innate immune response", leading to the hypothesis that high levels of miR-30d might inhibit the expression of type-I IFN target genes, a condition that could contribute to establish an immune "cold" microenvironment.

In this work I have investigated the impact of miR-30d on the regulation of IFN response and dissected the mechanisms by which ablation of miR-30d leads to upregulation of IFN signaling in BC cells. By using an LNA inhibitor and a miR-30d Decoy construct, I have demonstrated that inhibition of miR-30d in BC cells led to activation of the main components of the cGAS/STING signaling machinery, in particular phosphorylation of TBK1 and STING, nuclear translocation of the IRF3 transcription factor, and consequent secretion of type-I IFNs. The effects of miR-30d inhibition included normalization of fragmented Golgi structure, and concomitant activation of STING at Golgi apparatus in BC cells, thus suggesting that miR-30d might attenuate the

cGAS/STING pathway by inducing structural alterations of the secretory pathway, in particular of the Golgi. Furthermore, I found that miR-30d inhibition in BC cells promoted accumulation of nuclear DNA damage and of cytoplasmic dsDNA with activation of cGAS, which acts upstream of the STING DNA-sensing pathway.

In sum, this evidence is consistent with a model in which inhibition of miR-30d may both trigger upstream induction of the cGAS/STING pathway in cancer cells, by causing release of dsDNA in the cytosol, and further sustain its activity by normalizing the structure of the secretory pathway.

In addition, I observed that when miR-30d inhibition was combined with conventional chemotherapeutic agents in metastatic BC cells, the treatment led to a much stronger effect on the activation of the IFN signaling. Experiments with ex-vivo and in-vivo preclinical models are currently in progress to investigate whether inhibition of miR-30d could reactivate immune surveillance as well as to test synergies between miR-30d inhibition and cGAS/STING-inducing chemotherapeutic treatments.

The cGAS-STING/IFN signaling pathway is currently the focus of intense research due to its key role in establishing an anti-tumor immune microenvironment, a condition that impacts responsiveness to immune checkpoint inhibitors. Therefore, the findings obtained in this thesis suggest that targeting miR-30d could represent a valuable strategy to stimulate this pathway thus improving patients' responsiveness to immune therapies.

1. Introduction

1.1 The tumor microenvironment

Cancer is driven by genetic and epigenetic alterations that allow cells to over-proliferate and escape mechanisms that normally control their survival and migration. Many of these alterations map to signalling pathways that control cell-intrinsic processes, including growth and survival, metabolism and differentiation, among others[1,2]. Remarkably, tumors are complex ecosystems composed of heterogeneous populations of cancer cells embedded in a dynamic tissue microenvironment (TME), which crucially shapes tumor growth, stromal invasion and metastatic evolution, as well as response to therapies. The specific composition of primary and secondary tumor niches and the reciprocal interactions between tumor cells and TME components represent major factors that may aggravate tumor progression, leading to poor clinical outcomes. The TME includes a large variety of resident and infiltrating stromal and immune cells, secreted factors, and components of extracellular matrix (ECM)[3] (Fig. 1). Studying tumors from an ecological perspective implies that malignant phenotypes are not fully tumor cell-autonomous, but rather that functional cooperative networks exist among multiple subpopulations, including crosstalk among cancer cells inside the tumor mass and between cancer and stromal cells, which cooperate to shaping the TME[4]. Notably, alterations in oncogenes and tumor suppressors, in addition to regulate cell-intrinsic activities, also impact on TME composition and functions, corrupting them to support pro-malignant phenotypes[5,6]. Importantly, the relationship between tumors and their surrounding microenvironment has a dual nature. In fact, the TME can both support metastatic growth and survival, and, vice versa, limit it, competing for the availability of vital resources (e.g. oxygen, nutrients, metabolites) and triggering an immune response[7].

This evidence highlights the importance of understanding how tumor cells interact and communicate with both their surroundings and distant tissues, and how this interplay may regulate disease progression.

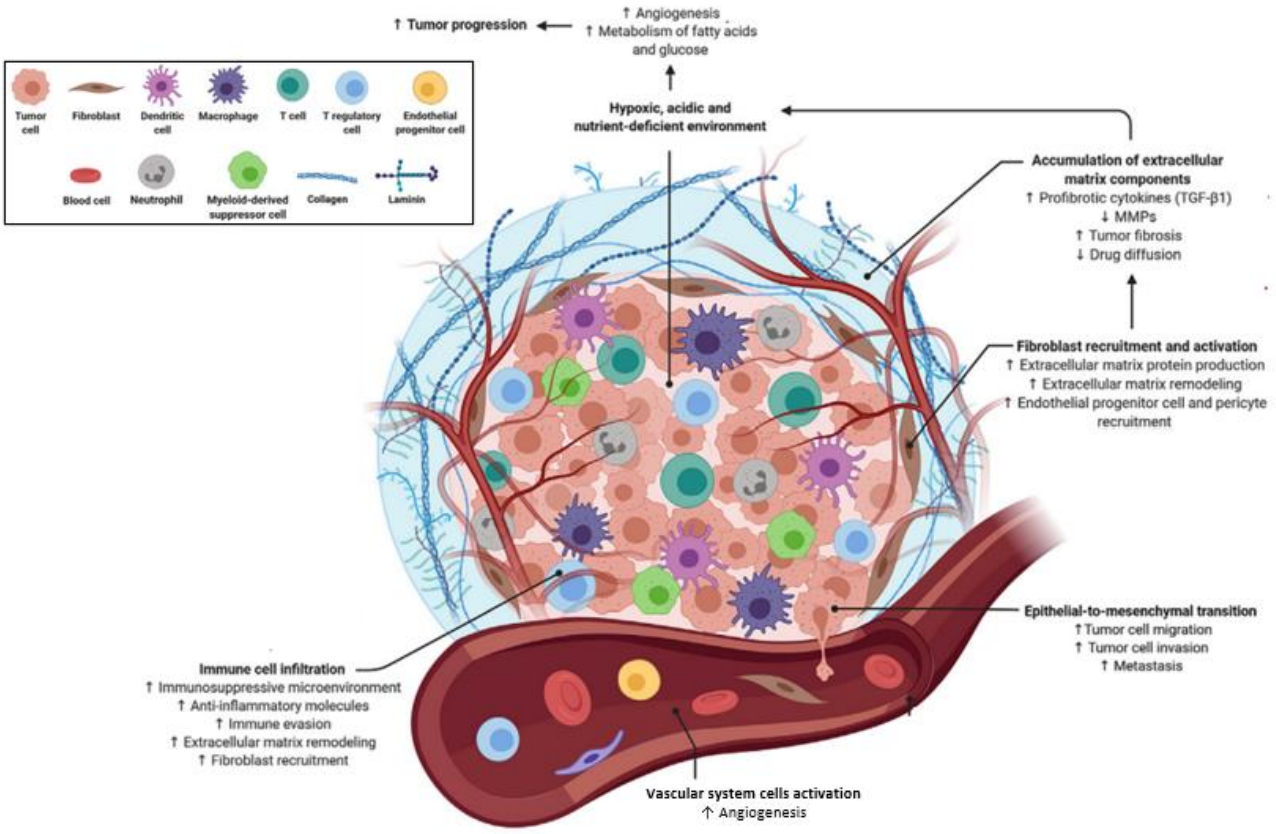

Figure 1. **The tumor ecosystem.** Schematic representation of the tumor mass and its surrounding TME, including the different cellular and non-cellular components and highlighting key processes that allow tumor and metastatic progression, such as remodeling of the ECM, fibroblast recruitment, immune suppression, and activation of cells of the vascular system (modified from[8]).

1.2 Stromal components of the TME

1.2.1 The extracellular matrix (ECM)

The extracellular matrix (ECM) is a major non-cellular component within all tissues, which serves to maintain their integrity by providing physical support to cells. It is composed of two main classes of macromolecules: proteoglycans and fibrous proteins, among which the most important are collagens, elastin, fibronectin and laminin[9]. Collagen and elastin fibers are stabilized through crosslinking by both the lysyl oxidase (LOX) and the transglutaminase enzyme families, thus resulting in the formation of larger and more rigid fibrils[10]. The ECM is a highly dynamic structure, whose molecular components are constantly deposited, degraded, and subjected to a myriad of post-translational modifications. Cells connect to ECM components via membrane receptors such as integrins, discoidin domain receptors, and syndecans. Notably, the ECM not only provides structural support for resident cells but also provides critical biochemical and biomechanical cues that drive morphogenesis, tissue-specific differentiation and maintain tissue homeostasis[11]. A bidirectional interdependence exists

between cells and the surrounding ECM: epithelial and stromal cells constantly secrete and remodel the ECM, whereas the latter in turn sends back signals that influence cell features and activities such as proliferation, adhesion, migration, and apoptosis[9].

Tumors may exhibit desmoplasia, characterized by increased deposition of ECM proteins, leading to tissue stiffening[12,13]. In addition, the high activity of LOX proteins creates thick linearized collagen fibrils[14,10]. Overall, deposition, remodeling and crosslinking alter the physical properties of the ECM, favoring its stiffening, while other physical cues relevant for tumor progression comprise solid stress (compression, stretch), and interstitial fluid pressure. In a process known as mechanotransduction[11,15] cells sense and respond to physical and mechanical stimuli via integrin-cytoskeleton mechanosignaling, affecting cell migration and inducing signaling pathways and gene expression changes relevant for tumor growth, progression and treatment outcome. Recent studies indicate that biomechanical alterations of the ECM, including high stiffness, cooperate with oncogenic mutations and are essential for tumor initiation and metastatic progression of solid tumors. Indeed, mechanical inputs have been shown to endow transformed cells with stem cell attributes, ability to evade the immune system and to induce proliferation and chemoresistance[11,16]. Therefore, it is not surprising that tissue fibrosis and high stromal stiffness correlate with tumor aggressiveness and poor patient prognosis in breast, pancreatic, lung and colon cancers[11,17–19].

1.2.2 Cancer-associated fibroblasts

Fibroblasts represent the most abundant stromal cell type, whose main functions include production, degradation, and remodeling of ECM and basement membrane components, and are therefore essential in maintaining matrix homeostasis. In addition to ECM organization, fibroblasts also play key roles in regulating epithelial differentiation and modulating the immune response[11,20,21]. Under physiological conditions, fibroblasts are in a quiescent state, whereas stress or injuries, such as those occurring during inflammation, wound healing, and fibrosis, stimulate their activation into myofibroblasts[22]. In cancer, activated fibroblasts are named cancer-associated fibroblasts (CAFs). These cells undergo morphological changes and increase migratory and proliferative abilities[23,24]. CAFs are commonly identified by the expression of the cytoskeletal protein smooth muscle α-actin (α-SMA), however, they can express distinct arrays of markers, displaying a wide degree of heterogeneity. Recent studies indicate that multiple CAF subtypes coexist in the TME, each affecting the tumor in a unique way [25–27]. This said, a common feature of CAFs is an augmented production and remodeling of ECM constituents, which contribute to abnormal stiffening of the ECM[11,26]. CAFs ECM remodeling ability is attributed to the production of matrix metalloproteinases (MMPs) such as MMP1 and MMP3, and to a massive synthesis of LOX family proteins[11,26]. Furthermore, activated

CAFs are characterized by the secretion of a wide range of pro-oncogenic factors, including cytokines, chemokines and growth factors, aimed at supporting tumor progression. For instance, the release in the extracellular space of the chemokine CXCL12 has been amply proven to drive angiogenesis and cancer cell proliferation and to inhibit the migration of T-cells in solid tumors[28,29]. Of note, many CAFs-secreted factors directly influence immune cell recruitment and activation, in order to support the generation of a immunosuppressive TME[11,30,31]. CAFs also support metabolic rewiring of tumors, by increased secretion of several amino acids, lipids and lactate, which fuel cancer metabolism, supporting tumor growth. CAFs-derived exosomes also contribute to this process by directly supplying glucose and glutamine to cancer cells[32].

1.2.3 Tumor vasculature

New growth of the vascular network through angiogenesis and vasculogenesis[33] represents an important event within the TME, since cancer growth depends on an adequate supply of oxygen and nutrients. In addition, the abnormal vascularization of the tumor mass encourages the spread of cancer cells to adjacent tissues and to distant loci, leading to metastases. New blood vessels consist of endothelial cells, which line the insides of the blood vessels, and perivascular cells (pericytes for microvessels, and smooth muscle cells for arteries and veins), which surround the blood vessels externally and play a role in blood vessel contraction[34]. Within the tumor mass, hypoxic conditions lead to secretion of angiogenic signals (e.g., VEGF, PDGF, FGFs, IL-8, and angiopoietin) by malignant, stromal or inflammatory cells, triggering the transformation of normal endothelial cells into tumor endothelial cells (TECs), which up-regulate genes associated with cell proliferation, migration and tube formation[35]. After activation, TECs undergo morphological changes, which negatively affect blood vessels integrity by diminishing cell–cell interconnections[36]. Moreover, reduced coverage of tumor vessels by pericytes cooperates to destabilize vascular integrity and function. As a consequence, new blood vessels become leaky, leading to inflammation, and facilitating intravasation and extravasation of cancer cells. TECs promote inflammation at the tumor site through the activation of NF-κB and STAT3 signalling, and the subsequent secretion of pro-inflammatory chemokines[37]. These factors, together with increased vascular permeability, allow immune cells, including leukocytes and macrophages, to infiltrate the tumor site. While the induction of an acute inflammatory response has an antitumor role, its chronic activation may induce immune cells to develop phenotypes that support tumor aggressiveness (see below).

1.3 Immune-inflammatory components of the TME

The TME contains immune cells belonging to both adaptive and innate immune systems[7,8], whose

combined actions modulate malignant progression. The idea that the immune system keeps in check tumor growth was first postulated by Paul Ehrlich in 1909 and later termed 'cancer immunosurveillance hypothesis' by Thomas and Burnet in the mid-twentieth century[38]. This hypothesis has since been refined based on knowledge that the immune system cannot only protect against tumor development but can also select for tumors with decreased antigenicity and/or immunogenicity in a process referred to as cancer immunoediting. The current framework of cancer immunoediting is a dynamic process comprised of three distinct phases: elimination, equilibrium and escape, which highlight the dual host-protective and tumor-promoting actions of immunity[39].

A TME is usually referred to as "hot" or "cold" depending on whether it contains high or low levels of anti-cancer immune infiltrate, respectively. It is widely recognized that some immune cell types, such as CD8+ and CD4+ T-cells[40], natural killer (NK) cells[41] and N1 neutrophils[42] are endowed with tumor suppressive functions. These cells are able to orchestrate inflammatory reactions and/or directly eliminate cancer cells from tumor sites. NK cells are components of the innate immune system and are able to kill tumor cells and virus infected cells by inducing apoptosis, which can be mediated by granzymes and perforin or via expression of Fas ligand and TRAIL. Moreover, NK cells secrete cytokines such as IFN-γ and TNF-α, which act on other immune cells like macrophages and dendritic cells to enhance the immune response.

Cytotoxic T lymphocites (CTLs), i.e. $CD8^+$ T-cells, are the main effectors of the adaptive anti-tumor immune response, able to recognize tumor antigens and promote tumor cell death by both releasing cytotoxic granules and anti-tumor cytokines (e.g., IFN-ɣ and TNF-α) and by inducing pro-apoptotic processes in cancer cells. Cytotoxic $CD8^+$ T-cell activity is supported by $CD4^+$ T-cell population through the production of IFN-ɣ and IL-2[43]. Additionally, N1 neutrophils display a potent anti-tumor activity mainly due to the release of pro-inflammatory or immunostimulatory cytokines, such as IL-12, TNF-α, CCL3, CXCL9 and CXCL10, which facilitate recruitment and activation of $CD8^+$ T-cells. Importantly, the anti-tumor immune cells also play a key role in eradicating dormant disseminated tumor cells (DTCs) in secondary sites, thus preventing metastatic outgrowth. Consistent with this evidence, it has recently been demonstrated that recruitment of NK pool at the metastatic site is necessary to maintain DTCs in the dormant state. NK cells, by increasing interferon-γ (IFN-ɣ) signalling, support the function of cytotoxic T-cells against awakened DTCs. The contraction of the NK cell compartment supports the output of DTCs from the state of dormancy and consequently the metastatic outgrowth[41].

Conversely, other immune subsets are reported to support tumor progression, such as regulatory T cells (Tregs), myeloid-derived suppressor cells (MDSCs), N2 neutrophils and M2 macrophages. Tregs are a particular subtype of $CD4^+$ T-cells, which permit tumor growth by suppressing T cell cytotoxic activity (e.g. by CTLA-4 signalling)[44,45]. Some subtypes of B lymphocytes may also be

pro-tumorigenic by favoring the maintenance of the Treg cell population, suppressing NK cell factions and downregulating the secretion of several proinflammatory cytokines (e.g., IFN-ɣ, IL-17,TNF-α, IL-12) via the release of IL-10[46,47]. During tumorigenesis, MDSCs are mobilized to both primary and secondary tumor sites, where they promote angiogenesis and immune suppression through production of suppressive factors, cytokines and surface ligands[32,48,49]. For instance, MDSCs are able to suppress activation of cytotoxic T and NK cell populations through the production of reactive oxygen species (ROS) and arginase 1 (Arg-1), along with recruitment of immune suppressive cells such as Tregs[48]. In contrast to N1 neutrophils, N2 neutrophils have strong immunosuppressive and tumor-promoting activity, including promotion of tumor angiogenesis, invasion and metastasis via several factors, such as hepatocyte growth factor (HGF), oncostatin M, reactive oxygen and nitrogen species (ROS, RNS) and MMPs[50]. Lastly, extensive evidence confirmed that tumor-associated macrophages (TAMs) are crucial for tumor and metastatic progression[49]. Macrophages are functionally plastic, altering their polarization status in a range between M1 and M2 phenotypes. While M1 macrophages produce type-I proinflammatory cytokines with tumoricidal role (e.g TNF-α, IL-1, IL-6, IL-12, CXCL10, CXCL11, CXCL16, CCL5), on the contrary M2 macrophages produce type-II cytokines which are immune-suppressive and pro-tumorigenic factors, including Arginase-I, IL-10 and TGF-β. TAMs exhibit M2 phenotype, and influence tumor biology by producing growth-inducing molecules, regulating inflammatory response and adaptive immunity, enhancing angiogenesis and promoting ECM deposition and remodeling[14].

During tumor immunoediting, low immunogenic clones become selected and are allowed to survive in an immunologically unrestricted manner[51]. Many mechanisms have been reported that enable tumors to escape immune surveillance, including both immune evasion and immune suppression. Understanding these alterations is essential for conceiving therapeutic strategies that aim at promoting tumor cell clearance by the immune system using combination therapies that involve immune checkpoint inhibitors[52].

It is known that tumor cells, as well as non-immune components of the tumor microenvironment, can produce immunosuppressive factors, including growth factors[53], cytokines[54] and chemokines[6], which are involved in tumor immune escape (see section 1.4). For instance, CAFs are recognized to secrete interleukin IL-6, which recruits tumor-associated macrophages and promotes their transition to an immunosuppressive (M2) phenotype[55,56]. In turn, the infiltrating M2 macrophages secrete factors (e.g., TGF-β), which stimulate resident stromal fibroblasts to synthesize and secrete ECM proteins, MMPs and collagen-crosslinking enzymes[14]. Finally, high collagen density and ECM stiffening reduce both the recruitment and function of cytotoxic T-cells in tumors[57], and promote macrophage polarization towards M2 phenotype[58].

Immune suppression may also occur by altering the surface repertoire of activating and inhibitory

signals that immune cells use to distinguish malignant from healthy cells. For instance, overexpression of immune checkpoint ligands on the surface of malignant cells facilitates their immune escape. When the checkpoint (expressed by immune T-cells) and ligand partner protein (expressed by cancer cells) bind together, they send an "off" signal to T lymphocytes, which prevents the immune system from destroying cancer cells. Remarkably, cancer cells have been demonstrated to actively evade immune surveillance through upregulating the expression of programmed death ligand 1 (PD-L1), a well-known checkpoint ligand[59,60]. The rigidity of the ECM has been reported to increase the expression of PD-L1 on the surface of tumor cells, thus preventing tumor cell killing[61]. Of note, it has recently been demonstrated that CAFs are also able to reduce the activation of antitumoral $CD8^+$ cytotoxic T-cells by expressing inhibitory immune checkpoint signals, such as PD-L1[62–64].

As another means of immune evasion, cancer cells may acquire strategies to become undetectable by the immune system. This may entail cell contact-dependent mechanisms. For instance, a recent study revealed that disseminated cancer cells are able to bypass $CD8^+$ T-cell recognition by downregulating the exposure of HLA molecules[65], while expression of "don't eat me signals", like the cell surface molecule CD47, inhibits the phagocytic activity of macrophages and DCs. On the other hand, usually tumors appear to select activities that allow them to escape activation of innate immune signaling, which occurs via the cGAS-STING-IFN pathway.

1.3.1 The cGAS-STING pathway

The invasion of the cytoplasm by microbial DNA from infectious pathogens or by self-DNA from the nucleus or mitochondria represents a danger signal that alerts the host innate immune system. This occurs through activation of the cGAS-STING pathway, an evolutionarily conserved DNA sensing machinery able to both mediate cytotoxic effects and initiate a rapid innate immune response against microbial pathogens and viral infections. Recent advances have expanded the knowledge of the roles of cGAS-STING, revealing its involvement in anticancer immunity (Fig. 2). Several sources of DNA damage such as oxidative stress, radiation and chemotherapy, as well as low chromosome stability, nuclear damage and micronuclei, activated transposable elements and mitochondrial DNA, may contribute to generate cytosolic DNA within tumor cells. This activates the cGAS-STING pathway, culminating in the expression of interferon-related genes, and in the release of inflammatory cytokines and chemokines, capable of recruiting immune cells and initiating an immune response against cancer cells. Evasion of immune surveillance represents a key step during the emergence of malignancies, and consistently usually tumors appear to select activities that attenuate or corrupt cGAS-STING-IFN signalling, thus escaping immune surveillance.

1.3.2 Mechanisms of cGAS-STING pathway activation

The pathway component devoted to sensing cytosolic DNA is the cyclic GMP-AMP synthase (cGAS). This enzyme, able to detect double-stranded DNA (dsDNA) without sequence specificity, responds to both cytosolic foreign DNA from pathogens and to self-DNA, leaked into the cytosol due to genome instability or cellular damage. Upon activation, cGAS catalyzes the synthesis of a cyclic-dinucleotide second messenger, 2'3'- cyclic GMP-AMP (cGAMP), from ATP and GTP[66–69]. In particular, binding of dsDNA to cGAS causes the formation of liquid-liquid phase separated droplets, in which cGAS and dsDNA are spatially concentrated for efficient cGAMP synthesis[70]. cGAMP then binds directly to stimulator of interferon genes (STING), a ubiquitously expressed transmembrane protein localized on the endoplasmic reticulum (ER) [67,69,71]. This interaction induces a conformational change of inactive STING dimers, leading to active STING dimers, which are able to pack side-by-side to form tetramers and higher order oligomers[72]. In addition to inducing intracellular STING activation, cGAMP can be transferred to neighboring cells via gap junctions, thus initiating non cell-autonomous STING-mediated signalling[73,74]. Upon activation, STING translocates from the ER to the Golgi apparatus (GA) through COPII mediated vesicular transport[75,76]. Here it recruits the TBK1 kinase, which phosphorylates STING at the critical serine residues S366 and S358[77,78], allowing recruitment of the transcription factor IRF3, and its subsequent phosphorylation by TBK1. This causes IRF3 homo-dimerization and dissociation from STING[77,78], and exposure of a masked nuclear localization signal (NLS), leading to IRF3 accumulation in the nucleus where it forms a complex with the transcriptional coactivators CBP/p300 and induces the expression of type-I IFNs (i.e. IFNα and IFNβ) and of a set of pro-inflammatory cytokines[79]. In addition, IRF3 can also translocate to the mitochondria and induce apoptosis by interacting with Bax to promote pore formation[80]. A further activity of STING is to bind and stimulate IκB kinase to trigger the activation of NFκB[81], albeit to a lesser extent than IRF3[82]. NFκB activation promotes the expression of numerous inflammatory cytokines, including IFNα and IFNβ[83], TNF, IL-1β and IL-6 with antitumor effects[84]. Downstream IRF3 or NFκB activation, the binding of secreted type-I IFNs with the heterodimeric IFN receptor IFNAR1/IFNAR2 activates Janus kinase 1 (JAK1), which can phosphorylate members of the *signal transducer and activator of transcription* (STAT) family and induce the expression of a set of immune modulators termed interferon-stimulated genes (ISGs)[85]

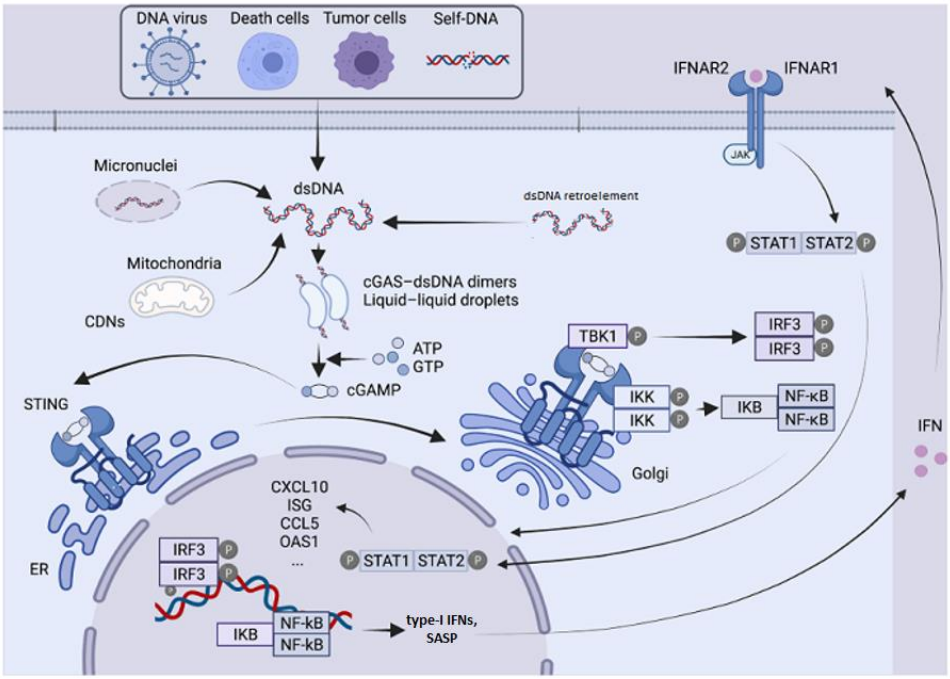

Figure 2. **Simplified scheme of the cGAS–STING pathway:** The recognition of cytosolic DNA by cGAS leads to its activation and consequent production of cGAMP, which in turn activates STING. Activated STING translocates to perinuclear Golgi and forms a clustered platform on which TBK1 kinase phosphorylates the transcription factor IRF3. Phosphorylated IRF3 enters the nucleus and triggers the expression of type-I interferon and other immune mediators. At the same time, STING also binds and stimulates IKK, triggering the transcriptional activation of NF-κB. Ultimately, it regulates the expression and secretion of pro-inflammatory cytokines such as type-I interferon (modified from[85]).

1.3.3 Effects of the cGAS-STING-IFN pathway on the immune components of the TME

The activation of the cGAS-STING-IRF3 pathway in cancer cells culminates in the expression of type-I IFNs and ISGs, which collectively alert the host immune system supporting the recruitment of immune cells, such as NK and cytotoxic T-cells[86]. These cells are able to orchestrate inflammatory reactions and directly eliminate cancer cells from tumor sites (Fig. 3). Importantly, the cGAS-STING pathway has also been robustly linked to the induction of cancer cell senescence, which mediates further tumor-suppressive effects[87–89]. Of note, the capability of cGAS-STING signalling to promote senescence is dependent on the secretion of chemokines and pro-inflammatory cytokines which are components of the senescence-associated secretory phenotype (SASP). These immune-stimulatory factors can either contribute to the tumor control in a tumor-cell autonomous manner or recruit immune cells for tumor clearance[90]. Notably, STING-mediated induction of SASP in an NFκB-dependent manner. The fact that SASP is driven by NFκB, and not by the IRF3–IFN pathway, suggests nonredundant roles of downstream STING effectors in regulating senescence[86].

In addition, tumor cells have also been found to induce the cGAS-STING-IFNs signalling in immune cells of the TME (*Fig.3*). Through an unestablished mechanism, tumor DNA is known to be

transferred into the cytosol of antigen-presenting cells (APCs), such as dendritic cells (DCs)[91]. Tumor-derived DNA, in turn, activates cGAS-STING signalling to enforce both IFNs production and tumor-antigen presentation on DC surface, triggering cross-priming of $CD8^+$ T cells for anti-tumor immunity[91,92]. In addition, tumor cells have been shown to secrete cGAMP in the extracellular space, which is taken up by DCs and activates STING-IFN response driving NK-mediated tumor killing[93]. Overall, this evidence supports the notion that cytosolic DNA sensing plays a crucial role in anti-tumor responses in both a tumor cell-autonomous and non-cell autonomous manner. Consistently, STING and/or cGAS expression is lost in many tumor-derived cell lines, suggesting that the cGAS-STING pathway is antagonistic to tumorigenesis[89,94,95]. Moreover, low expression of cGAS and STING in tumors is associated with increased disease aggressiveness and poor prognosis.[89,96].

Remarkably however, recent evidence has highlighted that the cGAS-STING pathway may also be involved in tumor promotion. Specifically, while acute cGAS-STING signalling plays a central role in anticancer responses, chronic inflammatory signaling through sustained activation of NF-κB downstream of the cGAS-STING signaling pathway has been reported to facilitate epithelial-to-mesenchymal transition, leading to increased migration and invasion of cancer cells[85]. Moreover, chronic cGAS-STING activation could paradoxically contribute to the generation of an immunosuppressive TME[97], also via upregulating the expression of immune checkpoint indoleamine-2,3-dioxygenase (IDO)[98]. As an example, in an epithelial cancer model, DNA damage detected by the cGAS-STING pathway promoted cytokine production leading to inflammation and carcinogenesis[99]. In a brain metastatic model, cGAMP produced by cancer cells was transferred to astrocytes through gap junctions, where it activated STING and induced the production of inflammatory cytokines, which in turn supported tumor growth[100].

Despite this evidence, since the acute activation of the cGAS-STING pathway has been widely demonstrated to have strong anti-cancer effects, it currently represents an important target for the development of cancer immunotherapy strategies[101,102]. Interestingly, classic anticancer therapies designed to directly target cancer cells, including ionizing radiation and chemotherapy, have been shown to activate the cGAS-STING pathway resulting in antitumor immunity. For example, the PARP inhibitor Olaparib, a chemotherapeutic drug used in the treatment of BRCA-mutated cancer, enhaces DNA damage and micronuclei formation, resulting in the activation of cGAS-STING signalling in tumor cells[103]. More recently, several cyclic dinucleotide and small molecule STING agonists have been tested in tumor models with the aim to stimulate STING signalling and hence upregulate cancer immunity, with promising effects[85]. Several clinical trials are currently ongoing using STING agonists alone or in combination with other cancer treatments[101].

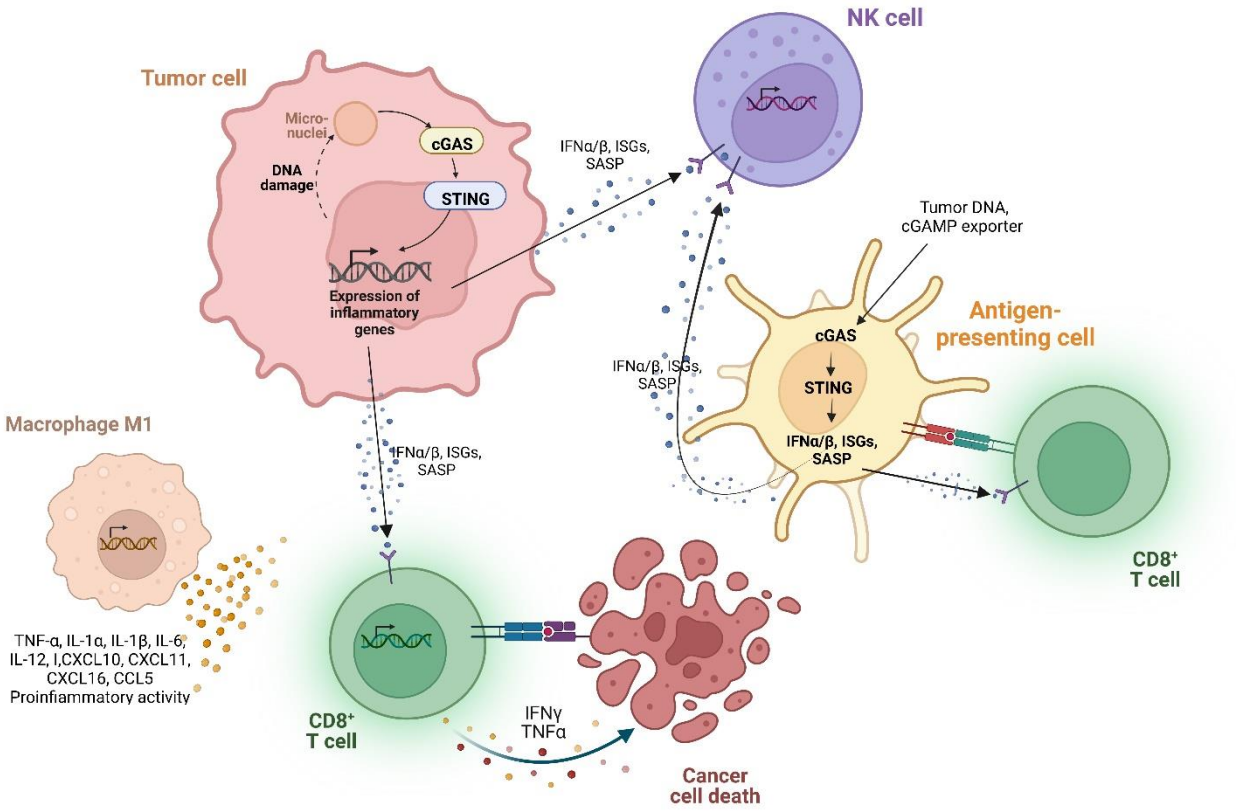

***Figure 3.* cGAS-STING signalling within the tumor microenvironment.** The cGAS-STING pathway is activated by cytosolic ds DNA in tumor cells and culminates in the release of type-I IFNs and immune-stimulatory cytokines, which trigger tumor cell killing by cytotoxic cell populations (CD8+ T cells and NK cells). In addition, tumor-derived DNA and cGAMP produced by tumor cells represent signals that activate the cGAS-STING pathway also in antigen-presenting cells, thus enhancing both the production of type-I IFNs and the consequent activation of tumor-killing immune cell populations (Created with BioRender.com).

1.3.4 Regulation of the cGAS-STING pathway

The cGAS-STING pathway must be strictly regulated to prevent its aberrant or sustained activation, which would result in pathological inflammatory/immune responses. A number of positive and negative regulators of cGAS and STING have been identified, which ensure sufficient and prevent excessive stimulation of this pathway, respectively[104]. Positive regulation of the cGAS-STING pathway includes ubiquitination of STING by TRIM32[105] and TRIM56[106], which enhances its interaction with TBK1, and palmitoylation at residues C88 and C91 in the Golgi which is required for type-I IFN induction[107]. Conversely, attenuation of the pathway may occur by cGAS cleavage by caspase 1[108] or by autophagic degradation of STING [109].

During open mitosis, the cGAS DNA sensor does not respond to chromosomal DNA. Inhibition of cGAS/STING/IFN-I signalling during mitosis has been proposed to depend on disruption of Golgi structure. In cells with artificially vesiculated Golgi by addition of Brefeldin A or Golgicide, similar

to cells arrested in mitosis, correct processing of the STING protein on the Golgi apparatus (GA) would not occur, preventing the assembly of the STING-TBK1-IRF3 complex and execution of downstream IFN-I response[110]. In addition, nuclear activation of cGAS is also prevented[111]. In fact, although cGAS recognizes DNA in the cytoplasm, a pool of cGAS (even the majority in some cell types) resides in the nucleus[112,113]. Recently obtained electron microscopy structures have revealed that nuclear cGAS is tightly tethered to nucleosomes via the acidic patch of H2A-H2B histone dimers, which locks cGAS into a monomeric state and prevents it from binding to free DNA[114–116].

1.4 Regulation of cancer-TME communication

1.4.1 Roles of cancer cell secretion in TME reprogramming

Within solid tumors, tumor-stroma communication is crucial for establishing a supportive TME, thereby allowing tumor growth and progression. Although communication can occur in a contact-dependent manner by cell-cell interactions mediated by membrane receptor proteins or through gap junctions, it is mainly realized in a paracrine fashion, through secretion of soluble and insoluble factors[117] (Fig. 4).

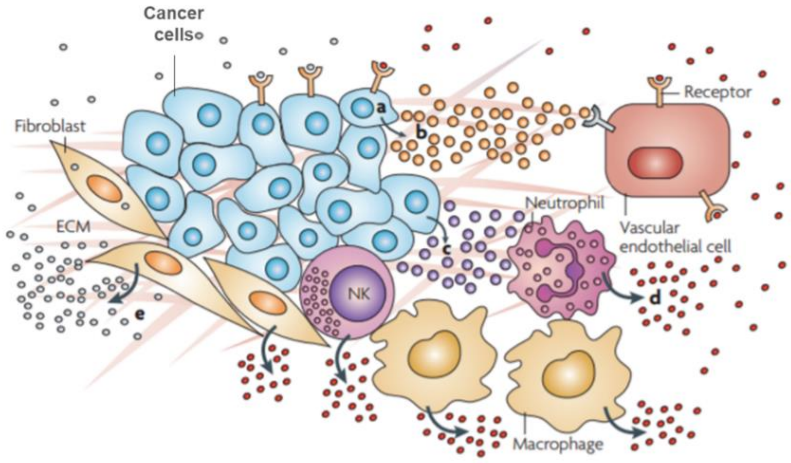

Figure 4. **Communication in the TME.** Simplified representation of the communication between cancer cells and different cell types of the TME (adapted from[118]).

Cancer cells are known to secrete more than their non-malignant counterparts [119], and their secretomes display both short-range and systemic effects[120]: studying cancer secretome components provides valuable resources for diagnosis, prognosis, and treatment of tumors[121]. Malignant secretomes may include a plethora of soluble proteins (i.e. growth and motility factors, extracellular matrix-degrading proteases, chemokines and immunoregulatory cytokines) but also lipids, metabolites, DNA fragments and several RNA types (i.e. mRNA, miRNA and lncRNA), as well as extracellular vesicles

(EVs) [122–124]. The amount of any constituent can vary due to alterations of de novo synthesis and half-life, or of trafficking processes[125].

Many secreted proteins have well-characterized roles in promoting tumor cell invasion and metastatic progression. For instance, secretion of growth factors such as TGF-β can drive EMT[126]. Secreted proteolytic enzymes, such as MMPs, have established roles in degradation of extracellular matrix components, facilitating both angiogenesis and cancer cell migration and invasion[127]. VEGF-A is a major pro-angiogenic factor in the TME and together with EGF, PDGF, TGF-β and chemokines, stimulates endothelial cells and pericytes towards neoangiogenesis[128]. Following its secretion, VEGF-A is sequestered in the ECM and is released by MMPs, abundantly produced by monocytes and macrophages, underlining the existence of a wide signalling network involving tumor, immune and stromal cells[2]. Tumor-secreted factors also act to reshape the TME towards an immunosuppressive state. Cancer cells secrete immunosuppressive cytokines, such as IL-1, IL-6, IL-10 and the growth factor TGF-β, which promotes the conversion of $CD4^+$ T lymphocytes into suppressive regulatory T-cells[129]. Secretion of VEGF-A results in the suppression of dendritic cells by inhibiting their maturation[130], similar to secretion of Indoleamine 2,3-dioxygenase (IDO), which pushes dendritic cells (DCs) and macrophages to an immunosuppressive phenotype and causes local suppression of effector T cells[131].

As a result of their metabolic reprogramming[132], tumors secrete multiple metabolites, some of which act as signalling molecules. A paradigmatic example is provided by the lactate generated during glycolysis, causing TME acidification. Extracellular lactate can be imported by tumor cell subpopulations exhibiting an oxidative metabolism, or by CAFs, where it is subsequently converted into pyruvate to foster the TCA cycle, thus resulting in efficient energy production and higher proliferative capacity[133]. Tumor-derived lactate can be up-taken by cytotoxic T lymphocytes, where it turns off the RLR receptor signalling, known to support the production of type-I interferons. Therefore, suppression of RLR signalling weakens immune surveillance and promotes cancer progression[134]. An immunosuppressive function has been also shown for extracellular adenosine and its associated nucleotides (i.e. ATP, ADP, AMP), which can impinge on T-cells activity[135]. Cancer cells also secrete in the extracellular milieu several bioactive lipid mediators that modify tumor-stroma communication[136]. The best characterized are prostaglandin E2 (PGE2), which stimulates angiogenesis and immunosuppression, and sphingosine-1-phosphate (S1P), involved in angiogenesis. It is important to underline that the crosstalk mediated by metabolites is bidirectional within the TME, in fact stromal/immune cells secrete metabolites able to rewire cancer cells' metabolism and functions. For instance, stroma-associated pancreatic stellate cells and CAFs are reported to secrete alanine and glutamine respectively, thus supplying TCA cycle in pancreatic tumor cells[137].

It has been estimated that microRNAs (miRNAs) regulate the expression of about 60% of human

protein-encoding genes[138]. Consistently with their roles as pleiotropic modulators of gene expression, miRNAs may act as either oncogenes (onco-miRNAs) or tumor suppressors when their expression is dysregulated in cancers compared to normal tissues[139,140]. miRNAs can be released into the extracellular milieu via extracellular vesicles (EVs) such as exosomes[141]. Alternatively, miRNAs bound to RNA-binding proteins like Argonaute2 (AGO2)[142,143], high density lipoproteins (HDL)[144], and RNA-binding protein nucleophosmin1 (NPM1)[145], can be exported into the stroma. Extracellular miRNAs operate as hormone-like molecules to influence the behavior of different cell types in a paracrine or endocrine manner[138], by modulating the expression of their target genes in recipient cells, thus reprogramming the TME and favoring tumor progression, PMN education[146,147] and metastatic outgrowth[148]. Notably, miRNAs secreted into the extracellular space can be then transported within body fluids, including peripheral blood[149]. It was reported that 10% of the known human miRNAs can be detected in plasma[150]. In general, many factors secreted by primary tumors can reach distant sites through the circulatory system, where they may reprogram and educate different cell types, as well as support the deposition and remodeling of the ECM, generating a receptive pre-metastatic niche (PMN) capable of attracting circulating tumor cells[120,124]. For instance, LOX proteins, once secreted into the circulation from primary breast tumors, colocalize with fibronectin at sites of future lung metastasis where they serve to crosslink collagen IV in the lung basement membrane, increasing the recruitment of BMDCs[151]. Thus, factors secreted by primary tumors can dictate metastasis organotropism.

It is important to underline that, if on the one hand tumor-dependent communication reprograms the composition and organization of the TME, on the other hand various stimuli deriving from both cellular and extracellular sources of the TME can reprogram cancer cell communication in favor of malignant outgrowth[152]. A hallmark of solid tumors is the presence of hypoxic regions, characterized by insufficient oxygen supply. The Hypoxia inducible factor 1 (HIF1) is a key mediator of the cell response to low oxygen conditions: this heterodimeric transcription factor consists of an oxygen sensitive α subunit (HIF1α) and a stably expressed β subunit (HIF1β)[153]. Activated HIF1 complex promotes the expression of several hypoxia-adaptation genes, including those involved in the processes of angiogenesis, cell proliferation, metabolic regulation and migration[154]. HIF1α expression is increased in various cancer types, such as breast, prostate, and colon cancer, and high expression of HIF1α in tumors correlates with poor patient prognosis[155]. HIF1 acts as a networking hub coordinating activities of multiple signalling molecules, and supporting the establishment a pro-tumorigenic crosstalk between cancer cells and surrounding TME[156]. The most important outcome of HIF1 activation is the induction of extensive neovascularization via secretion of the angiogenetic factor VEGF-A. This stimulates endothelial cells and pericytes to form new blood vessels and thus to cope low oxygen availability inside the tumor mass[157]. Furthermore, in a rapidly growing tumor

tissue, HIF1 supports fibroblasts activation through the secretion of several growth factors such as TGF-β, bFGF, PDGF-B, promotes the recruitment of macrophages through the production of chemoattractants (e.g. SEM3A, EMAPII, ET-1 and ET-2)[158], and recruits immunosuppressive Tregs and MDSCs via secretion of several chemokines and cytokines[159,160]. Finally, emerging evidence shows that HIF1α is both regulated by and contributes to the regulation of collagen cross-linking and ECM stiffening[11,158]. In this regard, breast cancer cells exposed to low oxygen levels have been reported to secrete LOX2 and LOX4 proteins, leading to collagen crosslinking and, consequently, BDMCs recruitment in both primary tumor site and lung metastases[151]. This implies that hypoxic signaling may exert its oncogenic effects also in secondary tumor sites and promote PMN education. Oncogenic signals influence the expression of several immune-related molecules, including immunoregulatory receptors, ligands, growth factors and other humoral factors, which influence various stromal cells and tumor cells[161]. Of note, mutations in many tumor suppressor and oncogenic pathways are known to promote escape of immune surveillance and suppression of antitumor immune responses, while stoking a tumor-promoting pro-inflammatory TME[5,6]. For instance, the release of Wnt ligands disrupts the cytotoxic function of $CD8^+$ T-cells and induces T-cell exhaustion[162,163]. Several reports have implicated the Ras/MAPK pathway in TME alterations, primarily due to production of cytokines and chemokines, such as IL-8, IL-6, TGF-β, GM-CSF[164–167]. Another relevant pathway is JAK/STAT, whose downstream TF STAT3 upregulates the expression of PD-L1 receptor on cancer cell surface and hence contributes to the evasion of immune surveillance[168]. YAP is a pervasively activated transcriptional regulator in human malignancies, involved in growth and progression of most solid tumors. YAP signalling has been shown to contribute to generate an immunosuppressive TME in several tumors. For instance, in prostate cancer YAP regulates the secretion of CXCL5 to recruit MDSCs[169]; while in pancreatic ductal adenocarcinoma YAP drives the expression and secretion of multiple cytokines and chemokines, promoting MDSCs accumulation and macrophage reprogramming[170].

1.4.2 Roles of missense mutp53 oncoproteins in TME reprogramming and immune escape

The p53 tumor suppressor provides a major barrier to neoplastic transformation and tumor progression by its unique ability to act as an extremely sensitive collector of stress inputs and to coordinate a complex framework of diverse effector pathways and processes that protect cellular homeostasis and genome stability[171]. In addition to coordinate responses to acute DNA damage (activation of cell cycle arrest and apoptosis), p53 regulates genomic integrity, metabolism, redox biology, stemness, senescence, immune response, and paracrine signaling in tumor suppression[172,173]. For instance, p53-mediated senescence leads to the production of a series of cytokines and growth

factors, which attract anti-tumor immune populations, contributing to the tumor suppressor function of p53[173].

Genome-wide analyses have shown that *TP53* is the most frequently mutated gene in human cancers.[174] While some cancer-associated somatic mutations in *TP53* result in loss of protein expression, more than 75% of *TP53* mutations are missense point mutations, resulting in the substitution of a single amino acid residue in the protein's central DNA-binding domain. In particular, six "hotspots" residues in this domain are more frequently affected by substitutions: R175H, G245S, R248Q, R249S, R273H and R289W[175]. Missense mutant forms of p53 (hereafter defined as mut-p53) not only lose their onco-suppressive functions, being uncapable of activating canonical p53 target genes, but also exert dominant negative effects over the wild-type form. Moreover, many mut-p53 proteins acquire new oncogenic activities independently of wild-type p53, termed gain-of-function (GOF)[176]: this occurs via interactions with a plethora of intracellular effectors that promote cancer progression by reshaping the tumor cells' transcriptomic and proteomic profiles[177]. Mut-p53 protein stabilization is a prerequisite for its oncogenic activities. It depends primarily on mut-p53 interaction with heat-shock family chaperones, particularly Hsp90[176,178,179], and has been shown to be exquisitely sensitive to mechanical stimuli, such as those deriving from a stiff ECM. Indeed, it has been shown that fibrotic regions in vivo often associate with mut-p53 accumulation[180]. Other extracellular environmental conditions, such oxygen or nutrient availability, can modulate mut-p53 oncogenic activities[176]. It has been shown that, under hypoxic conditions, HIF1α can bind mut-p53 and promote its localization on chromatin, leading to the promotion of a malignant transcriptional program[181]. In turn, mut-p53 appears to stimulate HIF1α stabilization through downregulation of the SHARP1 gene, a factor that promotes ubiquitin-mediated degradation of HIF1α, thus establishing a positive feedback loop[182].

Mut-p53 exerts its oncogenic activities by coopting a plethora of effector pathways. While most of these operate primarily to promote cancer cell-intrinsic phenotypes, many extend into the extracellular space[5]. In this regard, emerging evidence indicates that missense p53 mutants support the release of a pro-malignant secretome, including growth and angiogenic factors, onco-miRNAs and inflammatory cytokines and chemokines, which affect the surrounding TME, supporting aggressive tumor phenotypes, cancer-promoting inflammation and immune suppression (Fig.5)[5]. For instance, mut-p53 improves angiogenesis by inducing VEGF secretion[183] and also by upregulating ID4 proteins and, consequently, increasing post-transcriptional stabilization of the angiogenic factors IL8 and GRO1[184]. Moreover, mut-p53 is known to promote both invasion and EMT of cancer cells, driving the expression of the secreted serine protease inhibitor A1AT (alpha-1 antitrypsin)[185]. Remarkably, p53 mutants modulate tumor cell communication also through exosome secretion. Indeed, in colon cancer cells mut-p53 has been demonstrated to reprogram macrophages towards the

pro-tumorigenic M2 phenotype, by targeting them with miR-1246-enriched exosomes[186]. Considerably, it has been reported that mut-p53 itself can be packaged into small EVs and transferred from cancer cells to stromal fibroblasts where it exerts its oncogenic functions. In particular, in recipient fibroblasts mut-p53 activates Nrf2-mediated pathways and induce their conversion to a cancer- associated phenotype[187]. Numerous findings have revealed a strong relationship between mut-p53 and cancer inflammation, which largely depends on mut-p53 interaction with the transcriptional regulator NF-κB. Under TNFα stimulation, mut-p53 sustains chronic NF-κB activation and consequent expression of pro-inflammatory NF-κB target genes. Of note, contrary to its acute activation, the constitutive induction of NF-κB exerts pro-tumorigenic functions through the release of various chemokines in the extracellular environment. Among these, CXCL5, CXCL8 and CXCL1 are known to improve the migration and invasion of tumor cells[188]. mut-p53 can remodel the profile of secreted cytokines and chemokines also via NF-κB independent mechanisms, such as by suppressing the expression of sIL-1Ra, a specific antagonist of the inflammatory cytokine IL-1[189], and directly promoting the expression of inflammatory CXCL1[190].

Recent reports have highlighted the ability of mut-p53 to sustain a cold immune microenvironment by attenuating antitumor innate immunity[173]. In this context, Ghosh and colleagues demonstrated that several p53 mutants suppress downstream signaling of the cGAS-STING pathway, thus attenuating the type-I interferon response. In detail, by interacting with and sequestering the TBK1 protein, mut-p53 prevents the formation of the STING-TBK1-IRF3 trimeric complex, necessary for the activation and nuclear translocation of IRF3[191]. Additionally, mut-p53 has been reported to prevent efficient activation of T-lymphocytes, by both suppressing the expression of TAP1 and ERAP-1[192], important players of the antigen-presenting MHC-I complex, and promoting the expression of immune checkpoint ligands such as PD-L1[193]. Finally, loss or mutation of p53 in tumors has also been shown to modulate immune recognition, increasing the recruitment of suppressive myeloid cells and Tregs[173].

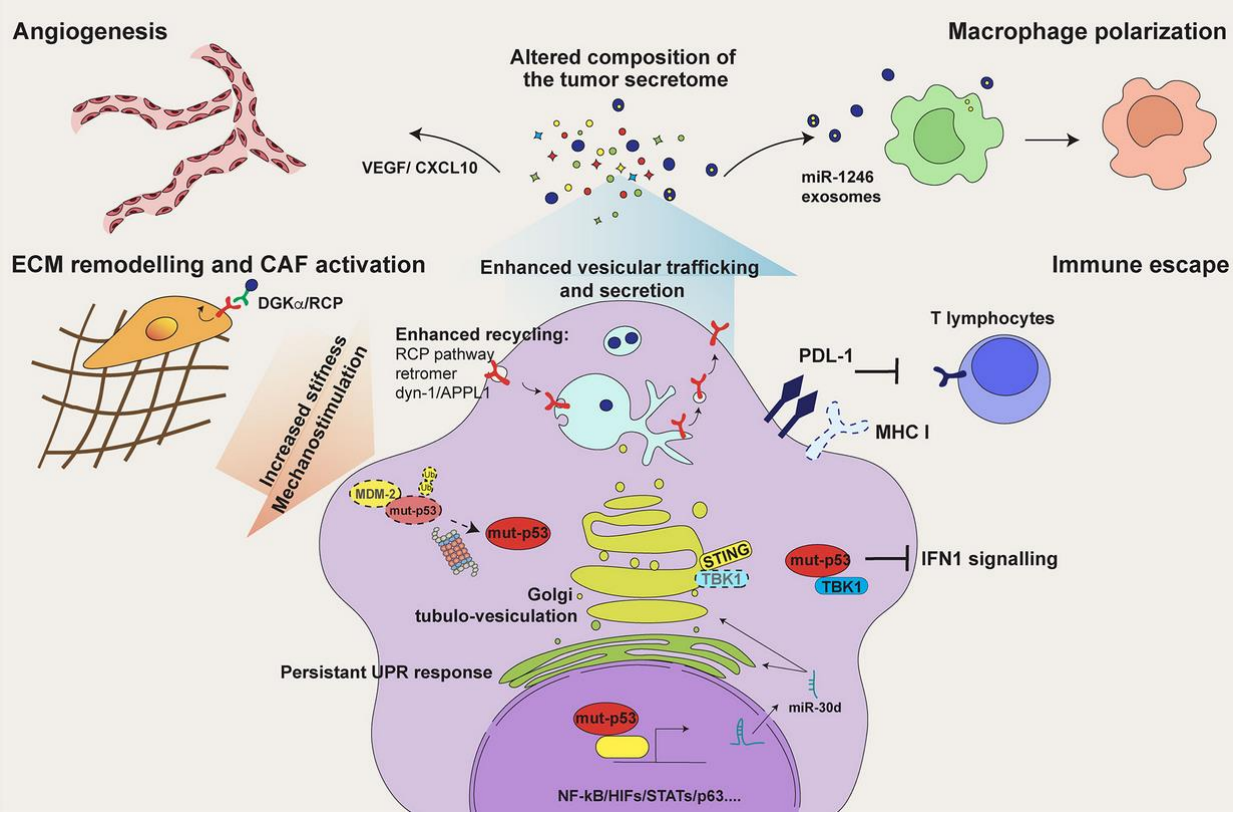

Figure 5. **Mut-p53 alters the communication of cancer cells with the surrounding TME.** Schematic representation of how missense p53 mutants shape the tumor cell secretome to reprogram the composition and function of the cellular stromal/immune infiltrate and support malignant growth (from[5]).

1.4.3 The mut-p53/miRNA-30d axis

Recently, a novel oncogenic axis affecting tumor-stroma crosstalk, which involves the microRNA miR-30d, was identified in our laboratory[194].

miR-30d is an intergenic miRNA located on the chromosome 8q24. It is a member of the miR-30 family, which in humans comprises six members, namely miR-30a, -30b, -30c1, -30c2, -30d and -30e. These miRNAs share a common seed sequence, but harbor different regulatory flanking elements, allowing them to target different transcripts[195]. Regarding its function in cancer, miR-30d has been reported to display different roles depending on the specific tumor type[196]. This is in agreement with the pleiotropic functions of miRNAs, which depend on the relative availability of specific target mRNAs in different cell contexts. For instance, in a pancreatic cancer xenograft model, miR-30d was reported to act as a tumor suppressor, blocking cell proliferation, migration and invasion of cancer cells through directly targeting SOX4, and, consequently, inhibiting the oncogenic PI3K-AKT signaling pathway[197]. Furthermore, high levels of miR-30d have been shown to inhibit ovarian cancer cell proliferation by promoting apoptosis through targeting Smad2, a protein involved in TGF-β signalling[198]. On the other hand, *MIR30D* gene has been found to be frequently amplified and/or

overexpressed in several human solid tumors[199], and its expression has been associated with aggressive neoplastic features. In cervical[200] and esophageal[201] squamous cell carcinoma, as well as in colorectal[202] and breast cancer[203], miR-30d has been shown to promote invasion and migration of tumor cells, while in prostate cancer it has been shown to favor angiogenesis and tumor growth[134]. Moreover, miR-30d has been shown to promote invasion and metastatic behavior of human melanoma cells through the generation of an immunosuppressive TME. Mechanistically, miR-30d was shown to directly target the Golgi-resident GalNAc transferase GALNT7, resulting in increased synthesis of the immunosuppressive cytokine IL-10, with consequent reduction of immune cell recruitment and activation[204]. Intriguingly, miR-30d has been reported to be released in the extracellular environment, both in exosomes and associated with proteins, and to be transferred between different cell populations[205,206]. Thus, miR-30d could exert oncogenic functions also in receiving cells of the TME. Nevertheless, evidence regarding potential non cell-autonomous roles of miR-30d in controlling the communication within the tumor microenvironment are still lacking.

It has been shown that miR-30d expression is controlled, under hypoxic conditions, by the hypoxia-inducible factor HIF1α[207]. Our research group recently demonstrated that in breast cancer (BC) cells, missense mut-p53 proteins form an active transcriptional complex with HIF1α on *MIR30D* promoter, thus supporting miR-30d expression also in normoxic conditions[194]. Importantly, we proved that the overexpression of miR-30d, induced by mut-p53 and HIF1α oncoproteins, causes a structural and functional reprogramming of the ER and Golgi apparatus. In particular, we showed that miR-30d overexpression induces a GA modification known as tubulo-vesiculation, which is characterized by tubular connections between the Golgi cisterns and an increased number of COPI vesicles. GA tubule-vesiculation was clearly observed by ultrastructural analysis using correlative light electron microscopy (CLEM) upon overexpression of mut-p53^{R280K} or miR-30d in normal-like breast epithelial cells (Fig. 6a). Of note, miR-30d inhibition using a decoy construct was sufficient to restore the normal structure of GA stacks in mut-p53 overexpressing cells, confirming an epistatic relationship between mut-p53 and miR-30d.

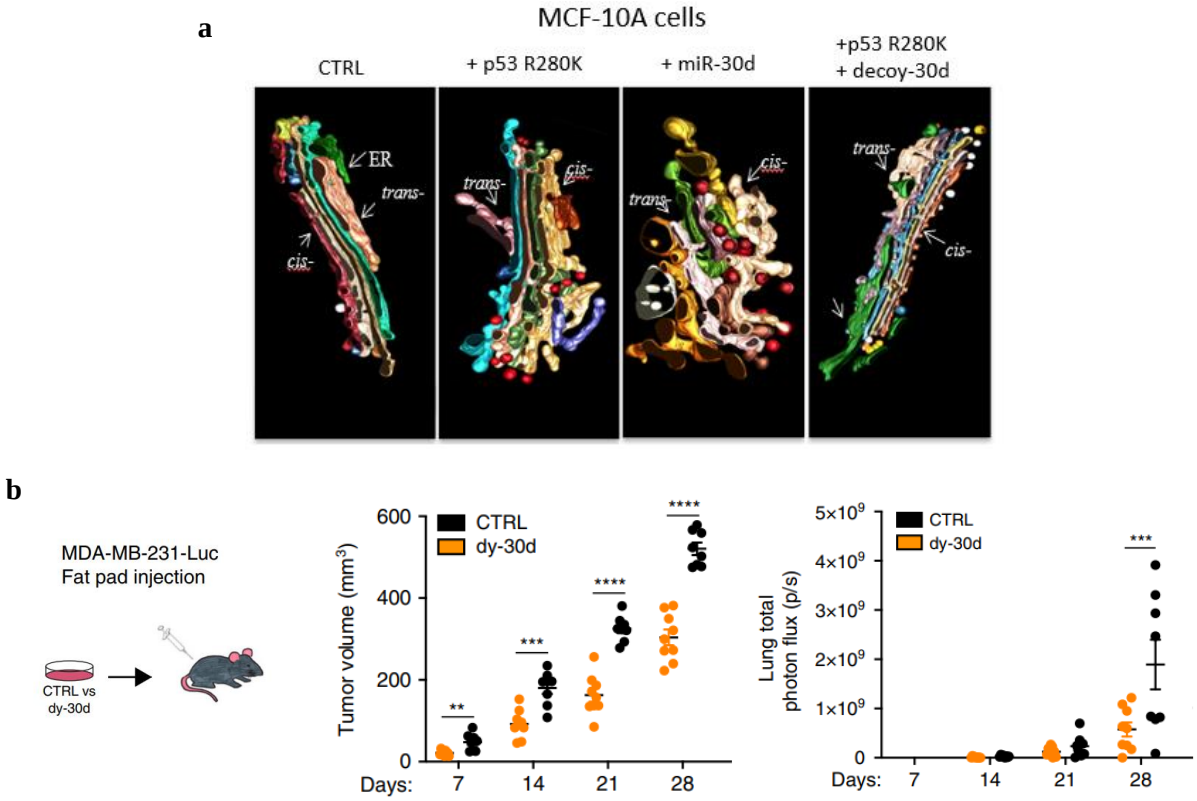

Figure 6. The mut-p53/miR-30d axis modifies Golgi structure and promotes tumor progression. a) CLEM analyses of the Golgi apparatus performed in MCF-10A cells upon overexpression of miR-30d or ectopic introduction of mut-p53^{R280K}, either alone or in combination with decoy-30d as indicated. Arrowheads indicate vesicular-tubular clusters in cells overexpressing miR-30d or mut-p53^{R280K}; **b)** Primary tumor volume and *in vivo* luciferase quantification of lung metastases measured at the indicated time points after orthotopic xenograft of MDA-MB-231–Luc control (CTRL, n = 8) or miR-30d decoy (dy-30d, n = 9) cells in SCID mice (from[194]).

GA tubulo-vesiculation has been previously described as an indicator of increased secretory rate in cells[208,209]. In agreement, our findings revealed that the mut-p53/miR-30d axis causes the formation of tubular continuities across Golgi cisternae, and such alterations promote rapid diffusion of cargoes within the Golgi, resulting in increased rate of secretory trafficking. This culminates in the release of a pro-malignant secretome, which contributes to generate a permissive tumor microenvironment. We found that miR-30d inhibition using a decoy construct significantly delayed both tumor growth and metastasis formation over a 4 weeks period in breast xenografts of MDA-MB-231 breast cancer (BC) cells in immunocompromised mice (Fig. 6b)[194]. Of note, the tumor-promoting effect of the mut-p53/HIF1α/miR-30d axis relied on production of a tumorigenic secretome, exerting paracrine effects on the TME both at primary and distant sites. Consistently, miR-30d inhibition in BC cells strongly decreased ECM deposition/remodeling, stromal neo-vascularization, and CAFs activation in both primary and metastatic tissues. Importantly, experiments of metastatic niche preconditioning in mouse xenografts models highlighted that miR-30d pro-tumorigenic functions are largely dependent on secreted factors that act by reshaping the TME[194].

2. Preliminary results

Recently, work from our research group highlighted that miR-30d supports growth and metastatic progression of breast cancer by directing tumor cell-extrinsic activities, which reshape the TME at local and distant sites[194]. Interestingly, analysis of TCGA data indicated that miR-30d is found overexpressed in some tumor types that are generally considered cold, i.e. breast, pancreas and prostate[210,211]. Consistently, overexpression of miR-30d in melanoma cells has been previously associated with immune-suppressive outcomes[204]. Therefore, we became interested in identifying miR-30d dependent activities in cancer cells that might influence the antitumor immune response. To this aim, we performed functional analysis of transcriptomic data, previously obtained upon stably inhibiting miR-30d in the human metastatic BC cell line MDA-MB-231[194]. Specifically, over-representation analysis of differentially expressed genes was performed using Gene Set Enrichment Analysis (GSEA) on gene sets of the Gene Ontology Biological Processes (GOBP) from the Broad Institute Molecular Signatures Database (http://software.broadinstitute.org/gsea/msigdb). From this analysis, a list of 532 positively enriched pathways has been identified: filtering for the keywords "Immune", "Interferon" and "DNA damage", we found 21 GO terms significantly up-regulated (Fig. 7a). These categories included "cellular response to DNA damage", "type I interferon production" and "antiviral innate immune response", among others. Remarkably, transformation-related DNA damage is known to trigger the activation of the DNA-sensing cGAS/STING pathway in cancer cells, with consequent expression of type-I IFNs, thus engaging anti-tumor innate immune surveillance[86]. In fact, GSEA analysis indicated a strong enrichment of "*type-I interferon production"* and "*INF-β production"* gene signatures upon miR-30d inhibition in metastatic BC cells (Fig.7b). On the other hand, analysis of publicly available transcriptomic data obtained from[204] highlighted enrichment of the functional category "negative regulation of *type-I interferon response"* in genes induced by miR-30d overexpression in melanoma cells (Fig. 7c). This suggests that overexpression of miR-30d in tumors may correlate with reduced expression of IFN-I signature genes. To test this hypothesis, we analyzed human breast cancer data from TCGA database, and found a negative correlation between elevated expression of miR-30d and "type-I IFN production" signature (Fig. 7d).

Taken together, the above analyses suggest a putative inhibitory effect of miR-30d on DNA damage signaling and type-I IFN response, which might be expected to attenuate antitumor innate immunity during cancer progression.

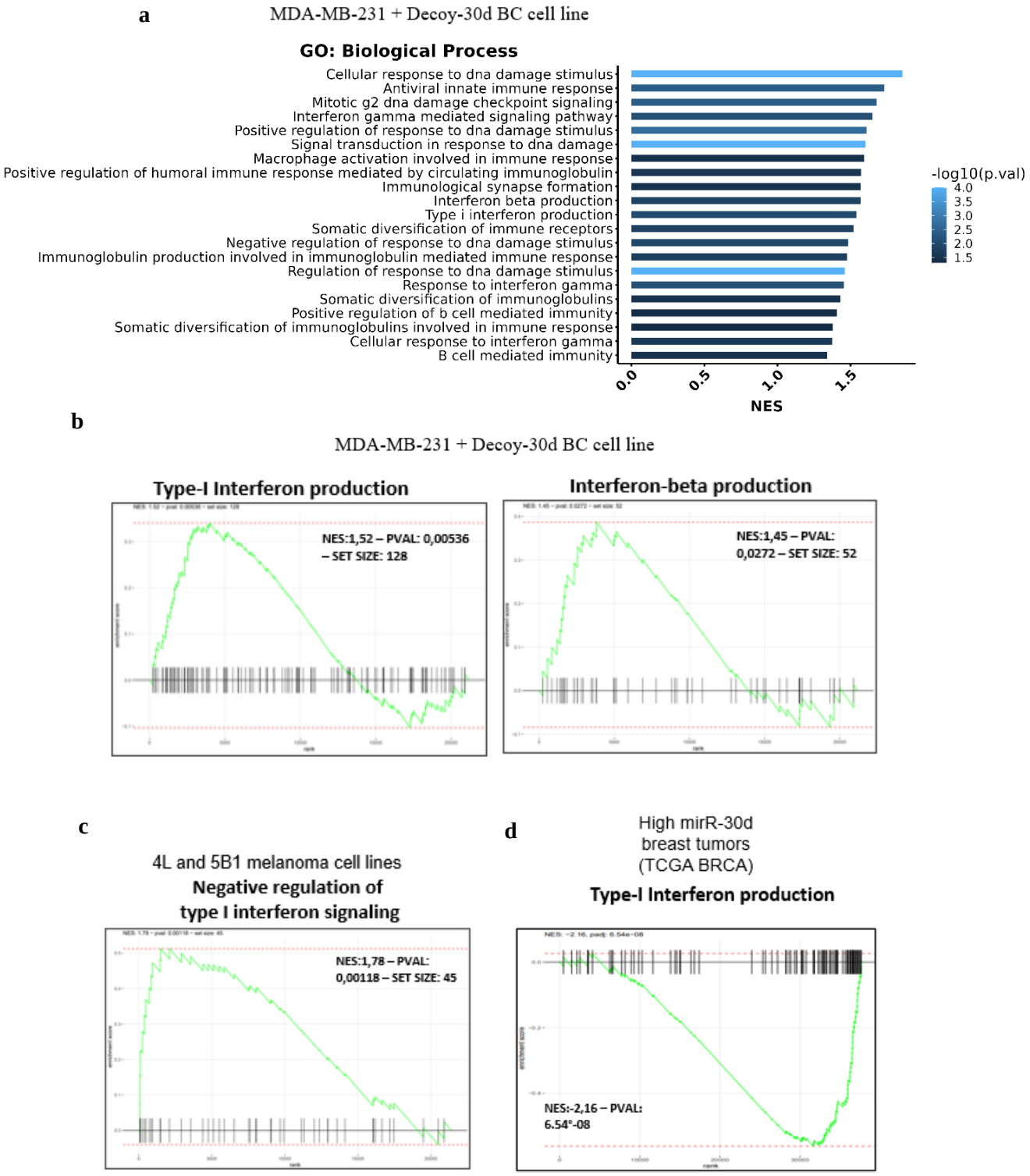

***Figure 7. miR-30d levels are inversely correlated with activity of innate immune pathways in human melanoma and BC cells and in BC tumor samples* . a)** Gene set enrichment analysis (GSEA) of differentially expressed genes performed on the sub-category Biological Processes of the GO database, filtered by functional categories of immunity, DNA damage, and interferons. **b)** Enrichment plots of gene signatures TYPE-I_INTERFERON_PRODUCTION and INTERFERON-BETA_PRODUCTION in the transcriptome of MDA-MB-231 cells stably transduced with Decoy-30d construct compared to control. **c**) Enrichment plot of gene signature NEGATIVE_REGULATION_OF_TYPE-I_INTERFERON_SIGNALING in the transcriptome of 4L and 5B1 melanoma cell lines transduced with miR30d-mimic construct compared to

control. **d)** GSEA of Type-I_Interferon_Production gene signature derived from high miR-30d TCGA BRCA data, using DAVID database.
The plots in b-d) were obtained using *fgsea* R package (version 1.22). All terms were significant ($p < 0.05$) following Benjamini–Hochberg correction ($n = 3$).
Analysis performed by Luca Triboli, graduate student in the lab.

3. Aim of the thesis

Preliminary data and previous work suggest that miR-30d might inhibit the expression of type-I IFN response genes in cancer cells, thus dampening antitumor innate immune response.

Therefore, my PhD project aims to: i) explore the impact of miR-30d and its inhibition on the regulation of type-I IFN signalling in BC cells and tumor organoids; ii) analyze the molecular and cellular mechanisms leading to the activation of the cGAS/STING/IFN-I pathway in BC cells following miR-30d inhibition; iii) test the synergy of combined miR-30d inhibition and chemotherapeutic agents on the activation of STING/IFN-I signalling.

4. Results

4.1 Inhibition of miR-30d increases the expression of IFN-I response genes in cancer cells

To determine whether miR-30d may affect activation of innate immune signaling, and particularly the expression of type-I IFNs and interferon-stimulated genes (ISGs) in cancer cells, I initially inhibited miR-30d activity in human breast cancer cells. To this aim, I employed the human MCF10.DCIS.com cell line[212,213], derived from ductal adenocarcinoma in situ, which represents a model of early-stage tumorigenesis and was shown to bear a functional cGAS/STING DNA-sensing machinery[212]. MCF10.DCIS.com cells were silenced for miR-30d expression by transient transfection with either a Decoy-30d construct or a specific locked nucleic acid (LNA) inhibitor (hereafter referred to as LNA-30d). The Decoy-30d construct, previously described by Capaci et al.[194], has been realized by cloning two copies of a miR-30d decoy sequence, which acts as a molecular sponge binding the mature miRNA, in the lentiviral vector pTWEEN 3′UTR EGFP[214]. The anti-miR-30d sequences are embedded within the EGFP 3'UTR sequence, so that binding of endogenous miR-30d to decoy sequences both sequesters the miRNA and prevents E*GFP* expression. As a control, the empty vector pTWEEN 3′UTR EGFP was used. The LNA-30d inhibitor is a short antisense oligonucleotide that sequesters miR-30d with perfect sequence complementarity in highly stable heteroduplexes, thus preventing its binding to target mRNAs. As a control, I used the scramble LNA Inhibitor (LNA-ctrl), which is similar in sequence length to LNA-30d but has no homology to any known mRNA. Efficient miR-30d inhibition upon transient transfection with either Decoy-30d construct or LNA-30d inhibitor in MCF10.DCIS.com cell, as compared to cells transfected with the respective control constructs, was verified by monitoring increased expression of known miR-30d target mRNAs (*KLHL20, CAPZA1, SNX16*)[215] by qRT-PCR (Fig. 8c). Furthermore, inspection of Golgi apparatus morphology, by immunofluorescence (IF) analysis with the Golgi marker GM130, indicated a shift from a tubulo-vesiculated to a more compacted structure and polarized localization (Fig. 8d) upon transfection with miR-30d inhibitors as compared to controls, similar to what previously observed[194].

I then analyzed the expression levels of a panel of type-I IFNs and interferon-stimulated genes (ISGs) by qRT-PCR in MCF10.DCIS.com cells depleted for miR-30d. As shown in Fig. 9a, inhibition of miR-30d by Decoy-30d resulted in a strong increase in the expression of *IFNα*, *IFNβ1* and of several *ISGs*, as compared to control-treated cells. Similar results were obtained when cells were treated with LNA-30d inhibitor (Fig. 8b).

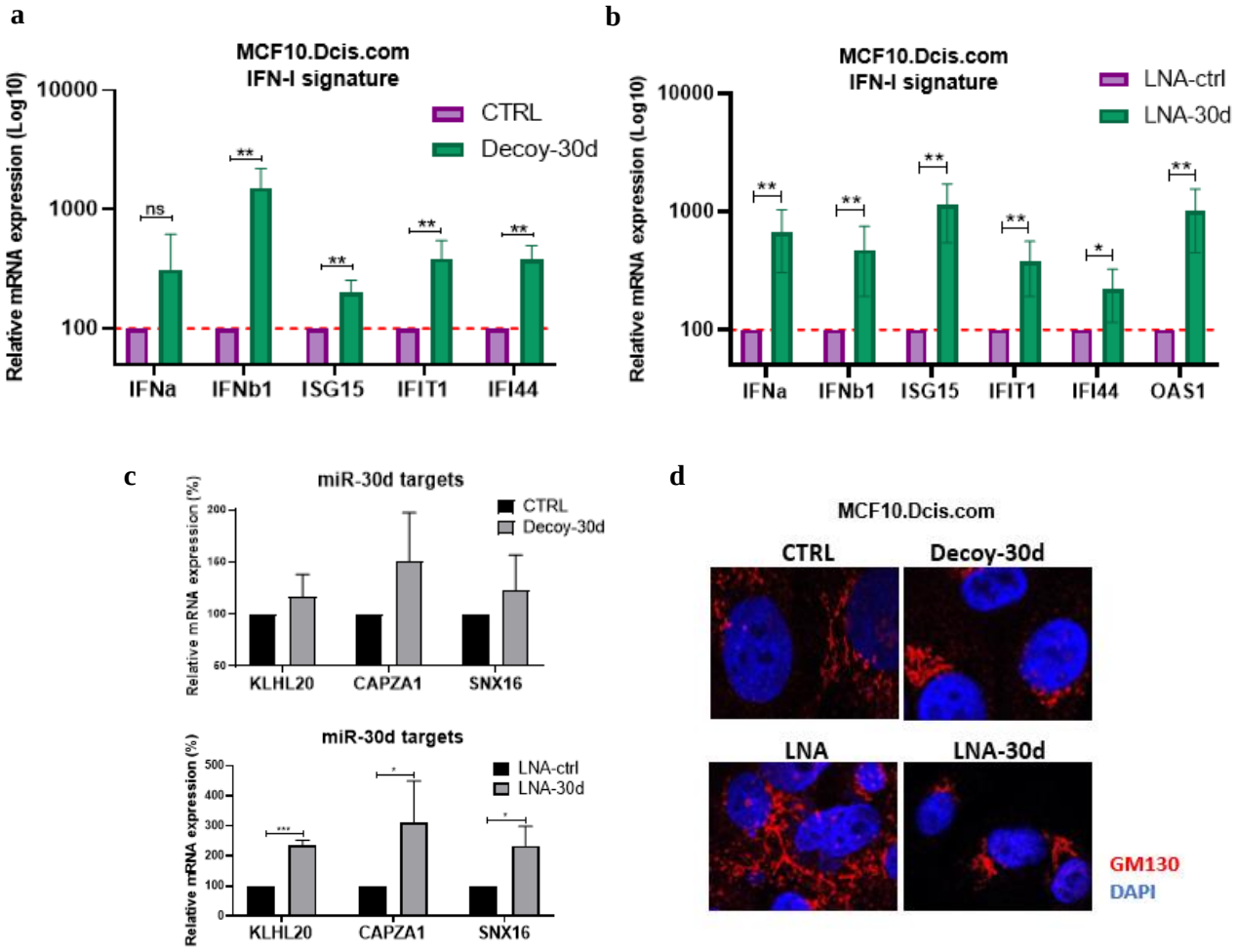

Figure 8. Inhibition of miR-30d induces the expression of IFN-I signature genes in human BC cells. **a)** MCF10.DCIS.com cells were transiently transfected with pTWEEN 3′UTR EGFP-Decoy-30d construct (Decoy-30d) or with pTWEEN 3′UTR EGFP empty construct (ctrl). After 48 h, the expression levels of the indicated IFN-I and interferon-stimulated genes were evaluated by RT-qPCR and normalized to *H3* mRNA expression as a reference. mRNA levels relative to control condition (red dotted line) are shown; **b)** MCF10.DCIS.com cells were transiently transfected with LNA-30d or with scramble LNA (LNA-ctrl). After 48 h, expression of *IFNs* targets was evaluated by RT-qPCR as in a). **c)** Expression of miR-30d target genes (*KLHL20, CAPZA1, SNX16)* was analyzed in MCF10.DCIS.com cells transiently transfected with Decoy-30d construct or control (upper panel) or with LNA-30d (lower panel). *H3* expression levels were used as a reference. **d)** Representative images showing IF staining of the Golgi marker GM130 in MCF10.DICIS.com cells treated as described above.
Graph bars represent mean ± s.d. of n≥3 biological replicates. P value: P < 0.05 [*], P < 0.01 [**], P < 0.001 [***] by two-tailed Student's t-test.

Based on these findings, I then sought to verify whether the increased transcription of *IFNα* and *IFNβ1* genes, observed upon miR-30d downregulation, correlated with the secretion of type-I IFNs in the culture medium (CM, conditioned medium). For this purpose, I performed HEK-Blue IFN-α/β assay, which allows the detection of secreted bioactive human extracellular type-I IFNs[216]. Specifically, this assay employs HEK293 cells engineered to express a SEAP (secreted embryonic alkaline phosphatase) reporter gene, under the control of the IFN-α/β-inducible ISG54 promoter

(hereafter called HEK-Blue IFN-α/β cells). Therefore, stimulation of HEK-Blue IFN-α/β cells with human type-I IFNs induces the production and secretion of SEAP protein reporter, whose activity can be measured with a colorimetric assay.

I thus incubated HEK-Blue IFN-α/β cells over-night with CMs collected from MCF10DCIS.com cells transiently transfected with either control or Decoy-30d construct. Consistently with gene expression results, I found a significant increase of SEAP reporter when HEK-Blue IFN-α/β cells were grown in the CM of MCF10DCIS.com cells depleted for miR-30d expression, implying that this medium contained a higher amount of type-I IFNs compared to control CM (Fig. 9).

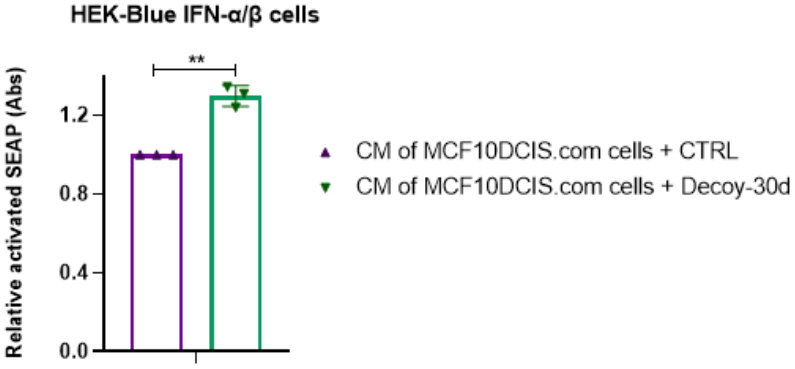

Figure 9. Downregulation of miR-30d increases type-I IFN secretion in BC cells. Measurement of IFN-α/β secreted in the conditioned medium of MCF10.DCIS.com cells transfected for 48h with either control or Decoy-30d construct, using HEK-Blue IFN-α/β assay. See main text for details. Graph bars represent mean ± s.d. of n≥3 biological replicates. P value: P < 0.05 [*], P < 0.01 [**], P < 0.001 [***] by two-tailed Student's t-test.

In contrast, in the non-neoplastic human breast epithelial cell line MCF10A, downregulation of miR-30d did not lead to any significant change in the expression of IFN-dependent signature (Fig. 10a,b).

a

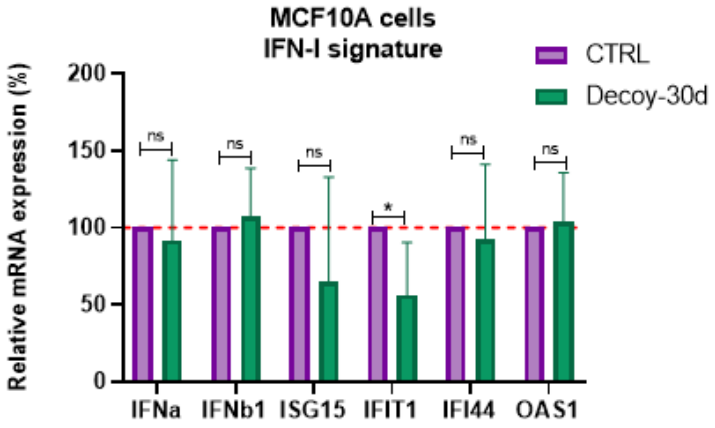

b

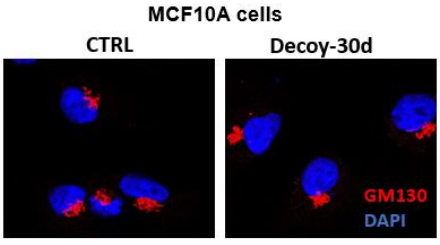

Figure 10. Inhibition of miR-30d does not induce the expression of IFN-I signature genes in non-neoplastic MCF10A human breast cells. a) MCF10A cells were transiently transfected with pTWEEN 3′UTR EGFP-Decoy-30d construct (Decoy-30d) or with pTWEEN 3′UTR EGFP empty construct (ctrl). After 48 h, the expression levels of the indicated IFN-I and ISGs were evaluated by RT-qPCR and normalized to *H3* mRNA expression as a reference. mRNA levels relative to control condition (red dotted line) are shown. **b)** Representative images showing IF staining of the Golgi marker GM130 in MCF10A cells treated as described above.
Graph bars represent mean ± s.d. of n≥3 biological replicates. P value: P < 0.05 [*], P < 0.01 [**], P < 0.001 [***] by two-tailed Student's t-test.

I then repeated the above analyses using mouse metastatic breast cancer (mBC) 4T1 cell line, as well as the human metastatic breast cancer cell lines MCF7 and MDA-MB-231 (Fig. 11a-c). In all cell lines analyzed, inhibition of miR-30d resulted in robustly increased expression of type-I IFNs and ISGs.

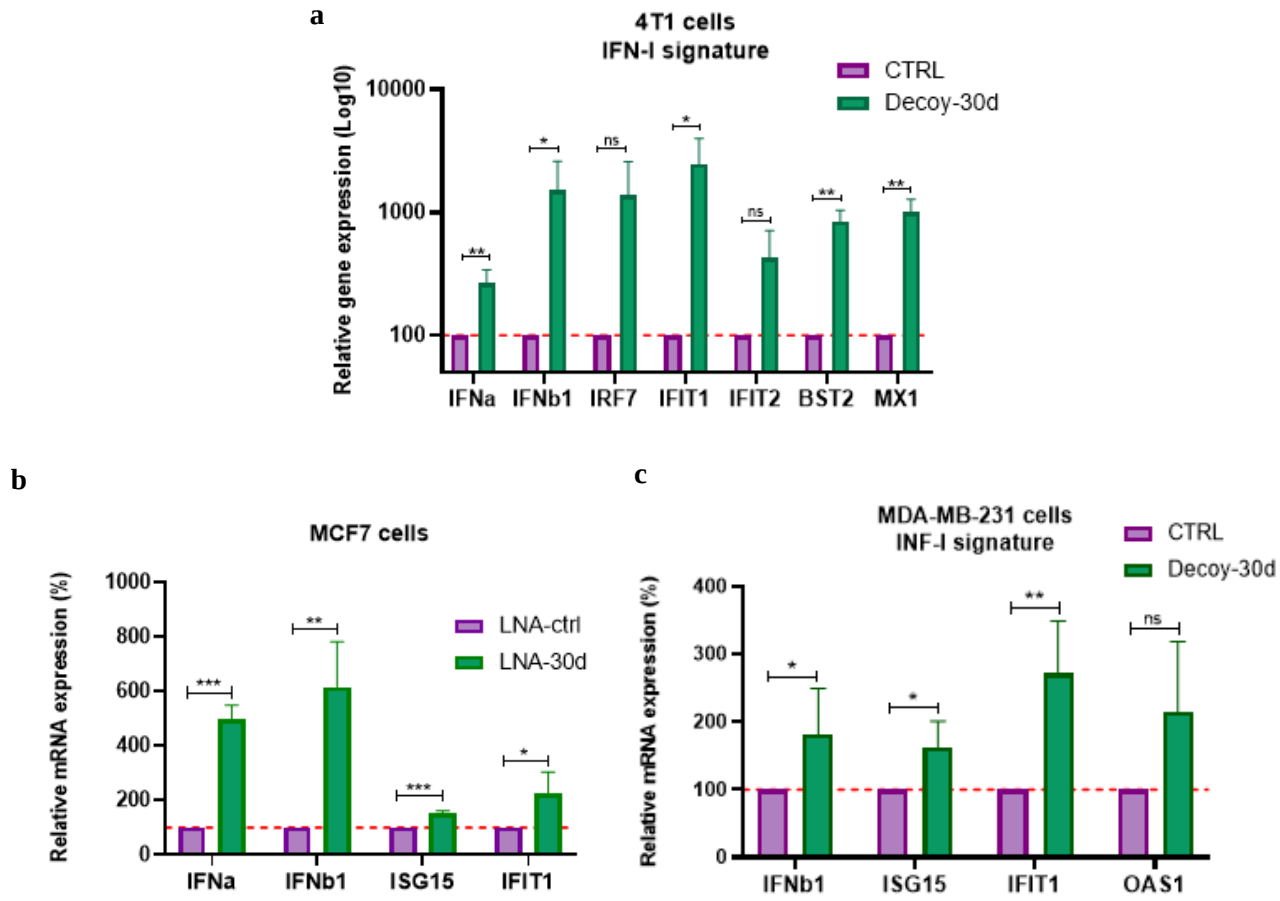

Figure 11. Inhibition of miR-30d induces the expression of IFN-I signature genes in human and mouse mBC cells. **a,c)** 4T1 and MDA-MB-231 cells were transiently transfected with pTWEEN 3′UTR EGFP-Decoy-30d construct (Decoy-30d) or with pTWEEN 3′UTR EGFP empty construct (ctrl). After 48 h, the expression of the indicated IFN-I and ISGs was evaluated by RT-qPCR and normalized to *H3* mRNA expression as a reference in human cells, and to *Gapdh* mRNA expression in mouse cells. mRNA levels relative to control condition (red dotted line) are shown; **b)** MCF7 cells were transiently transfected with LNA-30d or with scramble LNA (LNA-ctrl). After 48 h, expression of *IFNs* targets was evaluated by RT-qPCR as in a).

Graph bars represent mean ± s.d. of n≥3 biological replicates. P value: P < 0.05 [*], P < 0.01 [**], P < 0.001 [***] by two-tailed Student's t-test.

Next, I performed the same analysis in cell lines derived from different tumor types, including HCT-116 (human colorectal carcinoma), WM115 (human melanoma) and H1299 (human non-small lung carcinoma), observing in all cases an induction of type-I *IFNs* and *ISGs* expression after depletion of miR-30d (Fig. 12a-c).

Taken together, these findings indicate that inhibition of miR-30d in tumor-derived cell lines invariably results in induction of *IFNα, IFNβ1* and *ISGs* genes. This result is consistent with analyses performed on data from TCGA database, in which overexpression of miR-30d in human breast cancer was found to correlate with reduced expression of the IFN type-I production signature (preliminary data, Fig. 7d).

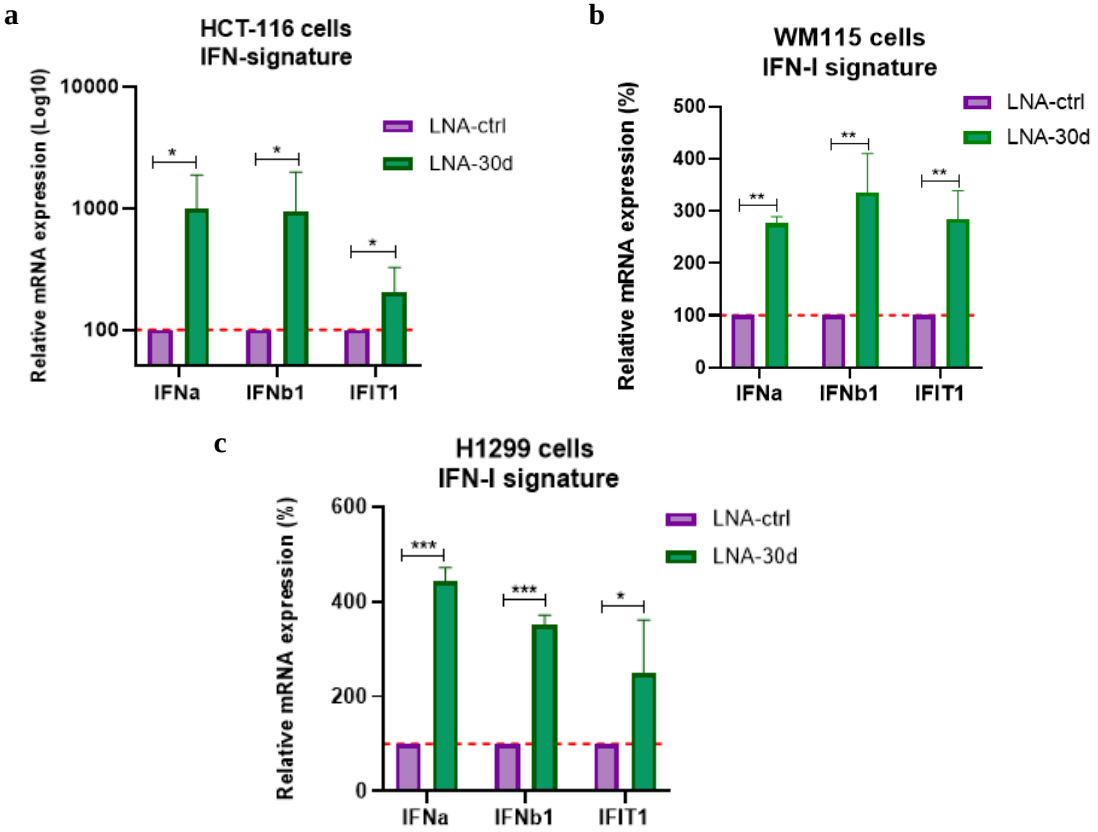

Figure 12. Inhibition of miR-30d induces the expression of IFN-I signature genes in cancer cells lines of colon, lung, and melanoma origin. **a-c**) HCT-116, WM115 and H1299 cells were transiently transfected with LNA-30d or with scramble LNA (LNA-ctrl). After 48h, the expression levels of the indicated IFN-I and ISGs were evaluated by RT-qPCR and normalized to *H3* mRNA expression as a reference.
Graph bars represent mean ± s.d. of n≥3 biological replicates. P value: P < 0.05 [*], P < 0.01 [**], P < 0.001 [***] by two-tailed Student's t-test.

4.2 miR-30d downregulation increases IFN-I signature expression via STING pathway

Type-I IFN genes *IFNα* and *IFNβ1*, as well as ISGs (including *ISG15, IRF7, IFIT1, IFIT2 OAS1*) whose expression is increased as a consequence of miR-30d inhibition, are targets of the transcription factor IRF3 and become induced upon activation of the cytosolic DNA sensing machinery cGAS/STING/TBK/IRF3[217,218]. Furthermore, expression of type-I IFNs and ISGs can be induced in a non-STING-dependent manner by several pathways, including Toll-like receptors (TLRs) (e.g., TLR3, TLR7/8, TLR9, MDA5, RIG-I, and IFI-16) and NFκB signalling[219].

I thus sought to understand whether the observed induction of this transcriptional signature upon miR-30d depletion is mediated by the cGAS/STING/IFN-I pathway. To this aim, I silenced *STING* expression by siRNA in MCF10.DCIS.com cells before transfection with Decoy-30d construct. As shown in Fig. 13a, STING silencing (Fig. 13b,c) prevented almost completely the induction of IFN-I signature genes upon inhibition of miR-30d. Consistently with this evidence, administration of Decoy-30d failed to induce the expression of a panel of IFN-I and ISGs in 4T1 *STING knock-out* cells (kindly provided by G. Scita) (Fig. 13d,e).

These results suggest that STING activity is involved in mediating the induction of IFN-I signature genes upon inhibition of miR-30d in BC cells.

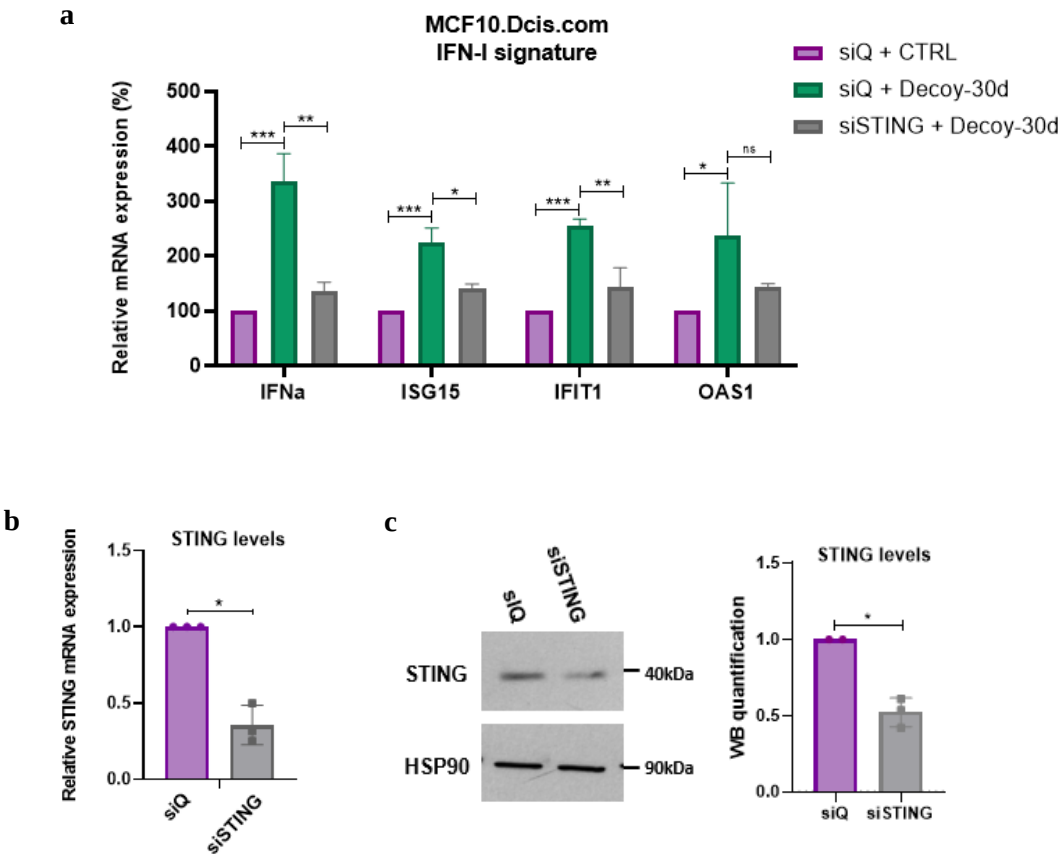

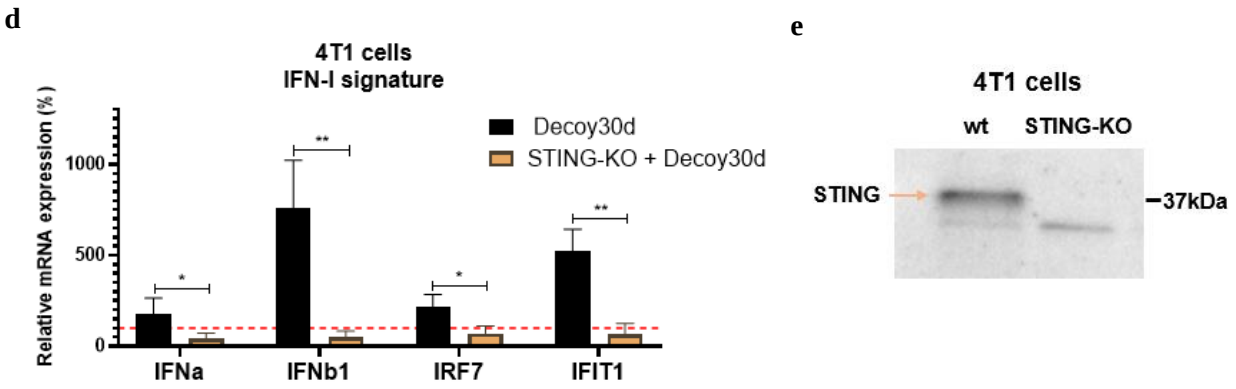

Figure 13. miR-30d downregulation increases IFN-I signature expression via STING pathway. **a)** MCF10.DCIS.com cells were transiently transfected with Decoy-30d construct or control, and with either *STING* siRNA (siSTING) or control siRNA (siQ) as indicated. After 48 h, the expression of the indicated INF-I and interferon-stimulated genes was evaluated by RT-qPCR and normalized to *H3* mRNA expression as a reference. mRNA levels relative to control condition (set at 100) are shown. **b**) Bar graph shows qRT-PCR analysis of *STING* mRNA expression in the experiment shown in a) Levels of *STING* were normalized to *H3* expression. **c**) Representative western blot analysis and quantification of STING protein expression in the experiment shown in a). HSP90 protein levels were used as reference for quantification. **d)** 4T1 and 4T1 *STING-KO* cells were transiently transfected with Decoy-30d construct or control, and the expression of IFN-dependent signature was evaluated after 48 h by RT-qPCR and normalized to *Gapdh* expression. mRNA levels relative to control condition (red dotted line) are shown. **e**) WB analysis of STING protein expression in 4T1 and 4T1 *STING-KO* cells.
Graph bars represent mean ± s.d. of n≥3 biological replicates. P value: $P < 0.05$ [*], $P < 0.01$ [**], $P < 0.001$ [***] by two-tailed Student's t-test. Blots are representative of n=3 biological replicates.

4.3 Inhibition of miR-30d activates cGAS/STING/TBK/IRF3 signalling in BC cells

Having demonstrated that inhibition of miR-30d induces expression of type-I IFNs and ISGs in cancer cells in a STING-dependent fashion, I postulated that miR-30d might impact on activation of cGAS-STING signaling in BC cells. In fact, due to genomic and/or nuclear damage[220], cancer cells are known to have high levels of cytoplasmic DNA, which results in a constitutive (although still inducible) activation of the cGAS/STING pathway[221].

On this premise, I investigated the activation status of the main components of the cGAS-STING signaling machinery in both human (MCF10.DCIS.com) and mouse (4T1) BC cell lines upon miR-30d inhibition. As a positive control for cGAS-STING activation, I employed the ATR inhibitor VE-821 (hereafter referred to as ATRi), recently shown to activate the cGAS-STING machinery by causing nuclear envelope breakdown and consequent cytoplasmic leakage of chromatin fragments[222]. Treatment with ATRi strongly induced both STING- and TBK1- activating phosphorylation events in either cell line, as shown by WB analysis (Fig.14a,b). Interestingly, cells depleted for miR-30d also showed a robust activation of both STING and TBK1 protein, that was comparable or even superior to that exerted by ATRi treatment (Fig.14a,b). Upon induction of the

pathway, STING activation requires its relocation from ER to the Golgi apparatus, where it forms a trimeric complex with TBK1 and IRF3 proteins, where TBK1 is activated by trans-autophosphorylation. In line with our previous evidence, miR-30d inhibition appeared to reduce alterations of GA structure in both MCF10.DCIS.com and 4T1 cells, as judged by a more compacted appearance and polarized localization of the organelle (Fig.14c,d). In this experimental setting, I observed TBK1 activation by immunofluorescence (IF) analysis, which highlighted a 4-5 fold increase in the appearance of phospho-TBK1 (pTBK1) foci colocalizing with the GA, in both MCF10.DCIS.com and 4T1 cells (Fig.14c-d).

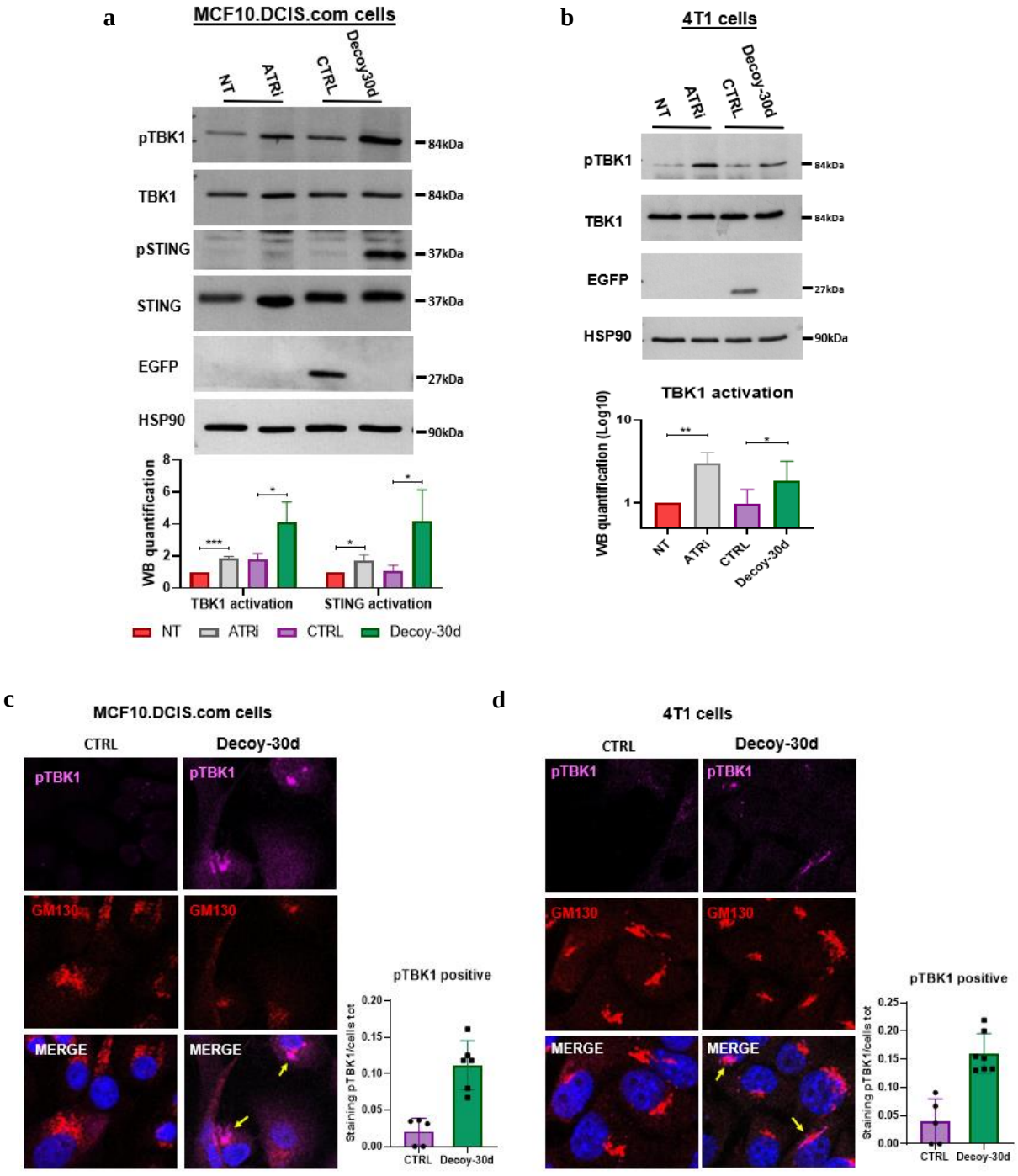

Figure 14. miR-30d downregulation activates cGAS/STING signalling in BC cells. **a)** WB analysis of STING/TBK1 activation in MCF10.DCIS.com cells transfected with control or Decoy-30d construct. As a positive control, VE-821 ATR-inhibitor (ATRi) 10uM was administrated for 16h. The bar graph shows quantification of WB analysis. TBK1 activation = fraction of p-TBK1 vs total TBK1; STING activation = fraction of p-STING vs total STING. **b)** WB analysis of TBK1 activation in 4T1 cells treated as described in (**a**). **c-d)** IF analysis of co-localization of phosphorylated TBK1 (p-TBK1) with the Golgi marker GM130 in MCF10.DCIS.com and 4T1 cells upon miR-30d downregulation. Nuclei were stained with DAPI. The graph shows the percentage of cells with activated TBK1 upon different treatments.

After its activation, pTBK1 phosphorylates the transcription factor IRF3, triggering its translocation to the nucleus, where it induces the expression of type-I IFNs and ISGs. I thus sought to monitor the effect of miR-30d inhibition on the subcellular distribution of IRF3. To this aim, MCF10.DCIS.com cells were transiently transfected with a GFP-IRF3 reporter construct[223] and with either control LNA or LNA-30d. In cells transfected with control LNA, GFP-IRF3 appeared mostly cytoplasmic, while LNA-30d transfection resulted in appearance of nuclear GFP-IRF3 in 75% of cells (Fig. 15).

Overall, these results indicate that downregulation of miR-30d supports the activation of cGAS-STING signaling in BC cells.

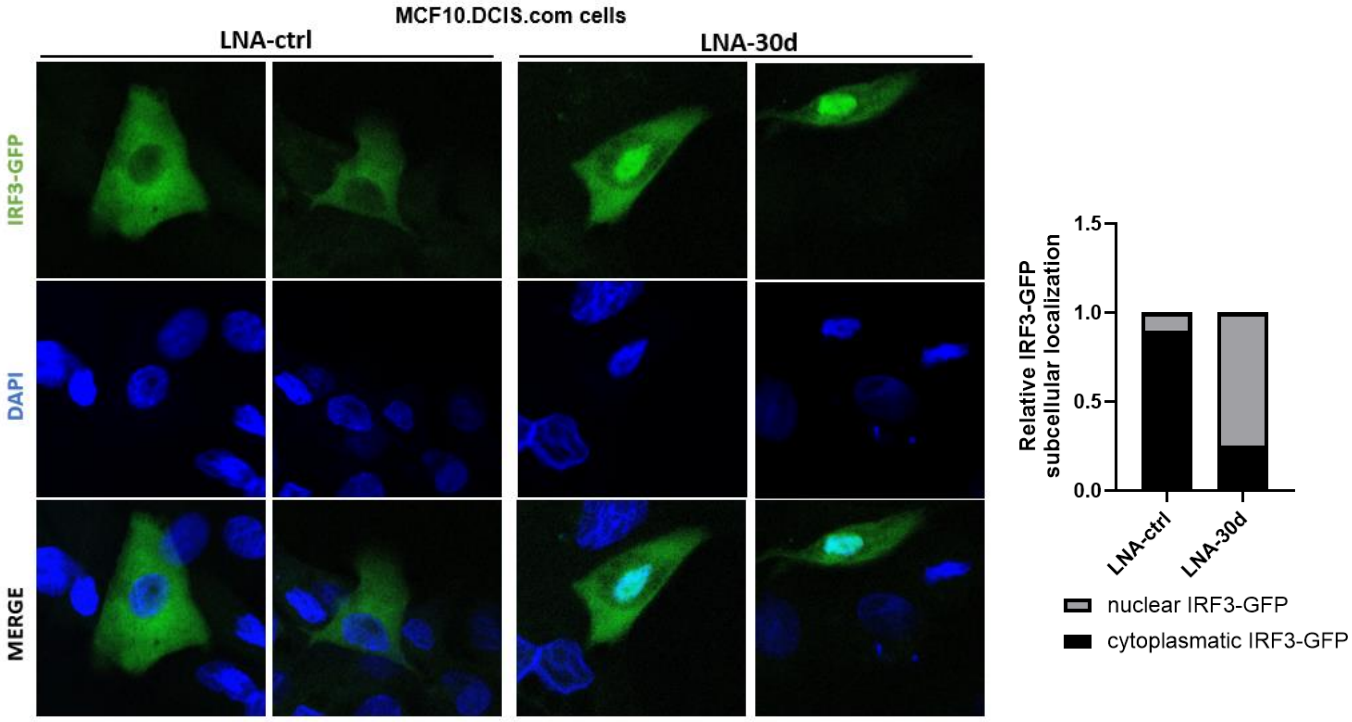

Figure 15. miR-30d downregulation induces nuclear translocation of IRF3 in BC cells. Left panels: representative confocal images of MCF10.DCIS.com cells transiently transfected with IRF3-GFP and with either control LNA or LNA-30d as indicated. The graph on the right shows the quantification of cells with activated IRF3 upon different treatments (n=2).

4.4 miR-30d depletion fails to decrease BC cell viability

Once activated downstream to cGAS-STING-TBK-pathway, IRF3 may induce either cell-autonomous or non-cell-autonomous surveillance mechanisms aimed at limiting cancer growth[86]. When translocated to the nucleus, IRF3 regulates the expression of type-I IFNs and other cytokines which, once released in the TME, signal to immune cells about the presence of tumor cells[86,217]. In addition, IRF3 can also translocate to the mitochondria and induce apoptosis by interacting with Bax to promote pore formation[80].

Thus, I asked whether activation of the IRF3 upon miR-30d depletion, in addition to the observed expression and secretion of type-I IFN (paragraph 4.1), could also affect BC cell viability in a cell autonomous manner. To explore this, I analyzed putative alterations of cell viability by ATPlite assay in 4T1 cells transiently transfected with either control or Decoy-30d construct. As shown in Fig. 16, a preliminary experiment did not highlight any significant change of cell viability in a time frame of 48h upon miR-30d depletion. This suggests that IRF3 activation caused by miR-30d depletion is not sufficient *per se* to induce cell death of BC cells in a cell-autonomous manner.

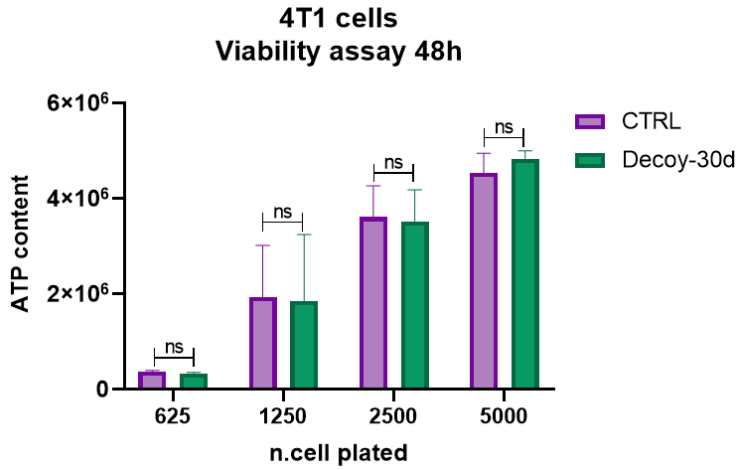

Figure 16. Downregulation of miR-30d does not affect BC cell viability. ATPlite assay in 4T1 cells transiently transfected with either control or Decoy-30d construct for 48h. The X-axis shows the number of cells plated in each well. (n=2)

4.5 miR-30d downregulation promotes accumulation of cytosolic DNA and cGAS activation in BC cells

The activation of cGAS/STING signalling relies on the function of cGAS to produce the cGAMP nucleotide required to activate STING upon recognition of cytoplasmic dsDNA. Remarkably, functional analysis conducted on the transcriptome of MDA-MB-231 cells inhibited for miR-30d[194] showed a significant enrichment of gene sets related to *cellular response to DNA damage*. This

finding appears particularly relevant given that cGAS/STING/IFN-I signaling is triggered by the accumulation of cytoplasmic dsDNA, which may derive from dsDNA ruptures [224].

I thus sought to explore whether miR-30d downregulation might impact on the accumulation of cytosolic dsDNA in BC cells. I performed immunofluorescence staining with an anti-dsDNA antibody: as shown in Fig. 17a, I observed a weak cytoplasmic staining for dsDNA already in control-transfected MCF10.DCIS.com cells. This is consistent with the notion that cancer cells undergo genomic damage and nuclear ruptures, which may lead to cytoplasmic dsDNA leakage[86,225]. Interestingly, after transfection with LNA-30d, I observed a clear increase of cytoplasmic dsDNA staining, with appearance of cytoplasmic dots and of perinuclear structures that are reminiscent of micronuclei, small nuclear-like bodies composed of chromosome fragments wrapped in fragile nuclear membranes (Fig. 17a,b).

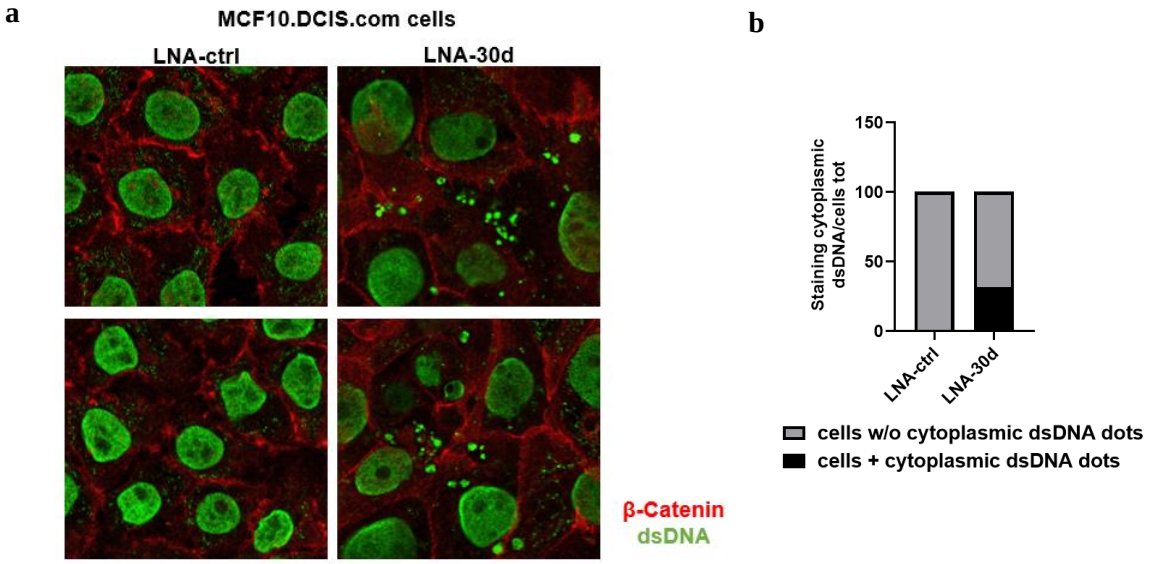

Figure 17. miR-30d downregulation promotes accumulation of cytoplasmic dsDNA in BC cells. **a)** Representative confocal images of IF staining of dsDNA with a specific Ab in MCF10.DCIS.com cells transiently transfected for 48h with LNA-30d or control LNA. Cell borders were marked by staining for β-Catenin. **b)** The graph shows the quantification of cells with cytoplasmic dsDNA dots upon different treatments (n=3).

I then sought to verify whether high levels of cytoplasmic DNA might associate with activation of the cytosolic DNA sensor cGAS upon miR-30d inhibition. In MCF10.DCIS.com cells transiently transfected with Decoy-30d, but not in control-transfected cells, perinuclear accumulation of cGAS spots was observed (Fig. 18a), suggesting activation of cGAS. To monitor cGAS accumulation and subcellular localization upon miR-30d inhibition I also transduced 4T1 cells with a cGAS-reporter, i.e. the lentiviral pTRIP-CMV-tagRFP-FLAG-cGAS (cGAS-RFP) construct, and with Decoy-30d or empty vector. As shown in Fig. 18b, this experiment indicated that treatment with Decoy-30d

promoted perinuclear accumulation of cGAS also in 4T1 cells. Importantly, upon downregulating miR-30d expression in MCF10.DCIS.com cells, I observed colocalization of activated cGAS with cytoplasmic dsDNA signals (Fig. 18c).

Overall, these data indicate that miR-30d depletion results in accumulation of cytoplasmic dsDNA and concomitant perinuclear activation of cGAS in BC cells.

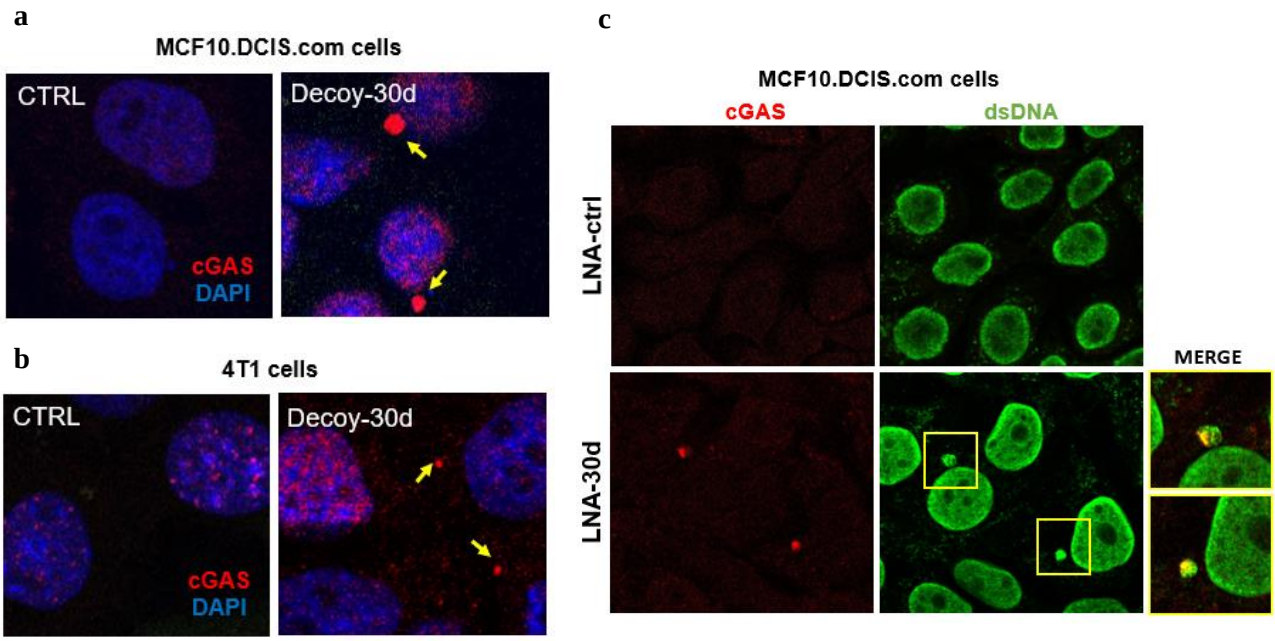

Figure 18. miR-30d downregulation promotes perinuclear accumulation of cGAS colocalizing with cytoplasmic dsDNA in BC cells. **a)** Representative confocal images of endogenous cGAS staining by IF with a cGAS antibody in MCF10.DCIS.com cells transiently transfected with Decoy-30d or empty vector for 48h. (n=3) **b**) Representative confocal images of cGAS-RFP reporter construct in 4T1 cells transiently transfected with Decoy-30d or empty vector for 48h. (n=3) **c**) Representative confocal images of endogenous cGAS (red) and dsDNA (green) IF staining in MCF10.DCIS.com cells transiently transfected for 48h with LNA-30d or control LNA (LNA-Q). (n=3)

I then asked whether accumulation of cGAS-activating cytoplasmic dsDNA could derive from increased genomic damage upon miR-30d inhibition. To address this issue, I evaluated the abundance of phosphorylated histone H2AX (γ-H2AX) foci, a marker of nuclear dsDNA breaks[226], in MDA-MB-231, MCF10.DCIS.com and 4T1 BC cells transiently transfected with LNA-30d or Decoy-30d construct. As a control, treatment with 1 μM of the DNA damaging drug etoposide was used. As shown in Fig. 19, this analysis revealed a strong increase in the number of γ-H2AX foci upon miR-30d depletion as compared to control-treated cells, suggesting that inhibiting miR-30d leads to accumulation of genomic damage.

Altogether, these results suggest that miR-30d inhibition results in accumulation of nuclear DNA damage and triggers upstream induction of the cGAS-STING-IFN-I pathway in cancer cells.

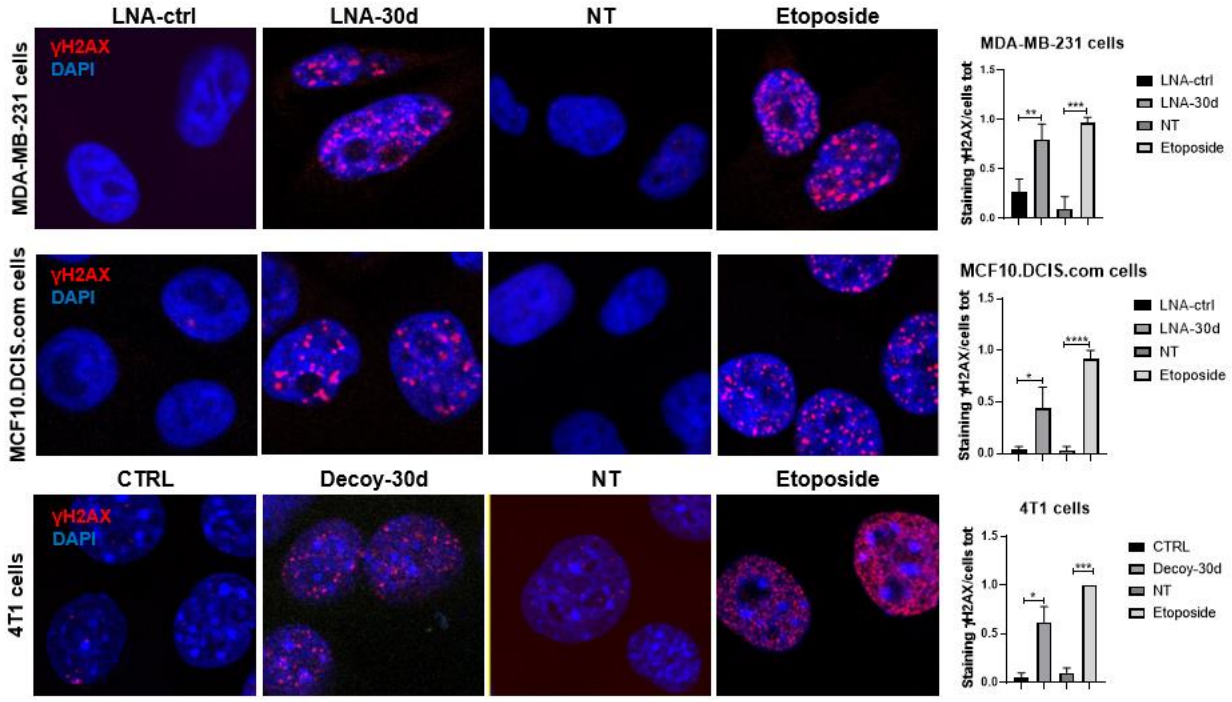

Figure 19. miR-30d downregulation promotes accumulation of nuclear DNA damage in BC cells. Representative IF analyses of γH2AX staining in MDA-MB-231, MCF10.DICIS.com and 4T1 mBC cells transfected for 48h with LNA-30d or Decoy-30d construct, respectively. Etoposide 1 µM was administered for 24h as a positive control. The graphs on the right show the percentage of γH2AX -positive cells upon different treatments (n=3).

4.6 The impact of miR-30d on IFN-I response may involve alterations of Golgi apparatus

Upon cGAS-dependent induction, STING pathway activation crucially depends on STING relocation from the ER to the Golgi apparatus (GA), and formation of a GA-resident activation complex between STING, TBK1 and IRF3 proteins. Structural alterations of the GA, such as those induced by miR-30d activity, are expected to impair execution of this pathway[110]. On this premise, I sought to verify if the effect of miR-30d on IFN-I signalling may also involve alterations of the secretory pathway, and in particular miR-30d dependent structural changes of the GA. Previous work from our group demonstrated that miR-30d impacts GA structure by downregulating DGKZ, an enzyme belonging to the diacylglycerol kinase family, which catalyzes the conversion of the membrane lipid diacylglycerol (DAG) into phosphatidic acid (PA). Mechanistically, downregulation of DGKZ increases local DAG concentration at membranes, promoting GA tubulo-vesiculation (Fig. 20a). Consistent with this notion, MCF10.DCIS.com cells, which express high levels of miR-30d, show a tubulo-vesiculated GA characterized by multiple mini-stacks dispersed within the cytoplasm (Fig. 20b). In these cells, miR-30d inhibition leads to GA compaction, while

concomitant silencing of DGKZ prevents normalization of GA, which appears highly fragmented (Fig. 20b,c). As shown in Fig. 20d, I observed that in this experimental setting DGKZ silencing largely prevented STING activation caused by miR-30d inhibition. This suggests that the attenuation of cGAS/STING signaling by miR-30d may involve alterations of the Golgi apparatus. Consistent with this observation, silencing of *DGKZ* strongly reduced Decoy-30d dependent induction of both *type-I IFNs* and *ISGs*, i.e. downstream targets of the cGAS-STING pathway (Fig. 20e).

These data support the hypothesis that high levels of miR-30d may attenuate the cGAS/STING/IFN signalling by inducing structural alterations of the GA, which may impact on the correct activation of STING/TBK proteins. Therefore, these findings collectively suggest that miR-30d inhibition may activate the cGAS/STING/IFN pathway in cancer cells at multiple levels: on one hand, it concurs to trigger cGAS/STING signalling by causing accumulation of DNA damage and cytosolic dsDNA, and on the other hand it may further unleash STING/TBK/IRF3 activation by promoting GA compaction.

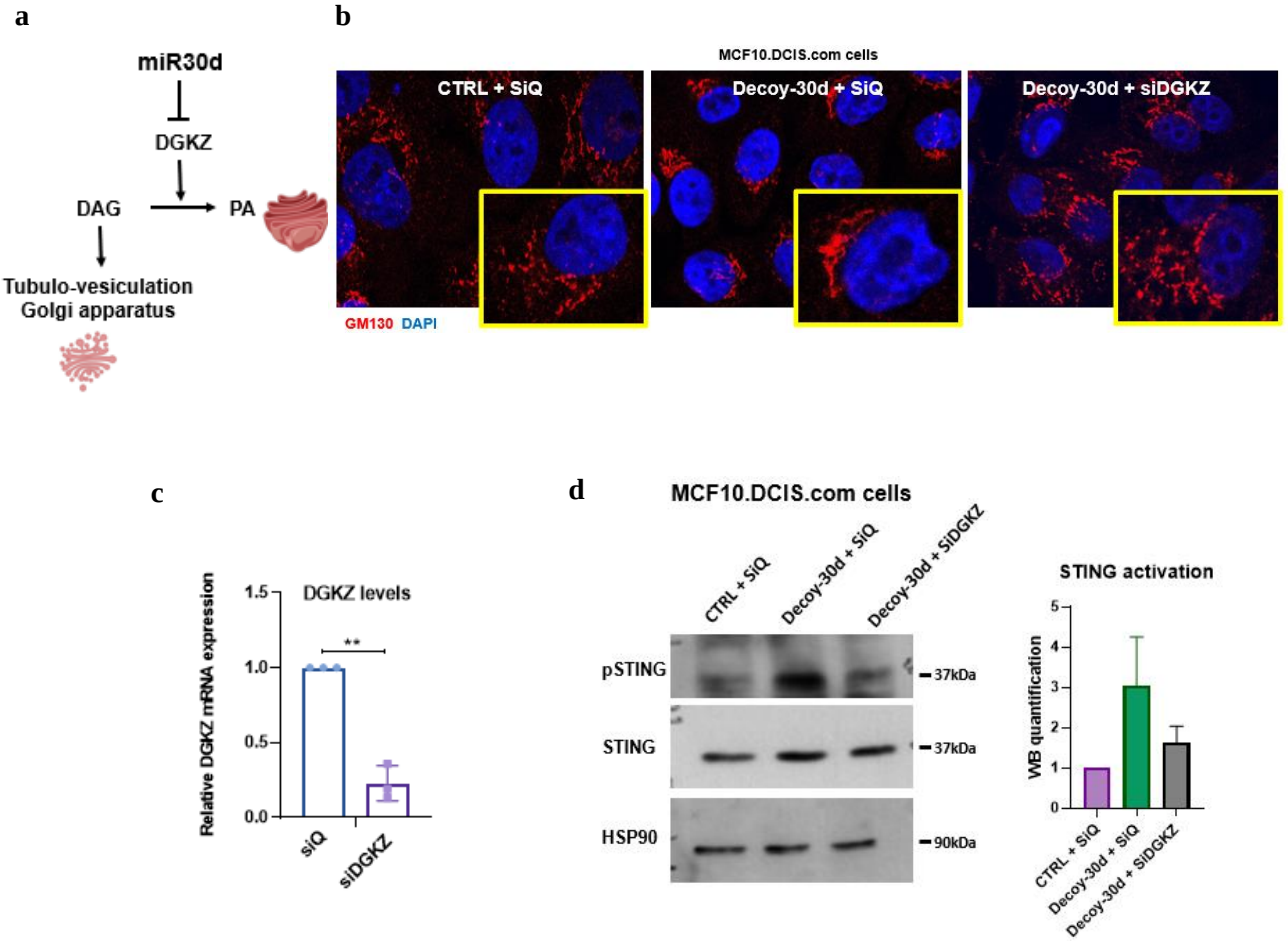

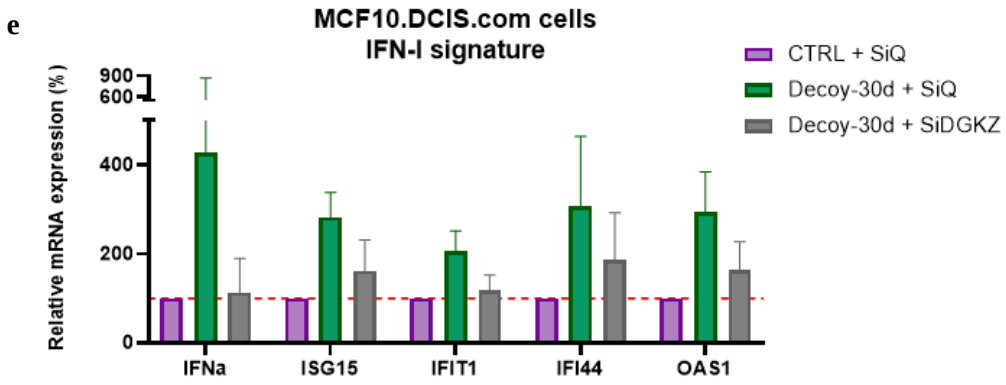

Figure 20. GA fragmentation by downregulating miR-30d target DGKZ prevents induction of the STING-IFN pathway upon miR-30d inhibition. **a)** Schematic representation of the effects of miR-30d on GA structure. Downregulation of DGKZ (Diacylglycerol kinase) increases local concentration of diacylglycerol (DAG) at membranes, promoting GA tubulo-vesiculation. **b)** Representative IF analysis of GA morphology by staining for GM130 in MCF10.DCIS.com cells transiently silenced for *DGKZ* (si*DGKZ*) and transfected with either control or miR-30d decoy construct for 48h. **c)** qRT-PCR analysis of *DGKZ* mRNA expression in MCF10.DCIS.com cells transiently transfected with either control siRNA (si*Q*) or *DGKZ* siRNA (si*DGKZ*). H3 expression was used as a reference for quantification. **d)** WB analysis of STING activation (= fraction of p-Sting vs total Sting) in MCF10.DCIS.com cells transfected as described in (b). Right panel shows quantification of WB analysis. **e)** RT-qPCR analysis of the indicated IFN-I and ISGs, conducted in MCF10.DCIS.com cells transfected as described in (c). *H3* expression was used as a reference for quantification.
Graph bars represent mean ± s.d. of n≥3 biological replicates. P value: $P < 0.05$ [*], $P < 0.01$ [**], $P < 0.001$ [***] by two-tailed Student's t-test. Blots are representative of n=3 biological replicates.

4.7 miR-30d downregulation displays synergistic effects with the cGAS/STING-inducing chemotherapeutic drug doxorubicin

Conventional chemotherapy regimens represent treatments of choice for a consistent fraction of patients bearing breast as well as other cancers. Notably, this represents the only systemic therapy with demonstrated efficacy in the most aggressive triple negative breast cancer (TNBC) subtype, and is an important adjunct to endocrine therapy in other BC subtypes[227]. A growing number of studies report that, in addition to well-known cytotoxic effects, chemotherapeutic treatments also exert immunostimulatory effects, due to DNA damage-dependent activation of the cGAS/STING pathway in proliferating cancer cells[102]. I thus sought to assess whether inhibition of miR-30d may synergize with chemotherapeutic treatments inducing cGAS/STING-dependent IFN-I response in BC cells. To this aim, I tested the ability of different chemotherapeutic drugs used in standard clinical practice to induce expression of type-I IFN genes in 4T1 TNBC cell line (not shown). In these experiments, the topoisomerase inhibitor doxorubicin behaved as a strong inducer of *Ifnα* and *Ifnβ1* genes, consistently with previous evidence[228] and with its reported ability to cause double-

strand DNA breaks and micronuclei formation by DNA intercalation or direct alkylation[102]. To test the effect of combining miR-30d inhibition with doxorubicin treatment, I then treated 4T1 cells stably expressing either control or Decoy-30d construct with 1µM doxorubicin. As shown in Figure 21, the effect of doxorubicin on type-I IFN genes expression increased up to 5-fold in cells expressing decoy-30d as compared to cell expressing control vector.

This result suggests that combination of miR-30d inhibition with administration of doxorubicin leads to a synergistic rather than additive effect in stimulating the IFN response.

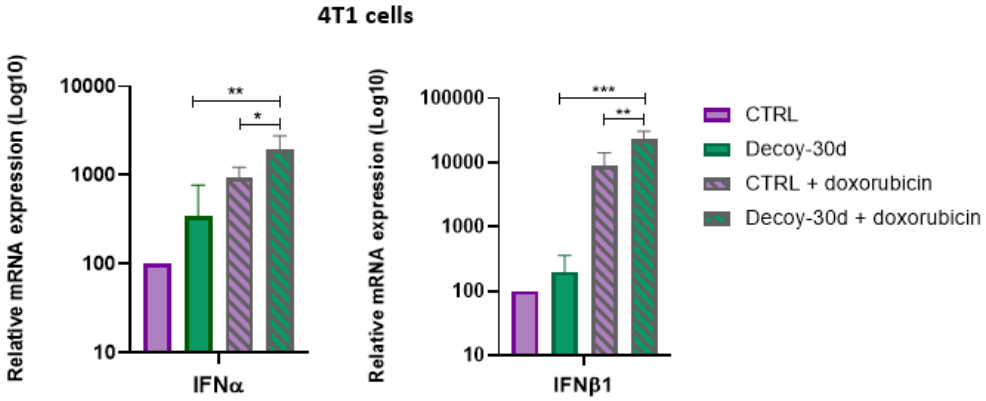

Figure 21. miR-30d downregulation displays a synergistic effect with doxorubicin in inducing Ifnα/β expression. 4T1 cells stably transfected with Decoy-30d construct or control were treated with 1µM doxorubicin. After 72 h, the expression of *Ifnα* and *Ifnβ1* genes was evaluated by RT-qPCR and normalized to *Gapdh* mRNA expression as a reference. mRNA levels relative to control condition (set at 100) are shown. Graph bars represent mean ± s.d. of n>4 biological replicates. P value: P < 0.05 [*], P < 0.01 [**], P < 0.001 [***] by two-tailed Student's t-test.

4.8 Inhibition of miR-30d induces expression of IFN response genes in ex-vivo organoid models of BC

To estimate the potential of using miR-30d inhibitors to stimulate the IFN-I response in breast tumors, I decided to employ tumor organoids, ex-vivo 3D culture systems representing well-established preclinical models in disease modelling and drug development. Organoids faithfully recapitulate genetic, phenotypic and architectural hallmarks of the original tumors, and can be grown in synthetic 3D matrices, whose composition and density may be experimentally modulated to recapitulate the features of tumor tissues[229].

First, I generated primary BC organoids from *Mouse Mammary Tumor Virus-Polyoma Middle T antigen* (MMTV-PyMT) mouse model of aggressive BC (Fig.22b). MMTV-PyMT organoids were transiently transfected for 48h with either control or LNA-30d inhibitor, and the expression of a panel of IFN-I and ISGs genes was then investigated by qRT-PCR. As shown in Fig. 22a,

administration of LNA miR-30d inhibitor to MMTV-PyMT organoids resulted in the induction of IFN-I signature genes as compared to control-treatment.

I also generated mBC organoids from spontaneous lung metastases recovered from an immunocompetent Balb/c mouse orthotopically transplanted in the fat pad with 4T1 cells (Fig. 22d). As shown in Fig. 22c, administration of LNA miR-30d inhibitor to metastatic 4T1m organoids resulted in increased expression of type-I IFNs and of several ISGs, as compared to control-treatment.

These data suggest that administration of miR-30d inhibitors may be effective in inducing the cGAS/STING/IFN pathway not only in 2D cell cultures but also in tumor tissues embedded in a solid ECM. Based on these results, it will be of interest to study the effect of miR-30d inhibition on patients' derived tumor organoids (PDOs) of breast and other tumor types.

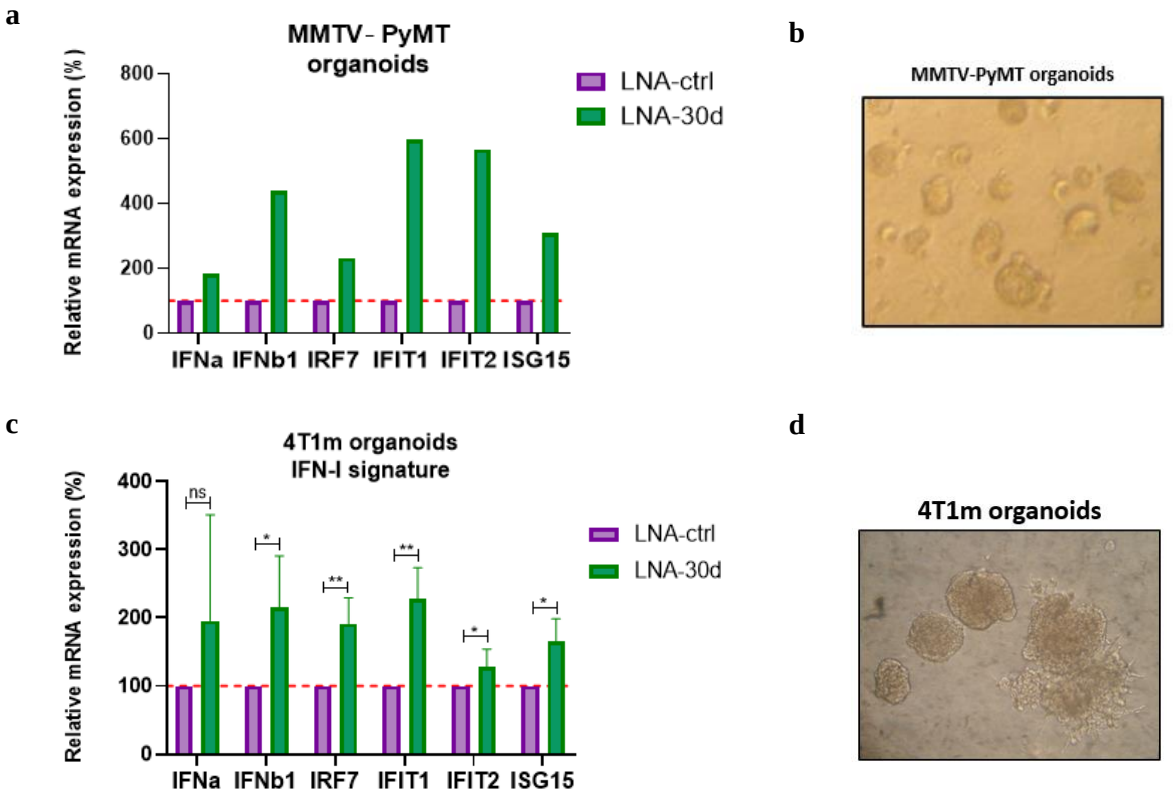

Figure 22. LNA miR-30d inhibitor induces the expression of IFN-I signature genes in primary and metastatic mouse BC organoids. **a,c)** Primary MMTV-PyMT and metastatic 4T1 (4T1m) organoids were transiently transfected with LNA-30d or with scramble LNA (LNA-ctrl). After 48h, the expression levels of the indicated IFN-I and ISGs were evaluated by RT-qPCR and normalized to *Gapdh* mRNA expression as a reference. **b,d)** Representative images of MMTV-PyMT and 4T1m organoids grown in Matrigel for 72h.

Graph bars represent mean ± s.d. of n=1 for a) and n=4 for c) biological replicates. P value: P < 0.05 [*], P < 0.01 [**], P < 0.001 [***] by two-tailed Student's t-test.

4.9 miR-30d downregulation promotes upstream activation of the cGAS/STING pathway in mBC-bearing mice

I then sought to investigate the effect of inhibiting miR-30d on cGAS/STING/IFN-I signalling in a mouse model of breast tumorigenesis. To this aim, I took advantage of a previous experiment performed in our lab to investigate the impact of miR-30d on tumor growth and metastasis *in vivo*[194]. This was obtained by orthotopically injecting SCID mice with luciferase-expressing human BC MDA-MB-231 cells, stably transduced with either control or Decoy-30d construct (Fig. 24a). Remarkably, in this experimental setting inhibition of miR-30d significantly delayed both tumor and metastatic growth over a 4 weeks period[194]. Primary tumors and lung tissues isolated from engrafted mice were subjected to immunohistochemical (IHC) analysis for evaluating the abundance of the DNA damage marker γ-H2AX and of cGAS. As shown in Fig. 24b, IHC clearly showed that both γ-H2AX and cGAS signals were consistently higher in both primary tumors and lung metastases recovered from mice injected with MDA-MB-231 cells downregulated for miR-30d expression as compared to control tumors, suggesting that the inhibition of miR-30d may enhance the activation of cGAS signalling *in vivo*.

Collectively, these results reinforce the notion that inhibition of miR-30d can increase the activation of the cGAS/STING pathway by causing nuclear DNA damage and subsequent activation of the DNA-sensor cGAS. Therefore, these data suggest that the reduction of tumor growth observed in mouse xenograft experiments upon stable inhibition of miR-30d might partly depend on enhancement of the cGAS/STING pathway, and consequent induction of anti-tumor innate immune surveillance.

Further analyses are currently ongoing to investigate putative changes in the immune composition of the TME upon miR-30d depletion.

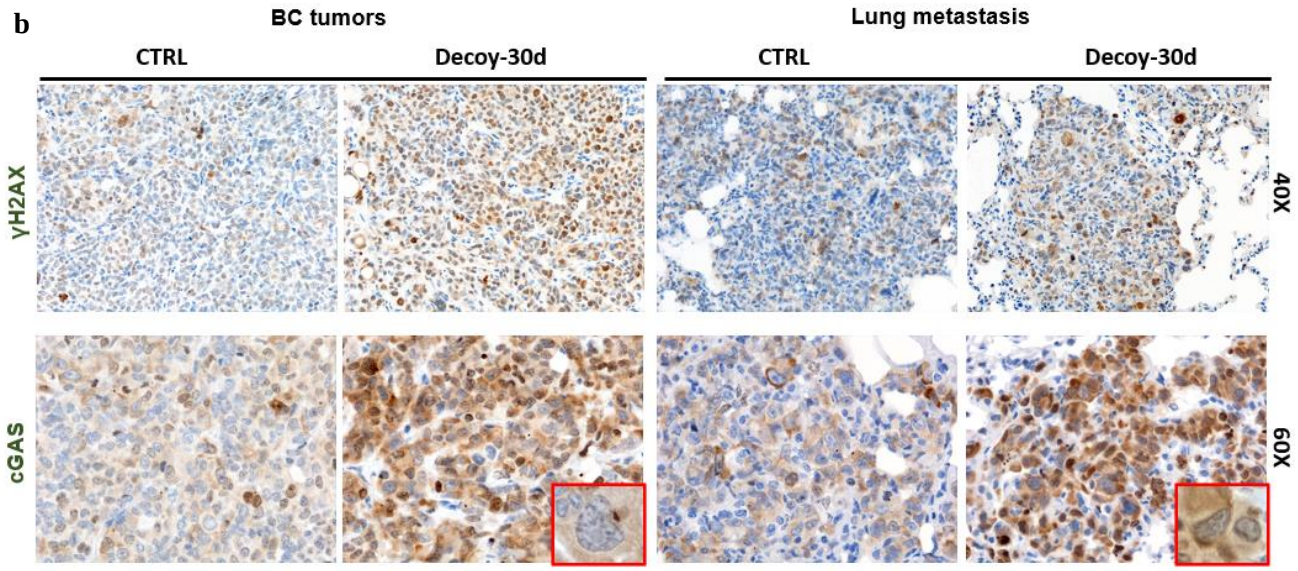

Figure 23. miR-30d downregulation increases γ-H2AX foci and cGAS accumulation in primary BC and derived metastases in vivo. a) Schematic representation of xenograft experiments: MDA-MB-231–Luc control (CTRL, n = 8) or miR-30d decoy (Decoy-30d, n = 9) cells were injected into the mammary fat pad of SCID mice and after 35 days primary tumors and lung metastases were recovered. **b)** Representative images of immunohistochemical analyses (IHC) of γ-H2AX foci and endogenous cGAS, in serial sections of primary tumors and lung metastases from mice treated as described in **a**).
All IHC staining were performed by postdoctoral researcher Valeria Cancila from C. Tripodo's Lab at the University of Palermo

4.10 High miR-30d levels correlate with a low immune score in BC patients

Based on the above results, I hypothesized that miR-30d depletion may attenuate the activation of the cGAS/STING/IFN-I pathway in BC cells and consequently promote an immunosuppressive TME during cancer progression. To test this hypothesis, I analyzed the correlation between miR-30d levels expression of STING-dependent gene signature, as well as immune cell recruitment, in clinical data from primary BCs. As shown in Fig. 24a, analysis of The Cancer Genome Atlas (TCGA) dataset highlighted that elevated levels of miR-30d correlated with lower expression of a STING gene signature. Furthermore, this analysis also showed a correlation between high miR-30d levels and a lower immune score (Fig. 24b).

Taken together, these data suggest that high levels of miR-30d could contribute to the generation of an immune-cold microenvironment by blunting cGAS/STING signalling.

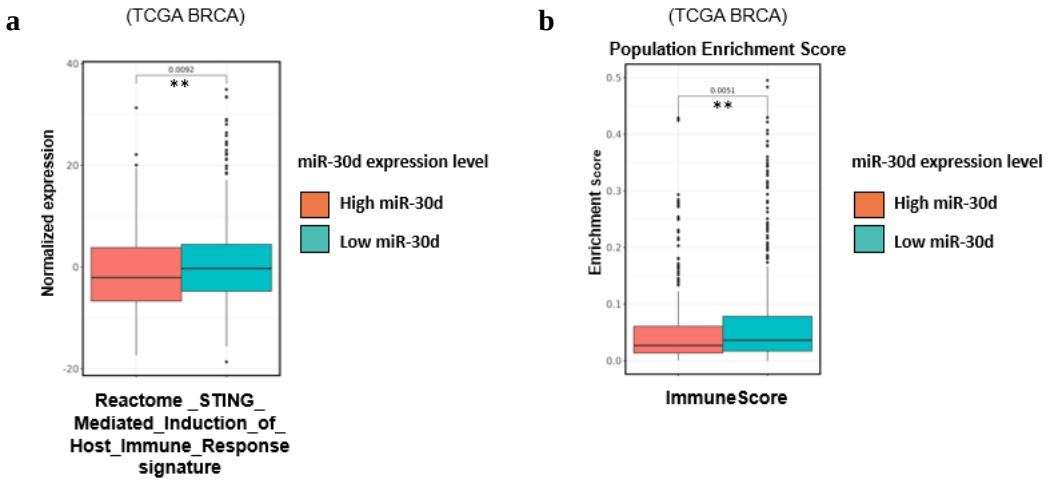

Figure 24. TCGA analysis of BC data showing the STING-dependent gene signature and immune score in relation to miR-30d levels. a) Normalized expression of "Reactome STING Mediated Induction of host Immune Response" gene signature calculated on TCGA BRCA patients divided by high and low levels of miR-30d expression. ***b)*** xCell derived ImmuneScore calculated on TCGA BRCA patients divided by high and low levels of miR-30d expression. Pvalue calculated with Wilcoxon T-test ($p < 0.0001$). Analysis performed by Luca Triboli.

4.11 Appendix: Analysis of circulating miR-30d levels in BC models

The data presented above provide evidence in support of a possible role of miR-30d in reducing the activation of cGAS/STING/IFN pathway in cancer cells, a condition known to promote a permissive TME through suppression of innate immunity and anti-tumor immune surveillance. This is consistent with our previous demonstration that miR-30d has a role in promoting breast cancer growth and metastatic progression in mouse models of BC[194] and with the notion that miR-30d is found overexpressed in BC[199] and its expression is induced by mut-p53 and HIF1a oncogenes[194], both associated with tumor aggressiveness and induction of immune evasion. miR-30d is known to be secreted by tumor cells and it is detectable in blood[201,230], suggesting that it may also exert paracrine effects in promoting immune evasion via blunting cGAS/STING signalling in both cancer cells and TME components, and these effects could impact both primary and secondary tumor sites.

Therefore, I evaluated whether circulating miR-30d could be detected in mice during cancer progression and whether miR-30d levels could follow the evolution of the disease and the response to therapy in breast cancer-bearing mice[196]. To explore this possibility, I conceived a pilot study to monitor circulating miR-30d levels during BC progression, by RT-qPCR analysis of peripheral blood samples from breast cancer-bearing mice. To this aim, luciferase reporter-expressing 4T1 mouse BC cells (4T1-Luc) were orthotopically transplanted in the fat pad of syngenic Balb/c mice.

Recipient mice developed both primary BC and metastatic lesions in the lungs, as detected by bioluminescence imaging in vivo (Fig. 25a,b). Peripheral blood was collected weekly from transplanted mice, and miR-30d levels were quantified from purified sera. As shown in Figure 25c, miR-30d serum levels remained constant during weeks 1-4, when primary tumor growth occurred, while showing a sharp increase at week 5, when all injected mice had developed large metastases, and were afterwards sacrificed.

These results indicated that serum levels of miR-30d increased upon tumor progression. However, this experiment could not discriminate whether miR-30d increase was dependent on either primary or secondary tumor growth, or both.

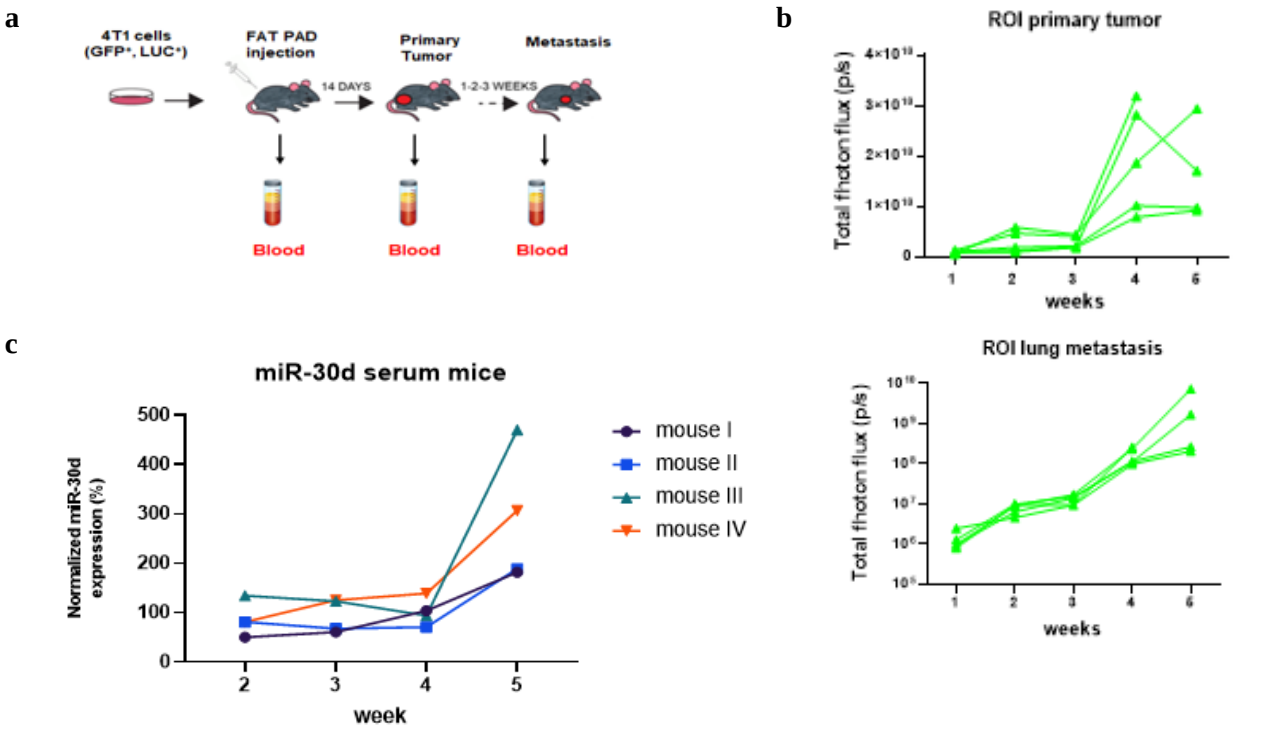

Figure 25. Circulating miR-30d levels increase during BC progression in mice. **a)** Schematic overview of the experimental workflow: 4T1-luciferase expressing (4T1-Luc) cells were transplanted into the fat pad of 4 Balb/c mice and peripheral blood was collected every week after inoculation. **b)** In vivo quantification of luciferase at different time points in primary tumors (left) and in lung metastases (right) was performed on the experimental model described in (a); **c)** RNA was extracted from a fixed amount of clarified sera (50 µl), adding a standard amount of cel-miR-39 to allow normalization. The levels of miR-30d relative to cel-miR-39 were evaluated by RT-qPCR. Time points t= 0 (before inoculation) and t= 1 (first week) are missing due to insufficient serum volume.

I then performed an experiment to investigate whether blood levels of miR-30d correlate with tumor response to therapeutic treatments. To this aim, 4T1 cells expressing mut-p53^{R280K} were injected in

the mammary fat pad of syngeneic Balb/c mice. Four days after inoculation, mice were treated for the next 24 days by intraperitoneal injection of either the chemotherapeutic agent 5-FU or the FDA-approved drug Dasatinib, a Src family inhibitor currently in phase II clinical trial for advanced BC[231,232]. Peripheral blood was taken at the experiment endpoint (Fig. 26a). As shown in Fig. 26b, treatment with Dasatinib resulted in a significant reduction of the primary tumor volume, while treatment with 5-FU did not significantly impact tumor growth. Under these conditions the levels of circulating miR-30d decreased in parallel with reduction of primary BC tumor growth (Fig.26c). In particular, while a consistent reduction in miR-30d blood levels was observed after treatment with Dasatinib, the reduction was not significant in mice treated with 5-FU. These initial observations suggest that miR-30d may represent a possible biomarker of BC disease progression and of tumor response. However, more experiments will be required to address this issue.

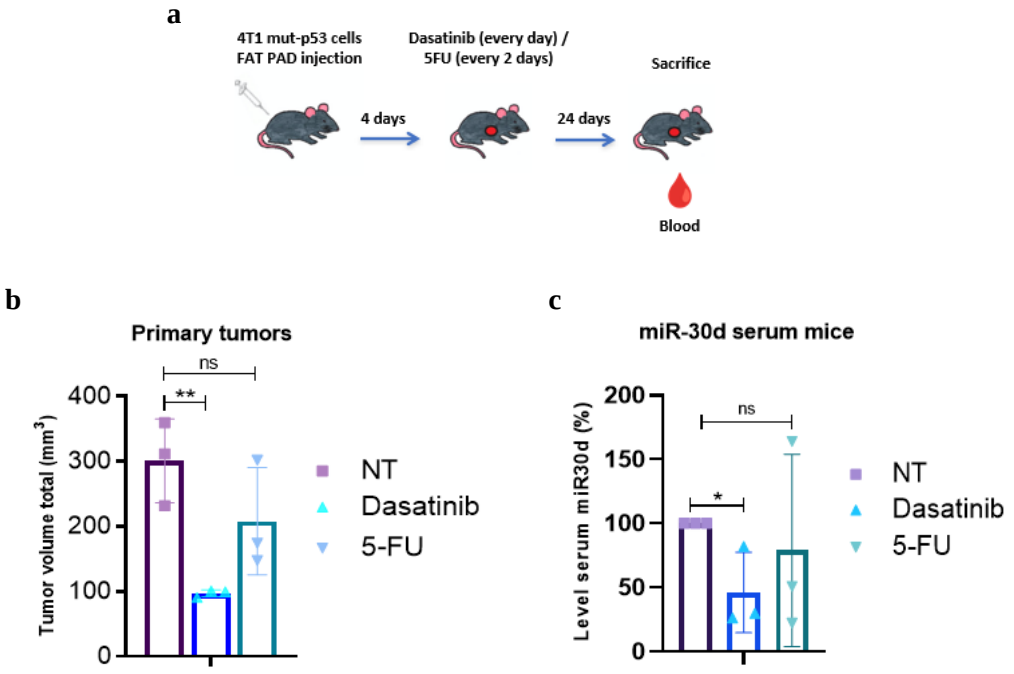

Figure 26. Circulating miR-30d levels are reduced upon regression of primary BC in vivo. **a)** Schematic overview of the experimental workflow: 4T1 mutp53^{R280K} cells were injected into the fat pad of Balb/c mice. The following day, 3 cohorts of 3 mice were treated with either 10 mg/kg Dasatinib, 25 mg/kg 5-fluorouracil (5-FU) or placebo (NT) until sacrifice. Peripheral blood was collected 4 weeks after injection, at the time of sacrifice. **b)** Bar graph of primary tumor volumes at week 4 of mice treated as described in a). Tumor volumes were calculated using the formula (d*d*D)/2, where "d" stands for smaller diameter and "D" for larger diameter. **c)** RNA was extracted from a fixed amount of clarified sera (35 µl), adding a standard amount of cel-miR-39 to allow normalization. The levels of miR-30d relative to cel-miR-39 were evaluated by RT-qPCR.
Graph bars represent mean ± s.d. of n=3 biological replicates. P value: P < 0.05 [*], P < 0.01 [**], P < 0.001 [***] by two-tailed Student's t-test.

5. Discussion

During tumor progression, cancer cells communicate with each other and with their surrounding tissue to shape a permissive microenvironment, which is critical for tumor growth and progression. This communication displays both local and systemic effects impacting on angiogenesis, ECM remodeling, metabolic rewiring, and modulation of immune/inflammatory cells, supporting both proliferation and metastatic dissemination of cancer cells and escape from immune surveillance. Understanding immune evasion mechanisms that are involved in generating non-immunogenic or "cold" tumors represents a key issue for improving the efficacy of anticancer immune therapies.

The cGAS–STING pathway is a cytoplasmic DNA-sensing machinery with relevant roles in innate immunity. Cancer cells often contain high levels of cytoplasmic DNA, due to genomic and nuclear damage, which result in constitutive, although still inducible, activation of the cGAS/STING pathway[224]. By production of type-I interferons and other immune mediators[86], this leads to activation of innate antitumor immunity. Consistently, many tumors appear to select for activities that either attenuate cGAS-STING-IFN signalling, thus escaping immune surveillance, or even corrupt it, thereby stoking tumor-promoting inflammation.

In line with these premises, I observed that overexpression of the microRNA miR-30d, which in breast tumors may occur downstream to HIF1α and mut-p53 oncogenes[194,207], correlates with reduced expression of IFN-I signature genes and with low immune score in breast cancer patients' datasets, suggesting that miR-30d could be involved in suppressing innate immune signalling in BC by attenuating the cGAS/STING/IFN-I pathway.

Inhibition of miR-30d activates STING/IRF3/IFN-I signalling in BC cells

In this thesis I demonstrated that the inhibition of miR-30d causes activation of cGAS/STING/IFN-I signaling in cancer cells, tumor organoids and tumor xenografts. In particular, I observed that depletion of miR-30d activates the expression of type-I IFNs and of several ISGs encoding for immune stimulatory chemokines and cytokines in BC cell lines, including ductal adenocarcinoma in situ and metastatic BC cell lines. In BC cells, induction of IFN-I signature genes after miR-30d ablation involved activation of cGAS/STING/TBK signaling and was accompanied by IRF3 nuclear translocation. Upon its activation IRF3 may trigger complementary responses that contribute to arresting tumor growth. Indeed, it either translocates into the nucleus to induce the expression of type-I IFNs and other cytokines that in turn engage

anti-tumor immune surveillance, or translocates to mitochondria and interacts with the pro-apoptotic Bax protein to induce apoptosis[80,86]. The results obtained showed evidence of nuclear IRF3-mediated response upon inhibition of miR-30d, while in contrast no decrease in cell viability was observed, suggesting that in cancer cells IRF3 activation alone is not sufficient to induce cell death. Further experiments will be required to fully investigate this aspect, by verifying the induction of apoptosis by specific assays. Consistent with the observed nuclear activation of IRF3, miR-30d inhibition induced an increase of IFNα and IFNβ secretion in BC cells. Remarkably, we previously observed that depletion of miR-30d leads to normalization of secretory trafficking in cancer cells[194], suggesting that the extracellular release of type-I IFNs is a consequence of the increased expression of interferon genes rather than to augmented rate of secretion. Induction of the cGAS/STING pathway may also lead to activation of the transcription factor NFκB[219,233], a master regulator of proinflammatory genes. However, preliminary results obtained in BC cells (not shown) indicate that miR-30d inhibition does not lead to significant changes of expression of NFκB target genes. Thus, these results suggest that induction of STING/IRF3 signalling, rather than NFκB activation, is responsible for the observed induction of IFN-I response genes upon inhibition of miR-30d.

Role of miR-30d in oncogene-driven immune evasion

Recently it has been reported that missense mut-p53 oncoproteins are able to attenuate antitumor innate immunity, by blunting activation of the STING/IFN-I pathway via direct inhibition of TBK1 protein[191]. Interestingly, when comparing the effects of miR-30d inhibition on induction of IFN-I response genes among cell lines with different *TP53* status, I observed lower levels of activation in a mut-p53 expressing BC cell line (MDA-MB-231) as compared to BC cells expressing either wild-type p53 (MCF10DCIS.com and MCF7) or null for p53 expression (4T1 cells). These results will require further validation in a wider panel of wild-type and mut-p53 expressing cell lines, however are in agreement with the reported role of mut-p53 in attenuating the STING/IFN-I pathway. It is tempting to speculate that the observed effect of mut-p53 as a suppressor of innate immune signaling could be also mediated by its ability to induce miR-30d expression, thus leading to repression of the cGAS/STING pathway at multiple levels. Importantly, these observations would imply that inhibition of miR-30d could result in efficient activation of this innate immunity pathway also in mut-p53 expressing tumors.

Remarkably, miR-30d is also a transcriptional target of the HIF1α oncoprotein, which may promote its transcription independently of the presence of mut-p53[207]. HIF1α is known to drive both innate and adaptive immune evasion in solid tumors by inducing the expression of

immunosuppressive factors (e.g., VEGF, TGF-β, IL-10 and PGE2) and immune checkpoint molecules (e.g., PD-L1 and HLA-G)[234]. Moreover, HIF1α was recently found to interfere with cGAS/STING pathway activation, further contributing to promote tumor cell evasion of immune surveillance. For instance, miR-25 and miR-93, two HIF1α-responsive microRNAs, have been implicated in creating an immunosuppressive tumor microenvironment by downregulating the expression of the DNA sensor cGAS[235]. It is thus conceivable that part of the immunosuppressive effects of HIF1α could be mediated by its ability to induce overexpression of miR-30d.

As a further validation of these findings, I aim to study the effects of miR-30d overexpression on the cGAS/STING pathway. This may be achieved either by employing constructs acting as miRNA mimics, or increasing expression of endogenous miRNA by hypoxic conditions. I expect that high levels of miR-30d, in contrast to its downregulation, would blunt cGAS/STING signaling.

miR-30d impacts on cGAS/STING/IFN-I pathway at multiple levels

Regarding the mechanisms underlying the effects of miR-30d on different levels of cGAS/STING pathway regulation, that may explain the observed activation upon miR-30d depletion, I started with an explorative bioinformatics analysis of publicly available data obtained in tumor cell lines upon perturbing miR-30d function. In this regard, functional analysis of transcriptomic data of human mBC cells suggested a putative effect of miR-30d on the cell response to DNA damage. Remarkably, cancer cells are prone to DNA damage, which triggers the activation of the DNA-sensing cGAS/STING/IRF3 pathway and the consequent expression of type-I IFNs and ISGs[86]. I observed a consistent increase of both number and size of dsDNA damage foci, as well as the appearance of structures reminiscent of micronuclei and of dsDNA staining in the cytoplasm upon miR-30d depletion. Furthermore, in this condition, I also highlighted an increase of perinuclear cGAS signal, which colocalized with cytoplasmic dsDNA. At present, it is not known how miR-30d might protect cancer cells from accumulating DNA damage and/or cytosolic dsDNA leakage. One intriguing possibility could be that miR-30d depletion might interfere with DNA repair. Given that cancer cells display DNA replication stress and intrinsic genomic instability, this could explain the selective ability of miR-30d inhibitors to induce IFN response in BC cells as compared to non-neoplastic breast epithelial cells, which are characterized by low genomic instability as compared to transformed counterparts. Further experiments are required to compare the effects of miR-30d inhibitors between normal and transformed cells. This said, it will be interesting to perform bioinformatic analyses to obtain hints on putative targets of miR-30d that may modulate DNA repair activities.

Another interesting observation was the appearance of nuclear blebs, micronuclei and cytoplasmic dsDNA upon miR-30d inhibition in cancer cells, which suggest nuclear envelope damage, leading to perinuclear accumulation of dsDNA and translocation of cGAS from the nucleus (where it resides in inactive form) to the cytoplasm (active form)[115,116]. Of note, cancer cells are subject to several challenges that undermine nuclear envelope integrity (e.g., mechanical stress), which, if not resolved, may culminate in nuclear envelope ruptures with consequent cGAS activation[220]. It will therefore be interesting to investigate whether tumor cells, by maintaining high levels of miR-30d, may limit nuclear envelope alterations and consequently allow survival of cancer cells through the generation of an immunosuppressed microenvironment. In addition, it has to be considered that cGAS is also known to be activated by mitochondrial dsDNA, therefore I plan to assess whether miR-30d may also have effects on mitochondrial structure and function.

While searching for the mechanistic underpinnings of miR-30d dependent attenuation of the cGAS/STING pathway, I also took into account the ability of miR-30d to cause tubulo-vesiculation of the Golgi apparatus[194], which has been shown by our research group to involve miR-30d dependent downregulation of the DGKZ kinase and of the retromer complex component VPS26B. In particular, downregulation of DGKZ increases the local concentration of diacylglycerol (DAG) at membranes, promoting Golgi tubulo-vesiculation. Interestingly, it has been previously suggested that alterations of Golgi structure, such as fragmentation, may prevent STING activation, resulting in attenuation of the STING/IFN-I pathway[76,110]. When I inhibited miR-30d in BC cells in the presence of DGKZ silencing, thereby interfering with decoy-dependent GA compaction, STING activation and induction of IFN-I response genes were largely prevented. This observation suggests that the ability of miR-30d inhibitors to induce GA compaction is required for activating the STING pathway and implies that the induction of structural alterations of the secretory pathway, which occur downstream to miR-30d overexpression in cancer cells, may contribute to attenuate STING signaling. It is conceivable that GA tubulo-vesiculation may specifically impact on the correct activation of STING and TBK1 proteins at Golgi membranes, blunting the downstream IFN-I signalling. My results would also imply that in tumor cells, which display high levels of intrinsic DNA damage, inducing normalization of GA structure may be sufficient to trigger the production of type-I IFNs and the secretion of antitumor innate immunity mediators. Remarkably, upon activation, STING translocates from the Endoplasmic Reticulum (ER) to the Golgi[86], and it is known that high levels of miR-30d alter the structure of the ER[194], thus it is possible that miR-30d might also influence the processing of STING protein by disrupting ER organization.

In sum, the evidence presented in this thesis is consistent with a model in which inhibition of miR-30d may both trigger upstream induction of the cGAS/STING pathway in cancer cells by causing release of dsDNA in the cytosol and sustain its activity by normalizing the structure of the secretory pathway.

Potential impacts of miR-30d on the immune tumor microenvironment

In line with the results described so far, I found that miR-30d inhibition in breast tumor xenograft experiments, where miR-30d inhibition was found to significantly delay both tumor growth and metastasis formation[194], correlated with accumulation of nuclear DNA damage and activation of the DNA-sensor cGAS in both primary tumors and metastatic lesions. Interestingly, miR-30d overexpression does not increase proliferation of breast cells (V. Capaci personal communication), moreover my data indicate that miR-30d depletion does not affect either cell growth or viability. This suggests that the increased growth advantage of miR-30d expressing tumors, as compared to those where miR-30d was inhibited, could be likely due to cell-extrinsic signaling, rather than to an intrinsic proliferative advantage. In fact, increasing evidence supports important roles of miR-30d in influencing the TME. Our research group demonstrated that miR-30d-dependent release of a pro-malignant secretome contributes to generate a permissive tumor microenvironment. In addition, it has been shown that miR-30d, in cluster with miR-30b, targets and downregulates the GalNAc transferase GALNT7 in human melanoma, resulting in increased synthesis and secretion of the immunosuppressive cytokine IL-10, which in turn both reduces the recruitment of $CD3^+$ T cells and increases tumor-promoting Treg cells at metastatic sites[204].

The obtained data are also consistent with a role of miR-30d in blocking immune surveillance in a non-cell autonomous fashion, by inhibiting the release in the TME of immunostimulatory chemokines and proinflammatory cytokines downstream of cGAS/STING signalling. My findings lead to the speculation that suppression of the STING-TBK1-IRF3 pathway by miR-30d may render tumors immunologically "cold", thereby allowing cancer cells that express high levels of miR-30d to grow in an immunologically unrestricted manner. In support of this hypothesis, analysis of TCGA data indicated that miR-30d is found overexpressed in tumor types that are commonly considered cold, i.e. breast, pancreas, and prostate[210,211]. Moreover, I found that in human BCs high expression levels of miR-30d correlated with lower expression of STING-dependent gene signature, as well as lower immune cell recruitment. Intriguingly, miR-30d has been shown to be secreted by various cell types in both physiological and pathological processes[205,206]. Secreted miRNAs have been shown to affect several oncogenic processes, among which invasion (miR-10b), activation of fibroblasts (miR-155), angiogenesis (miR-21, miR-494,

miR-9, miR-210), and modulation of immune response (miR-126, miR-34a, and others)[138,236]. Therefore, it would be interesting to explore the potential ability of cancer-secreted miR-30d to control cell populations within the TME in a paracrine fashion.

In sum, my future aim is to understand whether miR-30d might play paracrine effects in promoting cancer immune escape, and to explore the possibility that miR-30d, by dampening innate immune signaling in both cancer and stromal cells, could represent a tractable target whose inhibition may sensitize tumors to combined chemo- and immune therapy. In this respect, I plan to perform experiments in immunocompetent mouse models of BC to test whether miR-30d inhibition might reactivate immune surveillance and promote BC eradication. Specifically, I intend to investigate the impact of miR-30d depletion on primary and metastatic tumor growth, analyzing the effects on the tumor immune microenvironment by characterizing both anti-tumor and immuno-suppressive immune cell populations composing the tumor immune infiltrate, as well as to assess the possible involvement of the cGAS-STING pathway in these events. Furthermore, I also plan to test *in vivo* synergies between miR-30d inhibition and cGAS/STING-inducing chemotherapeutic treatments. Indeed, in this thesis I have shown that miR-30d inhibition may synergize with Doxorubicin, a DNA damage-inducing and STING-activating chemotherapeutic treatment. miRNA-based drugs have recently been hailed as therapeutic candidates for the treatment of a number of diseases, including cancer[237]. For instance, MRX34 is a synthetic miRNA mimic of the tumor suppressor miR-34, which represents the first miRNA to enter clinical trials and has shown convincing clinical results as a single-agent therapy in patients with melanoma, renal, and hepatocellular carcinoma[238]. MRG-106, an anti-miR-155 LNA, is currently in phase II clinical trials for the treatment of lymphomas and leukemias[239], while RGLS5579, an anti-miR-10, was recently announced for the treatment of glioblastoma multiforme[240]. Remarkably, this evidence implies that miRNA-based drugs may represent effective therapeutics not only for hematological cancers but also for treatment of solid tumors, which are typically more difficult to treat due to drug delivery and off-targeting issues. Moreover, these drugs might also be combined with STING agonists, which are currently being tested in clinical trials alone or in combination with a range of chemotherapeutic and immunotherapeutic drugs[241], and tested for their potential ability to sensitize poorly responsive tumors to immune checkpoint inhibitors.

In addition to BC, oncogenic roles of miR-30d have been reported in a wide range of tumors, including immunologically "cold" tumors[199–201,203]. Importantly, my results indicate that miR-30d inhibition induces IFN-I response genes in cell lines of different tumor origin, including colon and melanoma. In these contexts, the MIR-30D gene has been reported to be frequently amplified and overexpressed and its expression has been clearly associated with aggressive neoplastic features.

Indeed, miR-30d has been shown to promote invasion and migration of tumor cells in a xenograft model of colon cancer[202], while in melanoma cells it has been shown to exert an immune-suppressive role[204]. However, miR-30d has also been described to exert tumor suppressive roles, and these different behaviors might be due to expression of different sets of mirR-30d target genes in specific tumor contexts. For instance, high levels of miR-30d have been shown to inhibit ovarian cancer cell proliferation by promoting cell apoptosis through targeting Smad2, a protein involved in TGF-β signalling[198]. Furthermore, miR-30d was shown to prevent cell proliferation, invasion and migration in non-small cell lung cancer (NSCLC) by targeting the CCNE2 oncogene[242]. Interestingly, in lung carcinoma, although there is evidence attributing a tumor suppressor role to miR-30d, I have observed that its depletion results in induction of IFN-I signalling. This data suggests that reduced levels of miR-30d may favor the induction of the cGAS/STING/IFN-I pathway regardless of whether it plays oncogenic or tumor suppressive roles acting on different cellular pathways.

In perspective, the possibility to analyze miR-30d levels in cancer patients could help guiding treatment options, also taking into account that miR-30d is secreted in blood and may therefore be easily detected in liquid biopsies as a non-invasive diagnostic and prognostic cancer biomarker[149,150,243]. Remarkably, I found that miR-30d blood levels increase during BC and mBC progression and correlate with the size of the primary tumor in mice. I plan to monitor blood miR-30d levels also in BC patients and to correlate them with therapy response.

In conclusion, the results of this thesis provide further insight into the tumorigenic mechanisms that contribute to shaping a permissive TME during cancer progression. I found that ablation of miR-30d promotes the activation of cGAS/STING/IFN-I signalling in tumor cells resulting in the production of type-I interferons, which likely engage immune surveillance. I foresee that this study may prelude to preclinical research aimed at investigating the role of miR-30d in promoting an immune-cold, cancer-promoting tumor microenvironment, and testing whether depletion of miR-30d in both cancer cells and TME may stimulate innate immune signalling to restore an immunologically “hot” TME and limit tumor outgrowth.

6. Materials and methods

6.1 Cell culture and transfection

Cell lines

MCF10A is a normal human mammary cell line, whereas MCF10.DCIS.com is a ductal adenocarcinoma in situ cell line derived from RAS-mutated MCF10A cells[213], both expressing wtp53. MCF10A and MCF10.DCIS.com cells were maintained in Dulbecco'sModified Eagle's Medium (DMEM)/F12 (LONZA) (1:1) supplemented with 5% Horse Serum (HS), 100U/mL penicillin and 10µg/mL streptomycin, 20 ng/ml recombinant human epidermal growth factor (EGF), 10 µg/ml recombinant human insulin, 500 ng/ml hydrocortisone. MCF7 and MDA-MB-231 are human metastatic breast cancer cell lines expressing respectively wild-type p53 and missense mutant $p53^{R280K}$. MCF7 cells were cultured in Eagle's Minimum Essential Medium (EMEM, Sigma) supplemented with Fetal Bovine Serum (FBS), 100U/mL penicillin, 10µg/mL streptomycin, 1% Minimum essential medium non-essential amino acids (MEM NEAA), and 10µg/ml recombinant human insulin. MDA-MB-231 cells were cultured in Dulbecco's Modified Eagle's Medium (DMEM, LONZA) supplemented with 10% Fetal Bovine Serum (FBS) 100U/mL penicillinand 10µg/mL streptomycin.

4T1 is a p53-null mouse metastatic breast cancer cell line maintained in Dulbecco's Modified Eagle's Medium (DMEM)/F12 (LONZA) (1:1) supplemented with 10% Fetal Bovine Serum (FBS), 100U/mL penicillin, 10µg/mL and streptomycin.

H1299 is a p53-null non-small cell lung carcinoma (NSCLC) cell line, whereas WM115 is human metastatic melanoma cell line expressing wtp53, both were cultured in RPMI medium (Lonza) supplemented with 10% FBS. HCT-116 a human colorectal carcinoma cell line expressing wtp53 was maintained in DMEMsupplemented with 10% Fetal Bovine Serum (FBS) 100U/mL penicillin and 10µg/mL streptomycin.

HEK-293T and HEK-293GP human embryonic kidney cell lines were cultured in DMEM supplemented with 10% Fetal Bovine Serum (FBS) 100U/mL penicillin and 10µg/mL streptomycin. HEK-Blue IFN-α/β is a human embryonic kidney cell line specifically designed to monitor the levels of IFN-α/β in the conditioned medium (InvivoGen). These cells were maintained in DMEM, 4.5 g/l glucose supplemented with 2 mM L-glutamine, 10% heat-inactivated FBS, Pen-Strep (100 U/ml-100 µg/ml), 100 µg/ml Normocin, 30 µg/ml of blasticidin and 100 µg/ml of Zeocin.

Mouse and human cell lines were obtained from ATCC, InvivoGen or other laboratories collaborating on the project. Cells were all mycoplasma free.

Generation of mouse Mammary Tumor Organoid Cultures

Primary BC organoids were generated from tumor-bearing MMTV-PyMT mice. Metastatic BC organoids were generated from spontaneous lung metastases developed in Balb/c mouse after injection of 4T1 cells in the mammary fat pad of syngenic Balb/c mice.

For organoid generation, primary BCs and lung metastases were mechanically processed until small portions (1 mm^3) were obtained and these were then enzymatically digested for 3 hours at 37°C with a solution containing collagenase/hyaluronidase (Collagenase/Ialuronidase 10X in DMEM, Stem Cell). At the end of the digestion, the enzymes were inactivated by adding Advanced DMEM/F-12 medium (Ad-DF, Gibco). Red blood cells were eliminated by diluting NH_4Cl (4:1) in Hank's Balanced Salt Solution (HBSS). After 2 washes in HBSS, cells were enzymatically digested for 2/5 minutes with a solution containing trypsin (0.25%, TrypLE Express 1X, Gibco) and EDTA (0.01 M in PBS). Next, cell aggregates were incubated for 1 minute with a solution containing Dispase (5 U/mL, Stem Cell) and DNase-I (SigmaAldrich). When tissue processing is completed, approximately 1x10^6 epithelial cells were obtained from a mouse. Cells were resuspended in Matrigel (MATRIGEL® Matrix, Corning 356231) and plated in 24-well multiwells pre-warmed for 1 hour at 37°C. When Matrigel was solidified, Ad-DF medium containing Glutamax 1%, 50 μg/mL Primocin, 100U/mL penicillin, 10μg/mL streptomycin,10mM Hepes, and supplemented with the growth factors EGF (5ng/mL, Peprotech), B27 50X (1X, Gibco), and FGF basic (20 ng/mL, Peprotech).

Mouse BC organoids were maintained in Matrigel and in Ad-DM medium with the above supplementations. Organoids ≥ 50μm were counted by using brightfield microscopy.

In order to select 4T1 metastatic cells out of healthy lung cells, I grew metastatic BC organoids in presence of the purine analog 6-thioguanine (Sigma; A4882-250MG).

Transfections and viral transduction

Cells were transfected when the culture reached 50-80% confluence. For plasmid DNA transfections, the appropriate amount of DNA, depending on the total surface of the culture vessel, was used together with Lipofectamine LTX transfection reagents, following manufacturer's instructions. For siRNA and LNA-miRNA-inhibitor transfections, cells were transfected with

40nM siRNA oligonucleotides (Eurofins Genomics) or 20nM LNA-miRNA inhibitor (QIAGEN) together with Lipofectamine RNAiMax (Life technologies) in antibiotic-free medium according to manufacturer's instructions. As negative control siRNA the Qiagen AllStars Negative Control was used. Sequences of siRNAs/mimic/miRNA-inhibitors are reported below.

For organoid transfection, organoids were enzymatically digested at the single-cell level with TrypLE solution, transfected in suspension for 5 hours with 20nM LNA-miRNA inhibitor (QIAGEN) together with Lipofectamine RNAiMax (Life technologies) in antibiotic-free medium, then resuspended in Matrigel and plated in 24-well multiwells.

For retrovirus production, low-confluence HEK-293GP packaging cells were transfected using PEI 2X(1mg/ml) the appropriate plasmids in combination with the pMD2.G packaging vector. For lentivirus production, low-confluence HEK-293T packaging cells were transfected using calcium phosphate with the appropriate plasmids in combination with the pMD2.G and ps-PAX2 packaging vectors. After 48–72 h the virus-containing medium was collected and filtered with 0.45 µM syringe filter to remove cellular debris and was added to the target cells, which were then selected with puromycin (Sigma-Aldrich) and/or blasticidin (InvivoGen) 2 µg/ml each.

DNA constructs

- The lentiviral vector pTWEEN-EGFP-3'UTR (TW3) empty was kindly provided by R. De Maria, and the miR-30d decoy was cloned as described by Bonci et al [214]. Briefly, I engineered the empty vector by cloning two antisense sequences for miR-30d between the Xho-I and XbaI restriction sites located in the 3'UTR, thus obtaining the TWEEN-EGFP-decoy-miR-30d vector (referred to in the thesis as Decoy-30d).

  miR-30d decoy cloned sequence:

  FW: 5'-TCGAGCTTCCAGTCGGGGATGTTTACAAGAGAACTTAGAGAACTTCTTCCAGTCGGGGATGTTTACAT -3 '
  REV: 5'- CTAGATGTAAACATCCCCGACTGGAAGAAGTTCTCTAAGTTCTCTTGTAAACATCCCCGACTGGAAGC -3 '

- pTRIP-CMV-tagRFP-FLAG-cGAS lentiviral vector (Addgene #86676), encodes the DNA sensor, cGAS, associated with the red fluorescent protein (RFP).
- The lentiviral vector encoding the IRF3-GFP protein was kindly provided by ICGEB collaborators. It was generated by cloning the transcription factor IRF3 labeled with enhanced green fluorescent protein (eGFP) into a pWPI-based lentiviral vector (LV) as described by Maistriau et al [223].

Generation of stable cell lines

4T1 cells with stable inhibition of miR-30d were then obtained by lentiviral transduction with the Decoy-miR-30d construct: TWEEN-EGFP-decoy-miR-30d vector (see below). As a control, 4T1

cells were stably transduced with TWEEN-3'UTR-EGFP empty. Infected cells were selected using puromycin (Sigma-Aldrich) 2,5 µg/mL for at least one week.

Oligonucleotide	***Sequence***	***Manufacturer***
siSTING (human)	GCAUUACAACAACCUGCUA	Ambion
siDGKZ (human)	GAGGAACGACUUCUGUAAG	Eurofins MWG
MiRCURY Control LNA-miRNA inhibitor	Control A ACGTCTATACGCCCA	QIAGEN (#YCI0202524-DDA)
MiRCURY LNA-miR-30d inhibitor	mmu-miR-30d-5p GTCGGGGATGTTTAC	QIAGEN (#YCI0201748-DDA)

Viability ATPlite assay

After trypsinization, 4T1 cells were resuspended and seeded in 96-multi-well view-plate at a concentration of $4x10^3$ cells per well. Forty-eight hours after seeding, growing medium was removed and 4T1 cells were assayed for viability using ATPlite™ OneStep reagent (Perkin Elmer), according to the manufacturer's instructions. Luminescence intensity was measured using EnSpire plate fluorometer (Perkin Elmer). 3 biological replicates were performed, and for each experiment 2 technical replicates (2 wells) were used.

Measurement of IFNα/β levels in the conditioned medium

HEK-Blue IFN-α/β cell suspension (InvivoGen hkb-ifnab) was diluted at ~280,000 cells/ml and 180 µl were aliquoted to each well of a 96-well cell culture plate. Next, 20 µl of either conditioned medium, positive control (recombinant human IFN-β (103 U/ml)), or negative control (fresh culture medium) were added to each well. Reactions were incubated overnight at 37 °C in 5% CO2. At the end, 20µl of culture supernatant was added to 180µl of QUANTI-Blue solution (InvivoGen, rep-qbs) in a separate microplate that was incubated at 37°C for 30–180 min. Expression of the reporter protein SEAP was quantitated at 640 nm using a spectrophotometer (https://www.invivogen.com/hek-blue-ifn-ab#citations).

Commercial chemical reagents

The following compounds were used: VE-821 ATR-inhibitor (Sigma SML1415-5MG), Etoposide (Sigma E1383), Doxorubicin (Sigma D1515), Dasatinib (Selleck Chemicals S1021), 5-fluorouracil (Teva 51-21-8) and DMSO (Sigma Aldrich D4540). Treatments lasted as described in figure

legends.

6.2 Protein analyses

Protein extraction

Total cell extracts were lysed with Lysis Buffer (50mM Tris-HCl pH 7.5, 300mM NaCl, NP-40 1%, EDTA 1mM, all from Sigma-Aldrich) supplemented with PMSF 1 mM (Sigma-Aldrich), NaF 5mM (Sigma-Aldrich), Na_3VO_4 1mM (Sigma-Aldrich), 10μg/ml CLAP (Sigma-Aldrich). Protein concentration was determined with Bio-Rad Protein Assay Reagent (Bio-Rad). All the samples were then denatured in Laemmli Sample Buffer 2x or 6X and finally by heating at 95 °C for 5 min.

Western Blot analysis

Lysates were resolved by SDS-PAGE and transferred to nitrocellulose membranes (Amersham). Blocking was performed in Blotto-tween (PBS, 0.2% Tween-20, not fat dry milk 5%) or with TBST (0.2% Tween-20, Tris/HCl 25 mM pH 7.5) plus 5% not fat dry milk or 5% BSA (PanReac Applichem) depending on the antibody. Anti-mouse and anti-rabbit HRPO- conjugated (Sigma-Aldrich) were used as secondary antibodies. Membranes were analyzed by chemiluminescence using Pierce ECL™ Western Blotting Substrate or Pierce ECL™ Plus Western Blotting Substrate. Bands were quantified by densitometry of autoradiographic films using FIJI software[244].

The following primary antibodies with corresponding working concentrations were used:

cGAS (1:1000 Cell Signalling technology 15102), phospho S172-TBK1 (Cell Signalling technology 5483S), TBK1 (1:1000 Cell Signalling technology 3504), phospho S366-STING (1:1000 Cell Signalling technology 19781), STING (D2P2F) (1:1000 Cell Signalling technology 13647S), GFP (1:1000 Cell Signalling technology 2955), and HSP90 (1:10000 Santa Cruz sc-13119).

6.3 Imaging

Immunofluorescence analysis (IF)

For immunofluorescence analysis cells were fixed in 4% paraformaldehyde for 20 minutes, washed in phosphate buffered saline (PBS), permeabilized with 0.1% Triton X-100 for 10 minutes and blocked in 3% Fetal Bovine Serum (FBS)/PBS for 30 minutes. Antigen recognition was performed by incubation with primary antibody at 4°C for 14 h and with secondary antibodies (goat anti-

mouse, and goat anti-rabbit Alexa Fluor 488, 568, 647, Life Technologies) at 37°C for 1 h. Nuclei were counterstained with DAPI (Sigma Aldrich 32670-F) incubating for 15 min. The following antibodies and working concentrations were used for immunofluorescence analysis: cGAS (1:100 Cell Signalling technology 15102), phospho S172-TBK1 (1:50 Cell Signalling technology 5483), γH2AX (1:200 Millipore 05-636), dsDNA (1:1000 Abcam ab27156), β-catenin (1:100 Santa Cruz sc-7199), and GM130 (1:200 BD Biosciences 610822). Images were acquired with a ZEISS LSM 880 confocal microscope using x60 objective.

Tissue staining and immunohistochemical analysis (IHC)

Immunohistochemistry was carried out on FFPE mouse tissue sections. Briefly, sections 4 micron-thick were cut from paraffin blocks, dried, de-waxed, and rehydrated. Novocastra Epitope Retrieval Solution (pH6 or pH 9) was used to unmask antigens in a thermostatic bath at 98°C for 30 min. Subsequently, the sections were brought to room temperature and washed in PBS. After neutralization of the endogenous peroxidases with 3% H_2O_2 and Fc blocking by 0.4% casein in PBS (Novocastra), sections were incubated with primary antibodies cGAS (Cell Signalling technology 15102) for 90 minutes at room temperature or γ-H2AX (Abcam ab11174) overnight at 4°C in accordance with the manual's instructions. The immunostaining was revealed by a polymer detection method (Novolink Polymer Detection Systems Novocastra Leica Biosystems Newcastle Ltd Product No: RE7280-K) and 3,3'-diaminobenzidine (DAB) substrate-chromogen (ThermoScientific). Images were acquired with x40 and x60 objectives in the DM4000B microscope (Leica) using Leica Application Suite 4.12 software.

IHC staining were performed by postdoctoral researcher Valeria Cancila from C. Tripodo's Lab at the University of Palermo

6.4 Nucleic acids analyses

RNA extraction and qRT-PCR

Cells were harvested in Qiazol lysis reagent (Qiagen) for total RNA extraction, and contaminant DNA was removed by DNase treatment. Quantitative real time PCR (qRT-PCR) analyses were carried out on cDNAs retrotranscribed with iScript™ Advanced cDNA Synthesis Kit (Biorad 172-5038) and analyzed genes were amplified using SsoAdvancedTMSYBR® Green Master Mix (Biorad) on a CFX96™ Real-Time PCR System (Biorad). Histone 3 (H3) was used as reference gene in human cell lines while GADPH were used for mouse cell lines.

For the analysis of extracellular miRNA expression, 1 ml of culture medium or 50 µl or mouse sera

were diluted 1: 5 Qiazol previously added with cel-39 miRNA mimic (0.1 nM) according to the manufacturer's instructions. For RNA extraction from mice sera, RNeasy MinElute Cleanup Kit (Qiagen) was used. Intracellular and extracellular miRNAs were retrotranscribed and amplified with the miScript PCR system (Qiagen) following the manufacturer's instructions. RNU6B and SNORD25 small nuclear RNA and cel-39 miRNA mimic were respectively used as the housekeeping control genes for intracellular and extracellular miRNAs.

The data were analyzed with the Biorad CFX Manager software. Experiments were performed at least three times, and each sample is the average of a technical duplicate. The quantification is based on the $2^{-\Delta\Delta Ct}$ method using the proper housekeeping gene levels as normalization reference.

PCR primer sequences are thefollowing:

qPCR primers miRNA		
Gene target	***Accession numbers miScript***	***Catalog Numbers (Qiagen)***
SNORD25	NR_002565.1	MS00014007
RNU6B	NR_004394.1	MS00014000
Cel_miR-39_1	MIMAT0000010	MS00019789
hsa-miR-30d	MI0000255	MS00009387
qPCR primers mRNAs		
Gene target	**Primer sequence**	**Direction**
hCAPZA1	AATGAAGCCCAAACTGCCAA	FW
hCAPZA1	TTCCAGTCGATTTTGGTGCG	REV
hDGKZ	AGCAGTACTGTGTAGCCAGGAT	FW
hDGKZ	CACGGAAGGACGGCTTACAG	REV
hH3	GAAGAACCTCATCGTTACAGGCCTGGT	FW
hH3	CTGCAAAGCACCAATAGCTGCACTCTGGAA	REV
hIFI44	CCA CCG AGA TGT CAG AAA GAG	FW
hIFI44	TGG TAC ATG TGG CTT TGC TC	REV
hIFIT1	CCTCAGTCTTGCAGCCTCTC	FW
hIFIT1	TCACCATTTGTACACATCTCCACT	REV
hIFNα	ACTCATACACCAGGTCACGC	FW
hIFNα	GCAGGGGTGAGAGTCTTTGAA	REV
hIFNβ1	AGTAGGCGACACTGTTCGTG	FW
hIFNβ1	GCCTCCCATTCAATTGCCAC	REV
hISG15	GGTGGACAAATGCGACGAAC	FW
hISG15	TCGAAGGTCAGCCAGAACAG	REV
hKLHL20	GTGATGGCCTGGGTCAAATAC	FW
hKLHL20	GGGATCAGAGCCTACTGTGC	REV
hOAS1	GATTCTGCTGGCTGAAAGCAA	FW
hOAS1	CTGGGATCGTCGGTCTCATC	REV

hSNX16	GCACTTCCTCCAAAACGCTG	FW
hSNX16	AAATGGACCCGGTGGATCAT	REV
hSTING	CTTCACTTGGATGCTTGCC	FW
hSTING	CCCGTAGCAGGTTGTTGTAATG	REV
mBST2	TGTTCGGGGTTACCTTAGTCA	FW
mBST2	GCAGGAGTTTGCCTGTGTCT	REV
mGAPDH	ATCCTGCACCACCAACTGCT	FW
mGAPDH	GGGCCATCCACAGTCTTCTG	REV
mIFIT1	CCAAGTGTTCCAATGCTCCT	FW
mIFIT1	GGATGGAATTGCCTGCTAGA	REV
mIFIT2	AGTACAACGAGTAAGGAGTCACT	FW
mIFIT2	AGGCCAGTATGTTGCACATGG	REV
mIFNα	GGATGTGACCTTCCTCAG ACTC	FW
mIFNα	ACCTTCTCCTGCGGGAATCCAA	REV
mIFNβ1	CTGGCTTCCATCATGAACAA	FW
mIFNβ1	AGAGGGCTGTGGTGGAGAA	REV
mIRF7	CCTCTTGCTTCAGGTTCTGC	FW
mIRF7	GGAGCCTGTGGTGGGAC	REV
mISG15	AGCAATGGCCTGGGACCTAA	FW
mISG15	CACGGACACCAGGAAATCGT	REV
mMX1	GACCATAGGGGTCTTGACCAA	FW
mMX1	AGACTTGCTCTTTCTGAAAAGCC	REV

6.5 *In vivo* experiments

Generation of mouse BC models

- 4T1-Luc cells were generated by infection with a lentiviral vector encoding the firefly luciferase (Photinus pyralis) and were injected in the mammary fat pad of six- to eight-week-old syngeneic Balb/c mice. Five weeks after inoculation mice were sacrificed and peripheral blood was collected. This experiment was performed in collaboration with Alessandro Zannini and Camilla Tombari, post-doctoral researchers in our laboratory
- 4T1 cells overexpressing mutp53 R280K were injected in the mammary fat pad of syngeneic Balb/c mice. After 4 days of inoculation, mice were treated for the next 24 days with Dasatinib 10mg/kg (every 2 days) or 5-FU 25mg/kg (every day). These drugs were administered by intraperitoneal injection. Four weeks after inoculation mice were sacrificed and peripheral blood was collected. This experiment was performed in collaboration with R. Sommaggio and A. Rosato at IOV Padova.

Procedures involving animals and their care were in conformity with national (D. L. 26/2014 and

subsequent implementing circulars) and international (EU Directive 2010/63/EU for animal experiments) laws and policies, and the experimental protocol was approved by the Ethical Committee of the University of Padua (CEASA) and by the Italian Ministry of Health.

In vivo quantification of luciferase

Tumor masses generated following the inoculation of 4T1-Luc cells in syngenic Balb/c mice were monitored at different time points by whole-body bioluminescent imaging. Briefly, anesthetized animals (1–3% isoflurane, Merial Italia S.p.A, Italy) were given the substrate D-Luciferin (Biosynth AG, Switzerland) by intraperitoneal injection at 150 mg/kg in PBS (Sigma). The light emitted from the bioluminescent tumors or metastasis was detected using a cooled charge-coupled device camera mounted on a light-tight specimen box (IVIS Lumina II Imaging System; Caliper Life Sciences, Alameda, CA). Regions of interest from the displayed images were quantified as total photon counts (photon/s) using Living Image® software (Xenogen).

Collection of sera from mice

Peripheral blood was collected and immediately processed to recover the sera. It was first incubated at 37° C for 30 minutes to allow coagulation, and after two successive centrifugations at 4,000 rpm for 10 minutes at 4 ° C the serum was recovered. The sera collected in this way were stored at -80 ° C until they were used.

6.6 Omics data analyses and statistics

miR-30d microarray data analyses

RNAseq data from two GEO archives were analyzed: GSE133410[194] and GSE27718[204]. The first dataset includes MDA-MB-231 cell line stably transduced with the decoy construct for miR-30d and the matching control cells, each in biological triplicate. The second dataset includes 2 different melanoma cell lines, namely 4L and 5B1 cells, either with over-expressed miR-30d or matching control, each in four biological replicates.

Raw gene counts were downloaded from the two aforementioned repositories. Differentially expressed genes were obtained using the *limma* package (version 3.5.2;[245]). The input ranked gene list for the GSEA (version 4.3.2) software was retrieved subsetting the column "*t*" (statistical-corrected logFC) from the result table of *limma* (retrieved using the function *topTable)*. The GSEAPreranked analysis was performed by selecting the GO terms from GOBP database with as parameters: 1000 permutations and No_Collapse to gene symbols. The barplot in Figure 8a was

made using the R package *ggplot2* (version 3.4.0). The enrichment plots in Figure 8b and 8c were made by using the R package *fgsea* (version 1.22;[246]). All analyses were performed using R 4.2.2 and publicly available packages explicitly cited inthe manuscript. No custom functions were written for the analysis. From the GSEA results, I selected as differentially enriched GO terms the ones with a p.val<0.05.

The signature genes were obtained from The Molecular Signatures Database (MSigDB; http://software.broadinstitute.org/gsea/msigdb/).

These analyses were performed by Luca Triboli, graduate student in the lab.

TCGA gene expression dataset

The TCGA breast cancer dataset (TCGA-BRCA) was downloaded from the Genomic Data Commons Portal using functions of the *TCGAbiolinks* R package (version 2.23.1;[247]). Raw counts were normalized to z-score subtracting the mean expression across samples and diving it for the standard deviation of every single gene. The TCGA patients were divided into high and low miR-30d expression levels based on the z-score (high if >0 and low if <0). The enrichment plot in Figure 7d has been done using the R package fgsea[246] on all the immune gene signatures from MsigDB.

The boxplot of the Figure 24a has been derived summing the normalized expression (in z-score) of the genes from the signature "Reactome STING Mediated Induction of host Immune Response".

The ImmuneScore from the Figure 24b has been obtained using the function *xCellAnalysis* from the R package *xCell* (version 1.1.0;[248]). The boxplot was made using the R package *ggplot2* (version 3.4.0).

The signature genes were obtained from The Molecular Signatures Database (MSigDB; http://software.broadinstitute.org/gsea/msigdb/).

These analyses were performed by Luca Triboli, graduate student in the lab.

Statistics and reproducibility

All the experiments are representative of at least three independent replicates. For each blot and IF I showed the representative image of experiments performed with similar results at least three independent times. All graphs represent single data point mean ± SEM. Statistical tests were performed using GraphPad Prism8. P values were obtained using two-tailed Student's t-test with a 95% confidence threshold or using One-way ANOVA followed by Tukey's comparison test ($\alpha<0.05$) as indicated in figure legends.

7. List of abbreviations

APC	antigen-presenting cell
α-SMA	alpha smooth muscle actin
BC	breast cancer
BMDC	bone-marrow-derived cell
CAF	cancer-associated fibroblast
CCL	CC-chemokine ligand
cGAMP	cyclic GMP-AMP
cGAS	cyclic GMP-AMP synthase
CM	conditioned medium
CTL	Cytotoxic T lymphocites
CXCL	CXC-chemokine ligand
DC	dendritic cell
Decoy-30d	decoy construct for miR-30d
dsDNA	double-strand DNA
DTC	dormant tumor cells
ECM	extracellular matrix
EGF	epidermal growth factor
EMT	epithelial-to-mesenchymal transition
ER	endoplasmic reticulum
FAK	focal adhesion kinase
FBS	fetal bovine serum
GA	Golgi apparatus
GAPDH	glyceraldehyde 3-phosphate dehydrogenase
GFP	green fluorescent protein
GM-130	Golgi matrix protein 130
GO	gene ontology
GOF	gain of function
GSEA	gene set enrichment analysis
HIF	hypoxia-inducible factor
HLA	human leukocyte antigen

IF	immunofluorescence
IFN	Interferon
IHC	immunohistochemical
IL	interleukin
IRF	interferon response factor
ISGs	interferon stimulated genes
JAK1	Janus kinase 1
KD	knockdown
KO	knockout
LNA	locked nucleic acid
LOX	lysyl oxidase
mBC	metastatic breast cancer
MDSC	myeloid-derived suppressor cell
miRNA	microRNA
MMP	matrix metalloproteinase
mRNA	messenger RNA
mut-p53	mutant p53
NF-κB	Nuclear factor κB
NK	natural killer cell
NLS	nuclear localization signal
PD-1	Programmed cell death 1
PDGF	platelet-derived growth factor
PD-L1	programmed-death ligand
PMN	pre-metastatic niche
qRT-PCR	quantitative real-time PCR
ROS	reactive oxygen species
SASP	senescence associated secretory phenotype
siRNA	small interfering RNA
STAT	signal transducer and activator of transcription
STING	Stimulator of interferon genes
TAM	tumor-associated macrophage
TAZ	transcriptional coactivator with a PDZ-binding domain
TBK1	TANK-binding kinase 1
TECs	tumor endothelial cells

TGF	transforming growth factor
TME	tumor microenvironment
TNF	tumor necrosis factor
Treg	T regulatory cells
UTR	untranslated region
VEGF	vascular endothelial growth factor
WT	wild type
YAP	yes-associated protein

8. Acknowledgments

The project presented in this thesis was carried out at the International Centre for Genetic Engineering and Biotechnology (ICGEB, Trieste) under the supervision of Prof. Giannino Del Sal, whom I thank for giving me the opportunity to work in his lab during these three years.
I am deeply grateful to Prof. Fiamma Mantovani for following me with expertise during my scientific growth in the lab and for the critical discussions and corrections of the thesis.
Important contributions to this work were given by: Dr. Valeria Cancila (C. Tripodo's Lab at theUniversity of Palermo) who performed the IHC analysis and the graduate student Luca Triboli (G. Del Sal's Lab at the University of Trieste) who performed all bioinformatic analysis.
I'd like to thank Prof. Giorgio Scita and Prof. Fulvia Vascotto for kindly accepted to read this thesis.
A mention goes also to all past and present colleagues of Del Sal's laboratory team and all the colleagues at ICGEB for both helping and constantly encouraging me during my PhD. Among them, a special thanks to Dr. Camilla Tombari, who, before being a colleague, is a dear friend who have patiently supported me in these years, both in the lab and outside, and have strongly contributed to make my life happier and more cheerful.
Finally, I thank my parents, my sister, and my brother, to whom this thesis is dedicated, for pushing me to continue during these hard but exciting years.

9. References

1. Sanchez-vega, F. *et al.* Oncogenic Signaling Pathways in The Cancer Article Oncogenic Signaling Pathways in The Cancer Genome Atlas. 321–337 (2018) doi:10.1016/j.cell.2018.03.035.
2. Sever, R. & Brugge, J. S. Genetic and epigenetic mechanisms of cancer progression. *Cold Spring Harb Perspect Med2015;5a006098 21* (2015).
3. Lawson, D. A., Kessenbrock, K., Davis, R. T., Pervolarakis, N. & Werb, Z. Tumour heterogeneity and metastasis at single-cell resolution. *Nat. Cell Biol.* **20**, 1349–1360 (2018).
4. del Pozo Martin, Y. *et al.* Mesenchymal Cancer Cell-Stroma Crosstalk Promotes Niche Activation, Epithelial Reversion, and Metastatic Colonization. *Cell Rep.* **13**, 2456–2469 (2015).
5. Capaci, V., Mantovani, F. & Del Sal, G. Amplifying Tumor–Stroma Communication: An Emerging Oncogenic Function of Mutant p53. *Front. Oncol.* **10**, 1–9 (2021).
6. Gál, P. *et al.* How Signaling Molecules Regulate Tumor Microenvironment: Parallels to Wound Repair. *Molecules* **22**, 1–17 (2017).
7. Deepak, K. G. K. *et al.* Tumor microenvironment: Challenges and opportunities in targeting metastasis of triple negative breast cancer. *Pharmacol. Res.* **153**, 104683 (2020).
8. Mendes, B. B., Sousa, D. P., Conniot, J. & Conde, J. Nanomedicine-based strategies to target and modulate the tumor microenvironment. *Trends in Cancer* **7**, 847–862 (2021).
9. Humphrey, J. D., Dufresne, E. R. & Schwartz, M. A. Mechanotransduction and extracellular matrix homeostasis. *Nat. Rev. Mol. Cell Biol.* **15**, 802–812 (2014).
10. Setargew, Y. F. I., Wyllie, K., Grant, R. D., Chitty, J. L. & Cox, T. R. Targeting lysyl oxidase family meditated matrix cross-linking as an anti-stromal therapy in solid tumours. *Cancers (Basel).* **13**, 1–26 (2021).
11. Piersma, B., Hayward, M. K. & Weaver, V. M. Fibrosis and cancer: A strained relationship. *Biochim. Biophys. Acta - Rev. Cancer* **1873**, (2020).
12. Northey, J. J., Przybyla, L. & Weaver, V. M. Tissue force programs cell fate and tumor aggression. *Cancer Discov.* **7**, 1224–1237 (2017).
13. Mohammadi, H. & Sahai, E. Mechanisms and impact of altered tumour mechanics. *Nat. Cell Biol.* **20**, 766–774 (2018).
14. Xing, X. *et al.* Matrix stiffness-mediated effects on macrophages polarization and their LOXL2 expression. *FEBS J.* 0–1 (2020) doi:10.1111/febs.15566.
15. Stowers, R. S. *et al.* Matrix stiffness induces a tumorigenic phenotype in mammary epithelium through changes in chromatin accessibility. *Nat. Biomed. Eng.* **3**, 1009–1019 (2019).
16. Panciera, T. *et al.* Europe PMC Funders Group Reprogramming normal cells into tumor precursors requires ECM stiffness and oncogene-mediated changes of cell mechanical properties. **19**, 797–806 (2020).
17. Acerbi, I. *et al.* Human breast cancer invasion and aggression correlates with ECM stiffening and immune cell infiltration. *Integr. Biol. (United Kingdom)* **7**, 1120–1134 (2015).
18. Brauchle, E. *et al.* Biomechanical and biomolecular characterization of extracellular matrix structures in human colon carcinomas. *Matrix Biol.* **68**–**69**, 180–193 (2018).
19. Neesse, A., Algül, H., Tuveson, D. A. & Gress, T. M. Stromal biology and therapy in pancreatic cancer: A changing paradigm. *Gut* **64**, 1476–1484 (2015).
20. Kalluri, R. The biology and function of fibroblasts in cancer. *Nat. Rev. Cancer* **16**, 582–598 (2016).
21. Plikus, M. V. *et al.* Fibroblasts: Origins, definitions, and functions in health and disease. *Cell*

184, 3852–3872 (2021).
22. Barker, T. H. & Engler, A. J. The provisional matrix: setting the stage for tissue repair outcomes. *Matrix Biol.* **60**–**61**, 1–4 (2017).
23. Sahai, E. *et al.* A framework for advancing our understanding of cancer-associated fibroblasts. *Nat. Rev. Cancer* **20**, 174–186 (2020).
24. Ping, Q. *et al.* Cancer-associated fibroblasts: overview, progress, challenges, and directions. *Cancer Gene Ther.* **28**, 984–999 (2021).
25. Friedman, G. *et al.* Cancer-associated fibroblast compositions change with breast cancer progression linking the ratio of S100A4+ and PDPN+ CAFs to clinical outcome. *Nat. Cancer* **1**, 692–708 (2020).
26. Liao, Z., Tan, Z. W., Zhu, P. & Tan, N. S. Cancer-associated fibroblasts in tumor microenvironment – Accomplices in tumor malignancy. *Cell. Immunol.* **343**, 0–1 (2019).
27. Biffi, G. & Tuveson, D. A. Diversity and biology of cancerassociated fibroblasts. *Physiol. Rev.* **101**, 147–176 (2021).
28. Orimo, A. *et al.* Stromal fibroblasts present in invasive human breast carcinomas promote tumor growth and angiogenesis through elevated SDF-1/CXCL12 secretion. *Cell* **121**, 335–348 (2005).
29. Kim, S. K. & Cho, S. W. The Evasion Mechanisms of Cancer Immunity and Drug Intervention in the Tumor Microenvironment. *Front. Pharmacol.* **13**, 1–16 (2022).
30. Monteran, L. & Erez, N. The dark side of fibroblasts: Cancer-associated fibroblasts as mediators of immunosuppression in the tumor microenvironment. *Front. Immunol.* **10**, 1–15 (2019).
31. Davidson, S. *et al.* Fibroblasts as immune regulators in infection, inflammation and cancer. *Nat. Rev. Immunol.* **21**, 704–717 (2021).
32. Karta, J., Bossicard, Y., Kotzamanis, K., Dolznig, H. & Letellier, E. Mapping the metabolic networks of tumor cells and cancer-associated fibroblasts. *Cells* **10**, 1–25 (2021).
33. Lugano, R., Ramachandran, M. & Dimberg, A. Tumor angiogenesis: causes, consequences, challenges and opportunities. *Cell. Mol. Life Sci.* **77**, 1745–1770 (2020).
34. Hida, K., Maishi, N., Annan, D. A. & Hida, Y. Contribution of tumor endothelial cells in cancer progression. *Int. J. Mol. Sci.* **19**, 1–12 (2018).
35. Akino, T. *et al.* Cytogenetic abnormalities of tumor-associated endothelial cells in human malignant tumors. *Am. J. Pathol.* **175**, 2657–2667 (2009).
36. Al-Ostoot, F. H., Salah, S., Khamees, H. A. & Khanum, S. A. Tumor angiogenesis: Current challenges and therapeutic opportunities. *Cancer Treat. Res. Commun.* **28**, 100422 (2021).
37. Aguilar-Cazares, D. *et al.* Contribution of Angiogenesis to Inflammation and Cancer. *Front. Oncol.* **9**, 1–10 (2019).
38. Thomas, L. On immunosurveillance in human cancer. *Yale J. Biol. Med.* **55**, 329–333 (1982).
39. Vesely, M. D. & Schreiber, R. D. Cancer immunoediting: Antigens, mechanisms, and implications to cancer immunotherapy. *Ann. N. Y. Acad. Sci.* **1284**, 1–5 (2013).
40. Tay, R. E., Richardson, E. K. & Toh, H. C. Revisiting the role of CD4+ T cells in cancer immunotherapy—new insights into old paradigms. *Cancer Gene Ther.* **28**, 5–17 (2021).
41. Correia, A. L. *et al.* Hepatic stellate cells suppress NK cell-sustained breast cancer dormancy. *Nature* **594**, 566–571 (2021).
42. Ponzetta, A. *et al.* Neutrophils Driving Unconventional T Cells Mediate Resistance against Murine Sarcomas and Selected Human Tumors. *Cell* **178**, 346-360.e24 (2019).
43. Kim, H. J. & Cantor, H. CD4 T-cell subsets and tumor immunity: the helpful and the not-so-helpful. *Cancer Immunol. Res.* **2**, 91–98 (2014).
44. Ohue, Y. & Nishikawa, H. Regulatory T (Treg) cells in cancer: Can Treg cells be a new therapeutic target? *Cancer Sci.* **110**, 2080–2089 (2019).
45. Togashi, Y., Shitara, K. & Nishikawa, H. Regulatory T cells in cancer immunosuppression —

implications for anticancer therapy. *Nat. Rev. Clin. Oncol.* **16**, 356–371 (2019).
46. Ding, T., Yan, F., Cao, S. & Ren, X. Regulatory B cell: New member of immunosuppressive cell club. *Hum. Immunol.* **76**, 615–621 (2015).
47. Flynn, N. J., Somasundaram, R., Arnold, K. M. & Sims-Mourtada, J. The Multifaceted Roles of B Cells in Solid Tumors: Emerging Treatment Opportunities. *Target. Oncol.* **12**, 139–152 (2017).
48. Fleming, V. *et al.* Targeting myeloid-derived suppressor cells to bypass tumor-induced immunosuppression. *Front. Immunol.* **9**, (2018).
49. Cassetta, L. & Pollard, J. W. Targeting macrophages: Therapeutic approaches in cancer. *Nat. Rev. Drug Discov.* **17**, 887–904 (2018).
50. Wang, X., Qiu, L., Li, Z., Wang, X. Y. & Yi, H. Understanding the multifaceted role of neutrophils in cancer and autoimmune diseases. *Front. Immunol.* **9**, 1–10 (2018).
51. Vesely, M. D., Kershaw, M. H., Schreiber, R. D. & Smyth, M. J. Natural innate and adaptive immunity to cancer. *Annu. Rev. Immunol.* **29**, 235–271 (2011).
52. Nicolini, A., Ferrari, P., Rossi, G. & Carpi, A. Tumour growth and immune evasion as targets for a new strategy in advanced cancer. *Endocr. Relat. Cancer* **25**, R577–R604 (2018).
53. Eftekhari, R. *et al.* Study of the tumor microenvironment during breast cancer progression. *Cancer Cell Int.* **17**, 1–10 (2017).
54. Setrerrahmane, S. & Xu, H. Tumor-related interleukins: Old validated targets for new anti-cancer drug development. *Mol. Cancer* **16**, 1–17 (2017).
55. Cohen, N. *et al.* Fibroblasts drive an immunosuppressive and growth-promoting microenvironment in breast cancer via secretion of Chitinase 3-like 1. *Oncogene* **36**, 4457–4468 (2017).
56. Chomarat, P., Banchereau, J., Davoust, J. & Palucka, A. K. IL-6 switches the differentiation of monocytes from dendritic cells to macrophages. *Nat. Immunol.* **1**, 510–514 (2000).
57. Kuczek, D. E. *et al.* Collagen density regulates the activity of tumor-infiltrating T cells. *J. Immunother. Cancer* **7**, 1–15 (2019).
58. Larsen, A. M. H. *et al.* Collagen Density Modulates the Immunosuppressive Functions of Macrophages. *J. Immunol.* **205**, 1461–1472 (2020).
59. Robert, C. A decade of immune-checkpoint inhibitors in cancer therapy. *Nat. Commun.* **11**, 10–12 (2020).
60. He, X. & Xu, C. Immune checkpoint signaling and cancer immunotherapy. *Cell Res.* **30**, 660–669 (2020).
61. Park, S. Y. & Nam, J. S. The force awakens: metastatic dormant cancer cells. *Exp. Mol. Med.* **52**, 569–581 (2020).
62. Inoue, C. *et al.* PD-L1 induction by cancer-associated fibroblast-derived factors in lung adenocarcinoma cells. *Cancers (Basel).* **11**, 1–16 (2019).
63. Li, Z. *et al.* Cancer-associated fibroblasts promote PD-L1 expression in mice cancer cells via secreting CXCL5. *Int. J. Cancer* **145**, 1946–1957 (2019).
64. Nazareth, M. R. *et al.* Characterization of Human Lung Tumor-Associated Fibroblasts and Their Ability to Modulate the Activation of Tumor-Associated T Cells. *J. Immunol.* **178**, 5552–5562 (2007).
65. Rodríguez, J. A. HLA-mediated tumor escape mechanisms that may impair immunotherapy clinical outcomes via T-cell activation (Review). *Oncol. Lett.* **14**, 4415–4427 (2017).
66. Civril, F. *et al.* Structural mechanism of cytosolic DNA sensing by cGAS. *Nature* **498**, 332–337 (2013).
67. Ablasser, A., Goldeck, M., Cavlar, T., Deimling, T. & Witte, G. cGAS produces a 2′-5′-linked cyclic dinucleotide second messenger that activates STING. **498**, 380–384 (2013).
68. Sun, L., Wu, J., Du, F., Chen, X. & Chen, Z. J. Sun L, Wu J, Du F, Chen X, Chen ZJ (2013) Cyclic GMP–AMP synthase is a cytosolic DNA sensor that activates the type I interferon

pathway. Science 339(6121):786–791. *Science (80-.).* **339**, 786–791 (2013).
69. Gao, P. *et al.* Cyclic [G(2′,5′)pA(3′,5′)p] is the metazoan second messenger produced by DNA-activated cyclic GMP-AMP synthase. *Cell* **153**, 1094–1107 (2013).
70. Du, M. & Chen, Z. J. DNA-induced liquid phase condensation of cGAS activates innate immune signaling. *Science (80-.).* **361**, 704–709 (2018).
71. Zhang et al. Cyclic GMP-AMP Containing Mixed Phosphodiester Linkages Is An Endogenous High Affinity Ligand for STING. *Mol. Cell* **148**, 825–832 (2013).
72. Shang, G., Zhang, C., Chen, Z. J., Bai, X. chen & Zhang, X. Cryo-EM structures of STING reveal its mechanism of activation by cyclic GMP–AMP. *Nature* **567**, 389–393 (2019).
73. Bridgeman, A. *et al.* Viruses transfer the antiviral second messenger cGAMP between cells. *Science (80-.).* **349**, 1228–1232 (2015).
74. Gentili, M. et al. Transmission of innate immune signaling by packaging of cGAMP in viral particles. *Science (80-.).* **151**, 10–17 (2015).
75. Ishikawa, H., Ma, Z. & Barber, G. N. STING regulates intracellular DNA-mediated, type i interferon-dependent innate immunity. *Nature* **461**, 788–792 (2009).
76. Dobbs, N. *et al.* STING activation by translocation from the ER is associated with infection and autoinflammatory disease. *Cell Host Microbe* **18**, 157–168 (2015).
77. Tanaka, Y. & Chen, Z. J. STING specifies IRF3 phosphorylation by TBK1 in the cytosolic DNA signaling pathway. *Sci. Signal.* **5**, 1–12 (2012).
78. Zhang, C. *et al.* Structural basis of STING binding with and phosphorylation by TBK1. *Nature* **567**, 394–398 (2019).
79. Zhu, M., Fang, T., Li, S., Meng, K. & Guo, D. Bipartite Nuclear Localization Signal Controls Nuclear Import and DNA-Binding Activity of IFN Regulatory Factor 3. *J. Immunol.* **195**, 289–297 (2015).
80. Chattopadhyay, S. *et al.* Viral apoptosis is induced by IRF-3-mediated activation of Bax. *EMBO J.* **29**, 1762–1773 (2010).
81. Ishikawa, H. & Barber, G. N. STING is an endoplasmic reticulum adaptor that facilitates innate immune signalling. *Nature* **455**, 674–678 (2008).
82. de Oliveira Mann, C. C. *et al.* Modular Architecture of the STING C-Terminal Tail Allows Interferon and NF-κB Signaling Adaptation. *Cell Rep.* **27**, 1165-1175.e5 (2019).
83. Agalioti, T. *et al.* Ordered recruitment of chromatin modifying and general transcription factors to the IFN-β promoter. *Cell* **103**, 667–678 (2000).
84. Yum, S., Li, M., Fang, Y. & Chen, Z. J. TBK1 recruitment to STING activates both IRF3 and NF- κ B that mediate immune defense against tumors and viral infections. 1–9 (2021) doi:10.1073/pnas.2100225118/-/DCSupplemental.Published.
85. Gan, Y. *et al.* The cGAS/STING Pathway: A Novel Target for Cancer Therapy. *Front. Immunol.* **12**, 1–15 (2022).
86. Kwon, J. K. & Bakhoum, S. F. The cytosolic DNA-sensing cGAS–sting pathway in cancer. *Cancer Discov.* **10**, 26–39 (2020).
87. Dou, Z. *et al.* Cytoplasmic chromatin triggers inflammation in senescence and cancer. *Nature* **550**, 402–406 (2017).
88. Glück, S. *et al.* Innate immune sensing of cytosolic chromatin fragments through cGAS promotes senescence. *Nat. Cell Biol.* **19**, 1061–1070 (2017).
89. Yang, H., Wang, H., Ren, U., Chen, Q. & Chena, Z. J. CGAS is essential for cellular senescence. *Proc. Natl. Acad. Sci. U. S. A.* **114**, E4612–E4620 (2017).
90. Takasugi, M., Yoshida, Y., Hara, E. & Ohtani, N. The role of cellular senescence and SASP in tumour microenvironment. *FEBS J.* 1–14 (2022) doi:10.1111/febs.16381.
91. Woo, S. *et al.* STING-dependent cytosolic DNA. *Trends Immunol.* **41**, 830–842 (2015).
92. Diamond, M. S. *et al.* Type I interferon is selectively required by dendritic cells for immune rejection of tumors. *J. Exp. Med.* **208**, 1989–2003 (2011).

93. Marcus, A. *et al.* Tumor-Derived cGAMP Triggers a STING-Mediated Interferon Response in Non-tumor Cells to Activate the NK Cell Response. *Immunity* **49**, 754-763.e4 (2018).
94. Xia, T., Konno, H. & Barber, G. N. Recurrent loss of STING signaling in melanoma correlates with susceptibility to viral oncolysis. *Cancer Res.* **76**, 6747–6759 (2016).
95. Xia, Konno, and B. Deregulation of STING Signaling in Colorectal Carcinoma Constrains DNA-Damage Responses and Correlates With Tumorigenesis. *Methods Mol. Biol.* **176**, 139–148 (2016).
96. Song, S. *et al.* Decreased expression of STING predicts poor prognosis in patients with gastric cancer. *Sci. Rep.* **7**, 1–13 (2017).
97. John Kwon1, Samuel F. Bakhoum1, 2. The cytosolic DNA-sensing cGAS-STING pathway in cancer John. *Physiol. Behav.* **176**, 100–106 (2016).
98. Lemos, H. *et al.* STING promotes the growth of tumors characterized by low antigenicity via IDO activation myeloid-derived suppressor cell infiltration and IL-10 production in the TME. Depletion of CD8+ HHS Public Access. *Cancer Res* **76**, 2076–2081 (2016).
99. Ahn, J. *et al.* Inflammation-driven carcinogenesis is mediated through STING. *Nat. Commun.* **5**, 1–9 (2014).
100. Chen, Q. *et al.* Carcinoma-astrocyte gap junctions promote brain metastasis by cGAMP transfer. *Nature* **533**, 493–498 (2016).
101. Yum, S., Li, M., Frankel, A. E. & Chen, Z. J. Roles of the cGAS-STING pathway in cancer immunosurveillance and immunotherapy. *Annu. Rev. Cancer Biol.* **3**, 323–344 (2019).
102. Yum, S., Li, M. & Chen, Z. J. Old dogs, new trick: classic cancer therapies activate cGAS. *Cell Res.* **30**, 639–648 (2020).
103. Pantelidou, C. *et al.* Parp inhibitor efficacy depends on CD8+ T-cell recruitment via intratumoral sting pathway activation in brca-deficient models of triple-negative breast cancer. *Cancer Discov.* **9**, 722–737 (2019).
104. Motwani, M., Pesiridis, S. & Fitzgerald, K. A. DNA sensing by the cGAS–STING pathway in health and disease. *Nat. Rev. Genet.* **20**, 657–674 (2019).
105. Zhang, J., Hu, M. M., Wang, Y. Y. & Shu, H. B. TRIM32 protein modulates type I interferon induction and cellular antiviral response by targeting MITA/STING protein for K63-linked ubiquitination. *J. Biol. Chem.* **287**, 28646–28655 (2012).
106. Tsuchida, T. *et al.* The ubiquitin ligase TRIM56 regulates innate immune responses to intracellular double-stranded DNA. *Immunity* **33**, 765–776 (2010).
107. Mukai, K. *et al.* Activation of STING requires palmitoylation at the Golgi. *Nat. Commun.* **7**, 1–10 (2016).
108. Wang, Y. *et al.* Inflammasome Activation Triggers Caspase-1-Mediated Cleavage of cGAS to Regulate Responses to DNA Virus Infection. *Immunity* **46**, 393–404 (2017).
109. Prabakaran, T. *et al.* Attenuation of c GAS - STING signaling is mediated by a p62/ SQSTM 1-dependent autophagy pathway activated by TBK1 . *EMBO J.* **37**, (2018).
110. Uhlorn, B. L., Gamez, E. R., Li, S. & Campos, S. K. Attenuation of cGAS/STING activity during mitosis. *Life Sci. alliance* **3**, (2020).
111. Pathare, G. R. *et al.* Structural mechanism of cGAS inhibition by the nucleosome. *Nature* **587**, 668–672 (2020).
112. Gentili, M. *et al.* The N-Terminal Domain of cGAS Determines Preferential Association with Centromeric DNA and Innate Immune Activation in the Nucleus. *Cell Rep.* **26**, 2377-2393.e13 (2019).
113. Volkman, H. E., Cambier, S., Gray, E. E. & Stetson, D. B. Tight nuclear tethering of cGAS is essential for preventing autoreactivity. *Elife* **8**, 1–21 (2019).
114. Cao, D., Han, X., Fan, X., Xu, R. M. & Zhang, X. Structural basis for nucleosome-mediated inhibition of cGAS activity. *Cell Res.* **30**, 1088–1097 (2020).
115. Kujirai, T. *et al.* Structural basis for the inhibition of cGAS by nucleosomes. *Science (80-.).*

370, 1–9 (2020).
116. Michalski, S. *et al.* Structural basis for sequestration and autoinhibition of cGAS by chromatin. *Nature* **587**, 678–682 (2020).
117. J. Zullo, K. Matsumoto, S. Xavier, B. Ratliff, M. S. G. The cell secretome, a mediator of cell-to-cell communication. *Prostaglandins Other Lipid Mediat.* **120**, 17–20 (2015).
118. Cavallo, F., Calogero, R. A. & Forni, G. Are oncoantigens suitable targets for anti-tumour therapy? *Nat. Rev. Cancer* **7**, 707–713 (2007).
119. Gangoda, L. *et al.* Proteomic Profiling of Exosomes Secreted by Breast Cancer Cells with Varying Metastatic Potential. *Proteomics* **17**, 1–15 (2017).
120. Peinado, H. *et al.* Pre-metastatic niches: Organ-specific homes for metastases. *Nat. Rev. Cancer* **17**, 302–317 (2017).
121. Robinson, J. L., Feizi, A., Nielsen, J., Engineering, B. & Road, O. C. Diagnostic Potential of the Cancer Secretome. **26**, 2622–2635 (2019).
122. Chen, G. *et al.* Comprehensive Identification and Characterization of Human Secretome Based on Integrative Proteomic and Transcriptomic Data. *Front. Cell Dev. Biol.* **7**, 1–14 (2019).
123. Uhlén, M. *et al.* The human secretome. *Sci. Signal.* **12**, 1–9 (2019).
124. Xu, R. *et al.* Extracellular vesicles in cancer — implications for future improvements in cancer care. *Nat. Rev. Clin. Oncol.* **15**, 617–638 (2018).
125. Paltridge, J. L., Belle, L. & Khew-Goodall, Y. The secretome in cancer progression. *Biochim. Biophys. Acta - Proteins Proteomics* **1834**, 2233–2241 (2013).
126. Moustakas, A. & Heldin, C. H. *Mechanisms of TGFβ-induced epithelial–mesenchymal transition*. *Journal of Clinical Medicine* vol. 5 (2016).
127. Quintero-Fabián, S. *et al.* Role of Matrix Metalloproteinases in Angiogenesis and Cancer. *Front. Oncol.* **9**, 1–21 (2019).
128. Ucuzian, A. A., Gassman, A. A., East, A. T. & Greisler, H. P. Molecular mediators of angiogenesis. *J. Burn Care Res.* **31**, 158–175 (2010).
129. Vinay, D. S. *et al.* Immune evasion in cancer: Mechanistic basis and therapeutic strategies. *Semin. Cancer Biol.* **35**, S185–S198 (2015).
130. Lu, J. *et al.* VEGF-A-induced immature DCs not mature DCs differentiation into endothelial-like cells through ERK1/2-dependent pathway. *Cell Biochem. Funct.* **29**, 294–302 (2011).
131. Oiseth, S. J. & Aziz, M. S. Cancer immunotherapy: a brief review of the history, possibilities, and challenges ahead. *J. Cancer Metastasis Treat.* **3**, 250 (2017).
132. Schiliro, C. & Firestein, B. L. Mechanisms of metabolic reprogramming in cancer cells supporting enhanced growth and proliferation. *Cells* **10**, 1–41 (2021).
133. Pavlides, S. *et al.* The reverse Warburg effect: Aerobic glycolysis in cancer associated fibroblasts and the tumor stroma. *Cell Cycle* **8**, 3984–4001 (2009).
134. Lin, Z. yuan *et al.* MicroRNA-30d promotes angiogenesis and tumor growth via MYPT1/c-JUN/VEGFA pathway and predicts aggressive outcome in prostate cancer. *Mol. Cancer* **16**, 1–14 (2017).
135. Di Virgilio, F. & Adinolfi, E. Extracellular purines, purinergic receptors and tumor growth. *Oncogene* **36**, 293–303 (2017).
136. Beloribi-Djefaflia, S., Vasseur, S. & Guillaumond, F. Lipid metabolic reprogramming in cancer cells. *Oncogenesis* **5**, e189–e189 (2016).
137. Sousa, C. M. *et al.* Pancreatic stellate cells support tumour metabolism through autophagic alanine secretion. *Nature* **536**, 479–483 (2016).
138. Pan, Z., Niu, G., Cao, C. & Tian, Y. Role of microRNAs in remodeling the tumor microenvironment (Review). *Int. J. Oncol.* **56**, 407–416 (2020).
139. Smolarz, B., Durczyński, A., Romanowicz, H., Szyłło, K. & Hogendorf, P. miRNAs in Cancer (Review of Literature). *Int. J. Mol. Sci.* **23**, (2022).

140. Syeda, Z. A., Langden, S. S. S., Munkhzul, C., Lee, M. & Song, S. J. Regulatory mechanism of microrna expression in cancer. *Int. J. Mol. Sci.* **21**, (2020).
141. Vu, L. T., Gong, J., Pham, T. T., Kim, Y. & Le, M. T. N. microRNA exchange via extracellular vesicles in cancer. *Cell Prolif.* **53**, 1–11 (2020).
142. Arroyo, J. D. *et al.* Argonaute2 complexes carry a population of circulating microRNAs independent of vesicles in human plasma. *Proc. Natl. Acad. Sci. U. S. A.* **108**, 5003–5008 (2011).
143. Geekiyanage, H., Rayatpisheh, S., Wohlschlegel, J. A., Brown, R. & Ambros, V. Extracellular microRNAs in human circulation are associated with miRISC complexes that are accessible to anti-AGO2 antibody and can bind target mimic oligonucleotides. *Proc. Natl. Acad. Sci. U. S. A.* **117**, 24213–24223 (2020).
144. Vickers, K. C., Palmisano, B. T., Shoucri, B. M., Shamburek, R. D. & Remaley, A. T. MicroRNAs are transported in plasma and delivered to recipient cells by high-density lipoproteins. *Nat. Cell Biol.* **13**, 423–435 (2011).
145. Wang, K., Zhang, S., Weber, J., Baxter, D. & Galas, D. J. Export of microRNAs and microRNA-protective protein by mammalian cells. *Nucleic Acids Res.* **38**, 7248–7259 (2010).
146. Semina, E. V., Rysenkova, K. D., Troyanovskiy, K. E., Shmakova, A. A. & Rubina, K. A. MicroRNAs in Cancer: From Gene Expression Regulation to the Metastatic Niche Reprogramming. *Biochem.* **86**, 785–799 (2021).
147. Takano, Y. *et al.* Circulating exosomal microRNA-203 is associated with metastasis possibly via inducing tumor-associated macrophages in colorectal cancer. *Oncotarget* **8**, 78598–78613 (2017).
148. Solé, C. & Lawrie, C. H. MicroRNAs and metastasis. *Cancers (Basel).* **12**, 1–21 (2020).
149. Cui, M. *et al.* Circulating MicroRNAs in Cancer: Potential and Challenge. *Front. Genet.* **10**, (2019).
150. Szelenberger, R., Kacprzak, M., Saluk-Bijak, J., Zielinska, M. & Bijak, M. Plasma MicroRNA as a novel diagnostic. *Clin. Chim. Acta* **499**, 98–107 (2019).
151. Erler, J. T. *et al.* Hypoxia-induced lysyl oxidase is a critical mediator of bone marrow cell recruitment to form the pre-metastatic niche. *Cancer Cell* **15**, 35–44 (2011).
152. Ritchie, S., Reed, D. A., Pereira, B. A. & Timpson, P. The cancer cell secretome drives cooperative manipulation of the tumour microenvironment to accelerate tumourigenesis. *Fac. Rev.* **10**, (2021).
153. Choudhry, H. & Harris, A. L. Advances in Hypoxia-Inducible Factor Biology. *Cell Metab.* **27**, 281–298 (2018).
154. Muz, B., de la Puente, P., Azab, F. & Azab, A. K. The role of hypoxia in cancer progression, angiogenesis, metastasis, and resistance to therapy. *Hypoxia* 83 (2015) doi:10.2147/hp.s93413.
155. Jun, J. C., Rathore, A., Younas, H., Gilkes, D. & Polotsky, V. Y. Hypoxia-Inducible Factors and Cancer. *Curr. Sleep Med. Reports* **3**, 1–10 (2017).
156. Soni, S. & Padwad, Y. S. HIF-1 in cancer therapy: two decade long story of a transcription factor. *Acta Oncol. (Madr).* **56**, 503–515 (2017).
157. Lv, X. *et al.* The role of hypoxia-inducible factors in tumor angiogenesis and cell metabolism. *Genes Dis.* **4**, 19–24 (2017).
158. Petrova, V., Annicchiarico-Petruzzelli, M., Melino, G. & Amelio, I. The hypoxic tumour microenvironment. *Oncogenesis* **7**, (2018).
159. Fu, Z., Mowday, A. M., Smaill, J. B., Hermans, I. F. & Patterson, A. V. Tumour hypoxia-mediated immunosuppression: Mechanisms and therapeutic approaches to improve cancer immunotherapy. *Cells* **10**, (2021).
160. Arnaiz, E. & Harris, A. L. Role of Hypoxia in the Interferon Response. *Front. Immunol.* **13**, 1–14 (2022).

161. Nishida, N. Role of oncogenic pathways on the cancer immunosuppressive microenvironment and its clinical implications in hepatocellular carcinoma. *Cancers (Basel).* **13**, (2021).
162. van Loosdregt, J. & Coffer, P. J. The Role of WNT Signaling in Mature T Cells: T Cell Factor Is Coming Home. *J. Immunol.* **201**, 2193–2200 (2018).
163. Li, X. *et al.* WNT/β-catenin signaling pathway regulating T cell-inflammation in the tumor microenvironment. *Front. Immunol.* **10**, 1–12 (2019).
164. Sparmann, A. & Bar-sagi, D. Ras-induced interleukin-8 expression plays a critical role in tumor growth and angiogenesis. **6**, 447–458 (2004).
165. Ancrile, B., Lim, K. H. & Counter, C. M. Oncogenic Ras-induced secretion of IL6 is required for tumorigenesis. *Genes Dev.* **21**, 1714–1719 (2007).
166. Liu, S., Iaria, J., Simpson, R. J. & Zhu, H. J. Ras enhances TGF-β signaling by decreasing cellular protein levels of its type II receptor negative regulator SPSB1. *Cell Commun. Signal.* **16**, 1–15 (2018).
167. Pylayeva-Gupta, Y., Lee, K. E., Hajdu, C. H., Miller, G. & Bar-Sagi, D. Oncogenic Kras-Induced GM-CSF Production Promotes the Development of Pancreatic Neoplasia. *Cancer Cell* **21**, 836–847 (2012).
168. Doi, T. *et al.* The JAK/STAT pathway is involved in the upregulation of PD-L1 expression in pancreatic cancer cell lines. *Oncol. Rep.* **37**, 1545–1554 (2017).
169. Wang, G. *et al.* Targeting YAP-dependent MDSC infiltration impairs tumor progression. *J. Immunother. Cancer* **3**, 2015 (2015).
170. Murakami, S. *et al.* Yes-Associated protein mediates immune reprogramming in pancreatic ductal adenocarcinoma. *Oncogene* **36**, 1232–1244 (2017).
171. Marei, H. E. *et al.* P53 Signaling in Cancer Progression and Therapy. *Cancer Cell Int.* **21**, 1–16 (2021).
172. Boutelle, A. M. & Attardi, L. D. p53 and Tumor Suppression: It Takes a Network. *Trends Cell Biol.* **31**, 298–310 (2021).
173. Blagih, J., Buck, M. D. & Vousden, K. H. P53, Cancer and the Immune Response. *J. Cell Sci.* **133**, (2020).
174. Kandoth, C. *et al.* Mutational landscape and significance across 12 major cancer types. *Nature* **502**, 333–339 (2013).
175. Freed-Pastor, W. A. & Prives, C. Mutant p53: One name, many proteins. *Genes Dev.* **26**, 1268–1286 (2012).
176. Mantovani, F., Collavin, L. & Del Sal, G. Mutant p53 as a guardian of the cancer cell. *Cell Death Differ.* **26**, 199–212 (2019).
177. Alvarado-Ortiz, E. *et al.* Mutant p53 Gain-of-Function: Role in Cancer Development, Progression, and Therapeutic Approaches. *Front. Cell Dev. Biol.* **8**, 1–24 (2021).
178. Peng, Y., Chen, L., Li, C., Lu, W. & Chen, J. Inhibition of MDM2 by hsp90 Contributes to Mutant p53 Stabilization. *J. Biol. Chem.* **276**, 40583–40590 (2001).
179. Li, D., Marchenko, N. D. & Moll, U. M. SAHA shows preferential cytotoxicity in mutant p53 cancer cells by destabilizing mutant p53 through inhibition of the HDAC6-Hsp90 chaperone axis. *Cell Death Differ.* **18**, 1904–1913 (2011).
180. Ingallina, E. *et al.* Mechanical cues control mutant p53 stability through a mevalonate-RhoA axis. *Nat. Cell Biol.* **20**, 28–35 (2018).
181. Amelio, I. *et al.* p53 mutants cooperate with HIF-1 in transcriptional regulation of extracellular matrix components to promote tumor progression. *Proc. Natl. Acad. Sci. U. S. A.* **115**, E10869–E10878 (2018).
182. Montagner, M. *et al.* SHARP1 suppresses breast cancer metastasis by promoting degradation of hypoxia-inducible factors. *Nature* **487**, 380–384 (2012).
183. Narendran, A. *et al.* Mutant p53 in bone marrow stromal cells increases VEGF expression and supports leukemia cell growth. *Exp. Hematol.* **31**, 693–701 (2003).

184. Fontemaggi, G. *et al.* The execution of the transcriptional axis mutant p53, E2F1 and ID4 promotes tumor neo-angiogenesis. *Nat. Struct. Mol. Biol.* **16**, 1086–1093 (2009).
185. Shakya, R. *et al.* Mutant p53 upregulates alpha-1 antitrypsin expression and promotes invasion in lung cancer. *Oncogene* **36**, 4469–4480 (2017).
186. Cooks, T. *et al.* Mutant p53 cancers reprogram macrophages to tumor supporting macrophages via exosomal miR-1246. *Nat. Commun.* **9**, (2018).
187. Ma, S. *et al.* Gain-of-function p53 protein transferred via small extracellular vesicles promotes conversion of fibroblasts to a cancer-associated phenotype. *Cell Rep.* **34**, 108726 (2021).
188. Yeudall, W. A. *et al.* Gain-of-function mutant p53 upregulates CXC chemokines and enhances cell migration. *Carcinogenesis* **33**, 442–451 (2012).
189. Ubertini, V. *et al.* Mutant p53 gains new function in promoting inflammatory signals by repression of the secreted interleukin-1 receptor antagonist. *Oncogene* **34**, 2493–2504 (2015).
190. Yan, W. & Chen, X. Identification of GRO1 as a critical determinant for mutant p53 gain of function. *J. Biol. Chem.* **284**, 12178–12187 (2009).
191. Ghosh, M. *et al.* Mutant p53 suppresses innate immune signaling to promote tumorigenesis. *Cancer Cell* **39**, 494-508.e5 (2021).
192. Zhu, K. *et al.* p53 induces TAP1 and enhances the transport of MHC class I peptides. *Oncogene* **18**, 7740–7747 (1999).
193. Dong, Z.-Y. *et al.* MA15.10 Potential Predictive Value of TP53 and KRAS Mutation Status for Response to PD-1 Blockade Immunotherapy in Lung Adenocarcinoma. *J. Thorac. Oncol.* **12**, S432–S433 (2017).
194. Capaci, V. *et al.* Mutant p53 induces Golgi tubulo-vesiculation driving a prometastatic secretome. *Nat. Commun.* **11**, 1–19 (2020).
195. Li, C. *et al.* Non-small cell lung cancer associated microRNA expression signature: Integrated bioinformatics analysis, validation and clinical significance. *Oncotarget* **8**, 24564–24578 (2017).
196. Zhao, Q., Yuan, X., Zheng, L. & Xue, M. miR-30d-5p: A Non-Coding RNA With Potential Diagnostic, Prognostic and Therapeutic Applications. *Front. Cell Dev. Biol.* **10**, 1–11 (2022).
197. Xu, X. *et al.* miR-30d suppresses proliferation and invasiveness of pancreatic cancer by targeting the SOX4/PI3K-AKT axis and predicts poor outcome. *Cell Death Dis.* **12**, (2021).
198. Yu, M. & Liu, J. MicroRNA-30d-5p promotes ovarian granulosa cell apoptosis by targeting Smad2. *Exp. Ther. Med.* 53–60 (2019) doi:10.3892/etm.2019.8184.
199. Li, N. *et al.* A combined array-based comparative genomic hybridization and functional library screening approach identifies mir-30d as an oncomir in cancer. *Cancer Res.* **72**, 154–164 (2012).
200. Zhou, Y. *et al.* Amplification and up-regulation of MIR30D was associated with disease progression of cervical squamous cell carcinomas. *BMC Cancer* **17**, 1–11 (2017).
201. Zhu, Y. *et al.* Serum expression and significance of MicroRNA-30d-5p in esophageal squamous cell carcinoma. *Int. J. Clin. Exp. Pathol.* **10**, 8677–8685 (2017).
202. Muhammad, S. *et al.* miRNA-30d serves a critical function in colorectal cancer initiation, progression and invasion via directly targeting the GNA13 gene. *Exp. Ther. Med.* 260–272 (2018) doi:10.3892/etm.2018.6902.
203. Han, M. *et al.* microRNA-30d mediated breast cancer invasion, migration, and EMT by targeting KLF11 and activating STAT3 pathway. *J. Cell. Biochem.* **119**, 8138–8145 (2018).
204. Gaziel-Sovran, A. *et al.* MiR-30b/30d Regulation of GalNAc Transferases Enhances Invasion and Immunosuppression during Metastasis. *Cancer Cell* **20**, 104–118 (2011).
205. Li, J. *et al.* Mir-30d Regulates Cardiac Remodeling by Intracellular and Paracrine Signaling. *Circ. Res.* E1–E23 (2021) doi:10.1161/CIRCRESAHA.120.317244.
206. Balaguer, N. *et al.* Heterogeneous nuclear ribonucleoprotein C1may control miR-30d levels in endometrial exosomes affecting early embryo implantation. *Mol. Hum. Reprod.* **24**, 411–425

(2018).
207. Camps, C. *et al.* Integrated analysis of microRNA and mRNA expression and association with HIF binding reveals the complexity of microRNA expression regulation under hypoxia. *Mol. Cancer* **13**, 1–21 (2014).
208. Trucco, A. *et al.* Secretory traffic triggers the formation of tubular continuities across Golgi sub-compartments. *Nat. Cell Biol.* **6**, 1071–1081 (2004).
209. Beznoussenko, G. V. *et al.* Transport of soluble proteins through the Golgi occurs by diffusion via continuities across cisternae. *Elife* **2014**, 1–27 (2014).
210. Maleki Vareki, S. High and low mutational burden tumors versus immunologically hot and cold tumors and response to immune checkpoint inhibitors. *J. Immunother. Cancer* **6**, 4–8 (2018).
211. Liu, Y. T. & Sun, Z. J. Turning cold tumors into hot tumors by improving T-cell infiltration. *Theranostics* **11**, 5265–5286 (2021).
212. Emanuela Frittoli, Andrea Palamidess, I. F. *et al.* Tissue uidiication promotes a cGAS/STING-mediated cytosolic DNA response in invasive breast cancer. *Res. Sq.* (2021) doi:DOI: 10.21203/rs.3.rs-845173/v1.
213. Miller, F. R. Xenograft models of premalignant breast disease. *J. Mammary Gland Biol. Neoplasia* **5**, 379–391 (2000).
214. Bonci, D. *et al.* The miR-15a-miR-16-1 cluster controls prostate cancer by targeting multiple oncogenic activities. *Nat. Med.* **14**, 1271–1277 (2008).
215. Agarwal, V., Bell, G. W., Nam, J. W. & Bartel, D. P. Predicting effective microRNA target sites in mammalian mRNAs. *Elife* **4**, 1–38 (2015).
216. Mejía-Calvo, I. *et al.* Validation of a cell-based colorimetric reporter gene assay for the evaluation of Type I Interferons. *Biotechnol. Reports* **22**, e00331 (2019).
217. Ablasser, A. & Chen, Z. J. CGAS in action: Expanding roles in immunity and inflammation. *Science (80-.).* **363**, (2019).
218. Schoggins, J. W. & Rice, C. M. Interferon-stimulated genes and their antiviral effector functions. *Curr. Opin. Virol.* **1**, 519–525 (2011).
219. Boukhaled, G. M., Harding, S. & Brooks, D. G. Opposing Roles of Type i Interferons in Cancer Immunity. *Annu. Rev. Pathol. Mech. Dis.* **16**, 167–198 (2021).
220. Gauthier, B. R. & Comaills, V. Nuclear envelope integrity in health and disease: Consequences on genome instability and inflammation. *Int. J. Mol. Sci.* **22**, (2021).
221. Shen, R. *et al.* DNA Damage and Activation of cGAS/STING Pathway Induce Tumor Microenvironment Remodeling. *Front. Cell Dev. Biol.* **9**, 1–14 (2022).
222. Kumar, A. *et al.* ATR mediates a checkpoint at the nuclear envelope in response to mechanical stress. *Cell* **158**, 633–646 (2014).
223. Maistriau, M. *et al.* A method for the detection of virus infectivity in single cells and real time: Towards an automated fluorescence neutralization test. *Virus Res.* **237**, 1–6 (2017).
224. Basit, A. *et al.* The cGAS/STING/TBK1/IRF3 innate immunity pathway maintains chromosomal stability through regulation of p21 levels. *Exp. Mol. Med.* **52**, 643–657 (2020).
225. Lim, S., Quinton, R. J. & Ganem, N. J. Nuclear envelope rupture drives genome instability in cancer. *Mol. Biol. Cell* **27**, 3210–3213 (2016).
226. Kuo, L. J. & Yang, L. X. γ-H2AX- A novel biomaker for DNA double-strand breaks. *In Vivo (Brooklyn).* **22**, 305–310 (2008).
227. Waks, A. G. & Winer, E. P. Breast Cancer Treatment: A Review. *JAMA - J. Am. Med. Assoc.* **321**, 288–300 (2019).
228. Luthra P, Aguirre S, Yen BC, Pietzsch CA, Sanchez-Aparicio MT, T. B. & Al., E. Topoisomerase II Inhibitors Induce DNA Damage-Dependent Interferon Responses Circumventing Ebola Virus Immune. *MBio* **8**, doi: 10.1128/mBio.00368-17 (2017).
229. Drost, J. & Clevers, H. Organoids in cancer research. *Nat. Rev. Cancer* **18**, 407–418 (2018).

230. Zheng, M. *et al.* Exosomal let-7d-3p and miR-30d-5p as diagnostic biomarkers for non-invasive screening of cervical cancer and its precursors. *Mol. Cancer* **18**, 1–8 (2019).
231. Finn, R. S. *et al.* Dasatinib as a single agent in triple-negative breast cancer: Results of an open-label phase 2 study. *Clin. Cancer Res.* **17**, 6905–6913 (2011).
232. Mayer, E. L. *et al.* A phase 2 trial of dasatinib in patients with advanced HER2-positive and/or hormone receptor-positive breast cancer. *Clin. Cancer Res.* **17**, 6897–6904 (2011).
233. Yum, S., Li, M., Fang, Y. & Chen, Z. J. TBK1 recruitment to STING activates both IRF3 and NF-κB that mediate immune defense against tumors and viral infections. *Proc. Natl. Acad. Sci. U. S. A.* **118**, 1–9 (2021).
234. You, L. *et al.* The role of hypoxia-inducible factor 1 in tumor immune evasion. *Med. Res. Rev.* **41**, 1622–1643 (2021).
235. Min-Zu Wu, Wei-Chung Cheng, et al. miR25/93 mediates hypoxia-induced immunosuppression by repressing cGAS. *Physiol. Behav.* **176**, 139–148 (2019).
236. Bell, E. & Taylor, M. A. Functional Roles for Exosomal MicroRNAs in the Tumour Microenvironment. *Comput. Struct. Biotechnol. J.* **15**, 8–13 (2017).
237. Romano, G., Acunzo, M. & Nana-Sinkam, P. Micrornas as novel therapeutics in cancer. *Cancers (Basel).* **13**, (2021).
238. Hong, D. S. *et al.* Phase 1 study of MRX34, a liposomal miR-34a mimic, in patients with advanced solid tumours. *Br. J. Cancer* **122**, 1630–1637 (2020).
239. Seto, A. G. *et al.* Cobomarsen, an oligonucleotide inhibitor of miR-155, co-ordinately regulates multiple survival pathways to reduce cellular proliferation and survival in cutaneous T-cell lymphoma. *Br. J. Haematol.* **183**, 428–444 (2018).
240. Hanna, J., Hossain, G. S. & Kocerha, J. The potential for microRNA therapeutics and clinical research. *Front. Genet.* **10**, (2019).
241. Le Naour, J., Zitvogel, L., Galluzzi, L., Vacchelli, E. & Kroemer, G. Trial watch: STING agonists in cancer therapy. *Oncoimmunology* **9**, 1–12 (2020).
242. Hosseini, S. M. *et al.* Clinically significant dysregulation of hsa-miR-30d-5p and hsa-let-7b expression in patients with surgically resected non-small cell lung cancer. *Avicenna J. Med. Biotechnol.* **10**, 98–104 (2018).
243. Wang, H., Peng, R., Wang, J., Qin, Z. & Xue, L. Circulating microRNAs as potential cancer biomarkers: The advantage and disadvantage. *Clin. Epigenetics* **10**, 1–10 (2018).
244. Schindelin, J. *et al.* Fiji: An open-source platform for biological-image analysis. *Nat. Methods* **9**, 676–682 (2012).
245. Ritchie, M. E. *et al.* Limma powers differential expression analyses for RNA-sequencing and microarray studies. *Nucleic Acids Res.* **43**, e47 (2015).
246. Korotkevich, G. & Sukhov, V. Fast gene set enrichment analysis. 1–29 (2016).
247. Colaprico, A. *et al.* TCGAbiolinks: An R/Bioconductor package for integrative analysis of TCGA data. *Nucleic Acids Res.* **44**, e71 (2016).
248. Aran, D., Hu, Z. & Butte, A. J. xCell: Digitally portraying the tissue cellular heterogeneity landscape. *Genome Biol.* **18**, 1–14 (2017).